Metal-Organic Coordination Polymers and Composites: Electrical Conductivity, Photoluminescence, and Electro-catalysis

A Thesis

Submitted in Partial Fulfillment of the Requirements

for the Degree of

Doctor of Philosophy

by

Barun Dhara

ID: 20113140

INDIAN INSTITUTE OF SCIENCE EDUCATION AND RESEARCH, PUNE

2017

Dedicated to

My Parents and Wife

भारतीय विज्ञान शिक्षा एवं अनुसंधान संस्थान, पुणे
INDIAN INSTITUTE OF SCIENCE EDUCATION AND RESEARCH (IISER), PUNE
(An Autonomous Institution, Ministry of Human Resource Development, Govt. of India)

Dr. NIRMALYA BALLAV
Associate Professor (Chemistry)
E-mail: nballav@iiserpune.ac.in
Web: http://www.iiserpune.ac.in/~nballav/

Dr. Homi Bhabha Road, Pashan
Pune 411 008, INDIA
Tel: +91 20 2590 8215
Fax: +91 20 2586 5315

CERTIFICATE

Certified that the work incorporated in the thesis entitled "***Metal-Organic Coordination Polymers and Composites: Electrical Conductivity, Photoluminescence, and Electro-catalysis"*** submitted by ***Mr. Barun Dhara*** was carried out by the candidate, under my supervision. The work presented here or any part of it has not been included in any other thesis submitted previously for the award of any degree or diploma from any other university or institution.

Date: 14th March, 2017

Dr. Nirmalya Ballav
(Research Supervisor)

भारतीय विज्ञान शिक्षा एवं अनुसंधान संस्थान, पुणे
INDIAN INSTITUTE OF SCIENCE EDUCATION AND RESEARCH (IISER), PUNE
(An Autonomous Institution, Ministry of Human Resource Development, Govt. of India)

Declaration

I ***Mr. Barun Dhara*** declare that, this written submission represents my ideas in my own words and where others' ideas have been included; I have adequately cited and referenced the original sources. I also declare that I have adhered to all principles of academic honesty and integrity and have not misrepresented or fabricated or falsified any idea/data/fact/source in my submission. I understand that violation of the above will be cause for disciplinary action by the institute and can also evoke penal action from the sources which have thus not been properly cited or from whom proper permission has not been taken when needed.

The work reported in this thesis is the original work done by me under the guidance of ***Dr. Nirmalya Ballav.***

Date: 14th March, 2017

Mr. Barun Dhara
(ID: 20113140)

Acknowledgment

I am deeply indebted to my research supervisor Dr. Nirmalya Ballav for teaching me a good conduct of scientific research in an economic way which I will carry forward in future. I am really thankful to him for guiding me and continuously supporting me in the last five years. His inspiration and continuous guidance make me choose a fruitful and effective research platform. I learned from him to design and engineer a research project in a very constructive manner. One of the most important achievement for me is to set up a new lab from a scratch.

I sincerely acknowledge to Indian Institute of Science Education and Research (IISER), Pune and its director Prof. K. N. Ganesh for providing excellent interdisciplinary research facilities and an outstanding research environment.

I am very much thankful to my Research Advisory Committee (RAC) members Dr. Sujit K. Ghosh (IISER Pune) and Dr. Avinash Kumbhar (Savitribai Phule Pune University, Pune) for their continuous support and invaluable suggestion in every step of my research work. I am thankful to Dr. G. V. Pavan Kumar, Dr. Shouvik Datta, Dr. Sunil Nair, Dr. Aparna Deshpande, Dr. Prasenjit Ghosh, Dr. Sreekumar Kurungot (NCL Pune), Dr. Peter M. Oppeneer (Uppsala University), Dr. Kartick Tarafder (National Institute of Technology Karnataka) for giving me their collective research inputs in collaborative way. I am extremely thankful to all the faculty members of IISER Pune and Prof. M. Jayakanan (Chair, Chemistry department) for giving us the four-probe I-V instrument.

I would like to thank my lab mates, Rajendra, Plawan, Shammi, Kriti, Dipayan, Debashree, Kaustav Da, Anupam, Mahendra and Utkarsh for their direct/indirect contribution to my PhD work. Important people in my PhD life are undergraduate students Vikash Kumar and former undergraduate student Vimlesh Bind. However, they are much younger to me, I learned many exciting things from them. While working or discussing with them, in every moment it reminds me that, there is chance to execute these hurdles. I am also thankful to our former group members Hetal, Shraddha, Srikant and Anita.

During my PhD work, hostel life is not fulfilled without my dearest friends Partha, Arindam Da, Joarder Da, Manna Da, Abhik, Koushik, Sudeb, Avishek, Sunil, Supratik, Maidul, Soumya, Rejaul, Shyama, Tanmoy, Rajkumar, and Amit.

I am thankful to Sushil, Arvind, Ashok, Anant, Sohini, Sneha, Sudeshna, Arundhati, Anupam Da, Abhigyan Da, Sagar, Gopal, Rahi, Sayan Da, Bijoy Da, Rajasekhar, Dinesh, Shiva Shankar, Wasim,

Jagadish, Chandra, Soumendra, Debanjan, Shiv Pal, Shanku, Ravikiran, Kiran, Santosh, Aamod, Suresh, Kajari, and many more ….

I would like to thank to my teachers Sidhu Da, Sintu Da, Suvra Di and Prasenjit Da. I am really delightful to get my childhood teacher Satya Kinkar Manna for extending my thinking power in multi-dimensions.

I am thankful to my best friends Montu, Sudip and Sanjay for giving me mental strength every moment.

I thank Dr. Umeshareddy Kacherki and Anuradha for library support and Ms. Archana, Parveen Nasa for SCXRD. I would like to thank to Sachin and Abhijeet for IT support. I would also like to thank Mr. Mayuresh, Mr. Tushar, Mr. Mahesh, Mr. Nitin, Mr. Anil, Mrs. Megha, and Mr. Prabhas for their administrative and official support during my research period at IISER, Pune.

I am very much thankful to madam (Dr. Tanushree Bhattacharjee) and Tani for encouraging me throughout my Ph.D. life. They always remind me that we are working as a family.

My dearest and nearest one who always encouraged me to step ahead on research problems, of course, that person is my wife Mrs. Mukti Pattanayak who teaches her students beyond the textbook knowledge and I am also one of them. I am grateful to her for her sacrifices, patience and support for gifting me a beautiful life.

I would like to thank my parents and my family for their encouragement and unconditional trust and support. They have helped me to overcome various difficulties and I wonder if I would be able to translate their dreams into reality.

I would also like to thank American Chemical Society (ACS), Royal Society of Chemistry (RSC), John Wiley & Sons (Wiley-VCH) and Elsevier for publishing a number of my research articles produced during my PhD tenure at IISER, Pune.

I am thankful to CSIR, DAE-BRNS, DST-Nano Mission, MHRD, and IISER Pune for the funding.

Barun Dhara

Table of Contents

Synopsis:

The thesis entitled "***Coordination Polymers and Composites: Electrical Conductivity, Photoluminescence and Electro-catalysis***" includes 4 chapters.

According to IUPAC, coordination polymer is a coordination compound with repeating coordination entities extending in 1, 2, or 3 dimensions. Coordination polymers (CPs) are primarily constructed through non-covalent interaction between multivalent organic ligand and metal ions and do not need to be crystalline, for example, metal-organic gel (MOG). In case, if it is crystalline and having potential void space can be termed as metal-organic framework (MOF). Owing to its structural diversity, CPs appear promising candidates for gas storage, gas separation, catalysis, proton conductivity, sensing, magnetism, light harvesting, electrical conductivity, photoluminescence, electro-catalysis, and recently emerging in the field of energy and environmental applications.

This thesis is aimed to shed new light in the domains of electrical conductivity, photoluminescence and electro-catalysis involving redox-active as well as redox-inactive CPs.

Chapter I. ***Introduction of Coordination Polymers***

In this chapter we describe a general introduction to CPs detailing some aspects of gas storage, gas separation, catalysis, proton conductivity, sensing, magnetism, light harvesting, electrical conductivity, photoluminescence, and electro-catalysis. This chapter serves as the overall literature review in the field as well as scopes available in the chosen topics.

Chapter II. ***Enhancement of Electrical Conductivity in Coordination Polymers***

Electrical conductivity of CPs can be modulated by adopting intrinsic (changing the ligand and/or metal ion) and extrinsic approach (filling the pores with suitable guest species). This chapter is subdivided into three sections.

Section IIA. ***Enhancement of Electrical Conductivity in Redox-Active Coordination Polymer***

In this section electrical conductivity enhancement is reported in a redox-active CP via in situ incorporation of conducting polymers. Specifically, conducting polypyrrole (PPy) and polythiophene (PTh) moieties were incorporated (without using any extraneous oxidizing agent) into the matrix of CP comprised of Fe(III) ions and benzene 1,3,5-tricarboxylic acid (BTC) ligand. Conductivity enhancement Fe-BTC→Fe-BTC-PPy/Fe-BTC-PTh was found to be ca. ~10^3 fold.

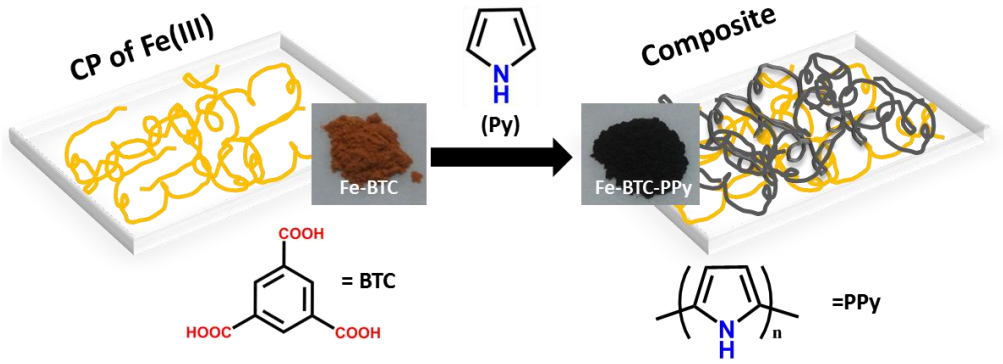

Scheme 1. *Schematic illustration of conducting polymer in redox-active CP matrix.*

Publication from this chapter

1. *In Situ* Generation of Conducting Polymer in a Redox-Active Metal–Organic Gel**.**

Barun Dhara, and Nirmalya Ballav.

RSC Adv. **2013**, 3, 4909-4913.

Section IIB. ***Enhancement of Electrical Conductivity in Redox-Inactive Coordination Polymer***

Remarkable enhancement of electrical conductivity is demonstrated upon incorporation of chains of conducting polypyrrole (PPy) into the 1D-nanochannels of a redox-inactive Cd(II)-based CP. Iodine (I_2) was used as an external oxidizing agent for an effective polymerization of Py monomers. Conductivity enhancement CP→CP-PPy was found to be ~10^9 fold. Such

observation is assigned to non-covalent electronic interaction between host (CP) and guest (PPy) as well as the confinement effect in nano-space.

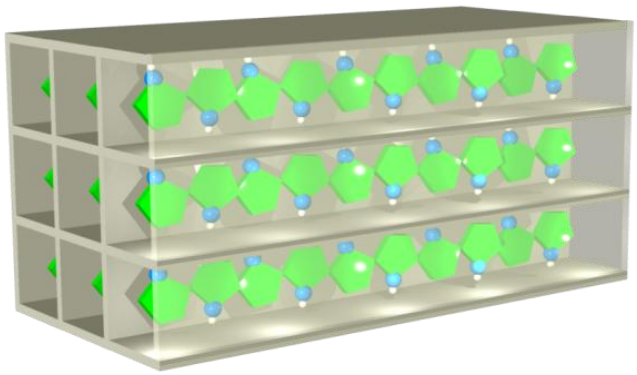

Scheme 2. *Schematic illustration of conducting polymer inside nanochannels of CP.*

Publication from this chapter

1. Increase in Electrical Conductivity of MOF to Billion-Fold upon Filling the Nanochannels with Conducting Polymer.

Barun Dhara, Sanjog S. Nagarkar, Jitendra Kumar, Vikash Kumar, Plawan K. Jha, Sujit K. Ghosh, Sunil Nair, and Nirmalya Ballav.

J. Phys. Chem. Lett. **2016**, 7, 2945–2950.

Section IIC. ***Modulation of Electrical Conductivity in Bimetallic Coordination Polymer***

In this section, an intrinsic approach of enhancing electrical conductivity in CP is reported. A bimetallic design principle of CP is explored. Specifically, bimetallic CPs of Fe(III) and Cr(III) ions coordinated to BTC ligand was prepared. Fe-BTC-Cr system exhibited very-high carrier mobility at matching mole ratio (1:1) – an enhancement of ~10^3-10^4 fold in comparison to those of monometallic parents Fe-BTC and Cr-BTC, respectively. Such an unusual increase in the mobility of bimetallic CPs is attributed to the formation of two-dimensional electron gas.

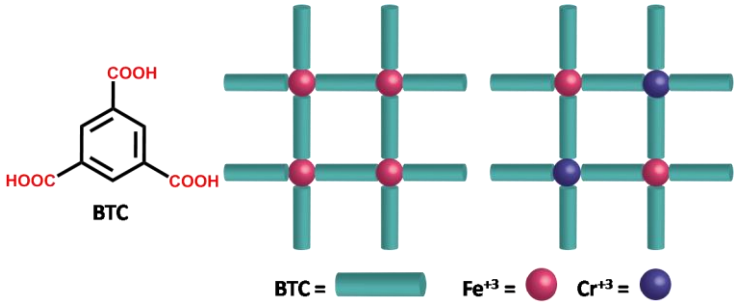

Scheme 3. *Schematic representation of monometallic and bimetallic CPs.*

Publication from this chapter

1. Giant Enhancement of Carrier Mobility in Bimetallic Coordination Polymers.

Barun Dhara, Vikash Kumar, Kriti Gupta, Plawan Kumar Jha, and Nirmalya Ballav.

(Submitted)

Chapter 3. ***Photoluminescence Property of Redox-Active Coordination Polymer***

Most of the CPs showing ligand-based photoluminescence property are reported to be comprised of redox-inactive metal ions such as Zn(II), Cd(II), Mg(II), In(III), and Al(III) ions. In this chapter, we have prepared a redox-active and intrinsically non-photoluminescent CP comprised of Fe(III) ions and terephthalic acid (TPA) ligand. In presence of small reactive organic molecules like pyrrole (Py), aniline (Ani), and bi-thiophene (BTh), the metal-organic gelation process was unaffected and at the same time it lead to the formation of highly photoluminescent composite materials. The photoluminescence turn-on response was primarily attributed to the redox-reaction between Fe(III) ions and the small organic molecules generating oxidized oligomers in the CP matrix.

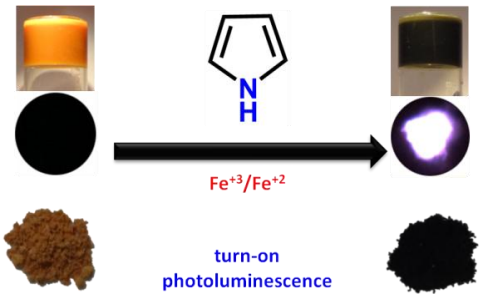

Scheme 4. *Photoluminescence turn-on response of redox-active CP.*

Publication from this chapter:

1. Redox-Induced Photoluminescence of Metal−Organic Coordination Polymer Gel.

Barun Dhara, Partha Pratim Patra, Plawan K. Jha, Shraddha V. Jadhav, G. V. Pavan Kumar, and Nirmalya Ballav.

J. Phys. Chem. C **2014**, 118, 19287–19293.

Chapter 4. ***Electro-catalytic Activity of Redox-Active Coordination Polymer***

Coordination polymers are recently emerging in the domain of renewable energy research such as electro-catalysis, supercapacitor, and battery. In this chapter, a redox-active CP made of Fe(III) ions and 4,4′,4″-tricarboxyltriphenylamine (TCA) ligand is prepared. The role of Fe-TCA material as such (without further treatment) as an electro-catalyst towards oxygen evolution reaction (OER) was checked. The catalytic performance of Fe-TCA is appearing better than those of previously reported Fe-based systems as OER catalysts. Theoretical insight is provided with the help of numerical simulations based on density functional theory (DFT).

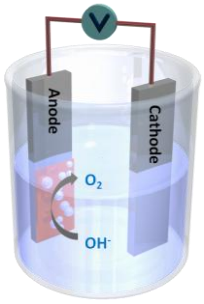

Scheme 5. *Schematic illustration of OER by employing redox-active CP as electro-catalyst.*

Publication from this chapter:

1. Coordination Polymers of Fe(III) and Al(III) ions with TCA Ligand: Distinctive Fluorescence, CO_2 Uptake, Redox-Activity and Oxygen Evolution Reaction.

Barun Dhara, Subrahmanyam Sappati, Santosh K. Singh, Sreekumar Kurungot, Prasenjit Ghosh, and Nirmalya Ballav.

Dalton Trans. **2016**, 45, 6901-6908.

Glossary of Acronyms

Å	Angstrom
AC	Alternative current
BTC	1,3,5-benzenetricarboxylate
°C	Degree Celsius
CCDC	Cambridge crystallographic data centre
CP	Coordination polymer
CPD	Cyclopentadiene
DC	Direct current
DMSO	Dimethyl sulfoxide
DOBDC	2,5-dihydroxybenzene-1,4-dicarboxylic acid
DSBDC	2,5-disulfhydrylbenzene-1,4-dicarboxylic acid
DSC	Differential scanning calorimetry
EDX	Energy-dispersive X-ray spectroscopy
EtOH	Ethanol
FESEM	Field emission scanning electron microscopy
FTIR	Fourier transform infrared-spectra
HER	Hydrogen evolution reaction
H_2NDC	2,6-naphthalenedicarboxylic acid
HOMO	Highest occupied molecular orbital
HPCA	4-pyridinecarboxylic acid
IRMOF	Isoreticular metal-organic framework
IUPAC	International union of pure and applied chemistry
LASER	Light amplification by stimulated emission of radiation
LUMO	Lowest unoccupied molecular orbital
LMCT	Ligand to metal charge transfer
MeOH	Methanol
MLCT	Metal to ligand charge transfer
MMOF	Magnetic metal-organic framework
MOF	Metal-organic framework

MOG	Metal-organic gel
MOM	Metal-organic material
MOP	Metal-organic polymer
NMR	Nuclear magnetic resonance
OER	Oxygen evolution reaction
OFET	Organic field effect transistor
PANI	Polyaniline
PCP	Porous coordination polyhedra
PL	Photoluminescence
PPy	Polypyrrole
PTh	Polythiophene
PXRD	Powder X-Ray diffraction
TCA	4,4′,4″-tricarboxyltriphenylamine
TCNQ	7,7,8,8-tetracyanoquinodimethane
TGA	Thermogravimetric analysis
TPA	Terephthalic acid
ZIF	Zeolitic imidazole framework

Publications included to Thesis

1. **Dhara, B.**; and Ballav, N. *In Situ* Generation of Conducting Polymer in a Redox-Active Metal-Organic Gel. *RSC Adv.* **2013,** *3*, 4909.

2. **Dhara, B.**; Nagarkar, S. S.; Kumar, J.; Kumar, V.; Jha, P. K.; Ghosh, S. K.; Nair, S.; and Ballav, N. Increase in Electrical Conductivity of MOF to Billion-Fold upon Filling the Nanochannels with Conducting Polymer. *J. Phys. Chem. Lett.* **2016,** *7*, 2945.

3. **Dhara**, **B.**; Kumar, V.; Gupta K.; Jha, P. K.; and Ballav, N. Giant Enhancement of Carrier Mobility in Bimetallic Coordination Polymers *(Under Revision).*

4. **Dhara, B.**; Patra, P. P.; Jha, P. K.; Jadhav, S. V.; Pavan Kumar, G. V.; and Ballav, N. Redox-Induced Photoluminescence of Metal–Organic Coordination Polymer Gel. *J. Phys. Chem. C* **2014,** *118*, 19287.

5. **Dhara, B.**; Sappati, S.; Singh, S. K.; Kurungot, S.; Ghosh, P.; and Ballav, N. Coordination Polymers of Fe(III) and Al(III) ions with TCA Ligand: Distinctive Fluorescence, CO_2 Uptake, Redox-Activity and Oxygen Evolution Reaction. *Dalton Trans.* **2016,** *45*, 6901.

Other Publications

1. **Dhara, B.**; Tarafder, K.; Jha, P. K.; Panja, S. N.; Nair, S.; Oppeneer, P. M.; and Ballav, N. Possible Room-Temperature Ferromagnetism in Self-Assembled Ensembles of Paramagnetic and Diamagnetic Molecular Semiconductors. *J. Phys. Chem. Lett.* **2016,** *7*, 4988.

2. Rana, S.; Rajendra, R.; **Dhara, B.**; Jha, P. K.; and Ballav, N. Highly Hydrophobic and Chemically Rectifiable Surface-Anchored Metal-Organic Framework Thin-Film Devices. *Adv. Mater. Interfaces* **2016,** *3*, 1500738.

3. Deshmukh, S. C.; Rana, S.; Shinde, S. V.; **Dhara, B.**; and Ballav, N.; Talukdar, P. Selective Sensing of Metal Ions and Nitro Explosives by Efficient Switching of Excimer-to-Monomer Emission of an Amphiphilic Pyrene Derivative. *ACS Omega* **2016,** *1*, 371.

4. Sk, R.; Shirolkar, M. M.; **Dhara, B.**; Kulkarni, S.; and Deshpande, A. Enhancing the Thermopower and Tuning the Resistivity in Bi_2Se_3 with Fe-Doping. *Chem. Phys.Lett.* **2015,** *638*, 94.

5. Jha, P. K.; **Dhara, B.**; and Ballav, N. Nanofibers to Nanocuboids of Polyaniline by Lead Nitrate: Hierarchical Self-assembly with Lead Ions. *RSC Adv.* **2014,** *4*, 9851.

Chapter-I

Introduction of Coordination Polymers

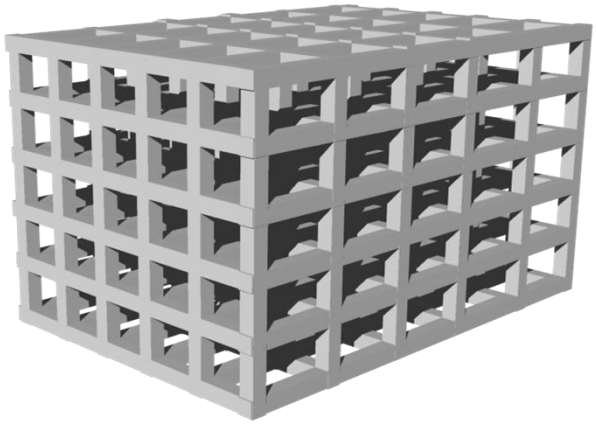

I.1. Introduction

In recent years, coordination polymers (CPs) have emerged as a new class of functional solid-state materials **(Figure 1.1)**. The synergetic reflection of the properties of the metal-ion and organic-ligand, and the void space available within the structure of CPs are the key factors behind such an emergence.[1] A high degree of structural flexibility as well as diversity of CPs offer application promise in the domains of gas storage,[2-15] separation,[16-23] catalysis,[12, 24-33] sensing,[34-40] photoluminescence,[39, 41-43] light-harvesting,[44-47] proton-conductivity (fuel cells),[48-52] energy storage (supercapacitors and batteries),[53-55] electrical conductivity,[56-58] electro-catalysis,[59-61] and magnetism.[10, 62-63] Notably, electrical conductivity, photoluminescence and electro-catalysis of CPs are not explored as extensively as the others leaving an important scope for us to improve, part of which has been undertaken in this thesis work.

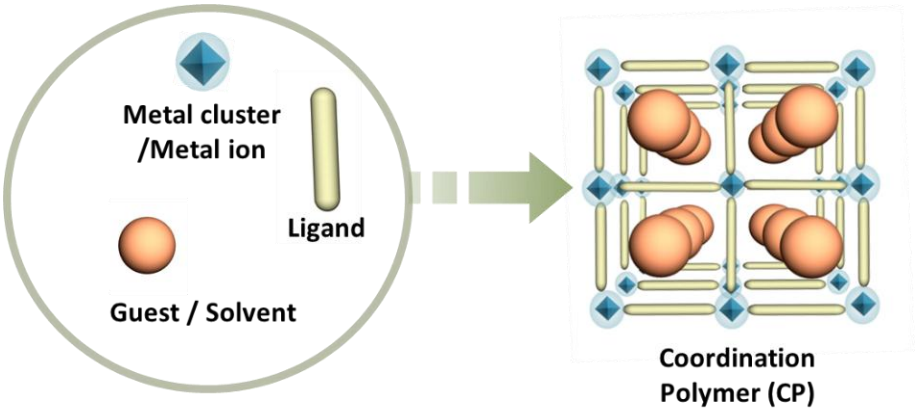

Figure 1.1: *Schematic representation of CP and synthesis.*

I.2. Physicochemical Properties of CPs

I.2.1. Gas Storage

The most attractive characteristic of porous CPs is high-specific surface area. In this context NU-109 and NU-110[64] have the highest surface area ~7000 m^2/g. Other benchmark materials are MOF-177 (~5640 m^2/g), MIL-101 (~5900 m^2/g) and UMCM-2 (~6000 m^2/g).[65-67] Such high-specific surface areas make these materials efficient candidates to capture various gas molecules inside their frameworks **(Figure 1.2)** challenging the conventional gas-adsorbing

materials like zeolites and activated carbon.[68] Also, porous MOFs are being pushed to the frontier of clean energy research, which has been particularly driven by the increasing threat of global warming together with decreasing stockpiles of fossil oil.

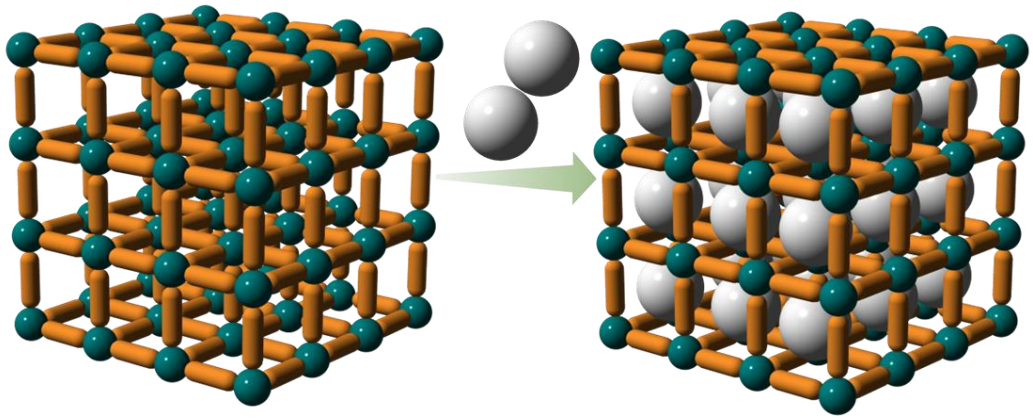

Figure 1.2: *Schematic illustration of gas storage by CP.*

I.2.2. Separation

In industries (mostly chemical, petrochemical and pharmaceutical industries), separation technology is very much important for producing pure compounds, mainly sought-out of monomers. Huge numbers of adsorbents have been explored such as zeolites for separation purpose. In this regard, CPs have gained more interest due to their tailor-made synthesis, customizable pore diameter, adjustable pore functionalization and selective host-guest interaction. Mainly, customize pore diameter and adjustable pore functionalization devoted the CPs for achieving selective gas separation **(Figure 1.3)**. For example, selective O_2 adsorption over N_2 could be precisely accomplished by tuning the pore diameter of the CPs because of the kinetic diameter of N_2 (3.64 Å) is more compared to O_2 (3.46 Å).[69] On the other hand, CO_2 has also been separated from gas mixture by amino functionalization into the pore surface or creating open metal sites in CPs.[70-72] CPs are also potential candidates for separation of solvent from isomeric solvent mixture which is very crucial and challenging task for industrial applications. One of such examples is xylene (mixture of o-xylene/*p*-xylene/*m*-xylene) separation by CPs. Although they have isomeric boiling point,[73-74] pre-functionalized linkers and structural flexibility makes them promising candidate for such selective separation.

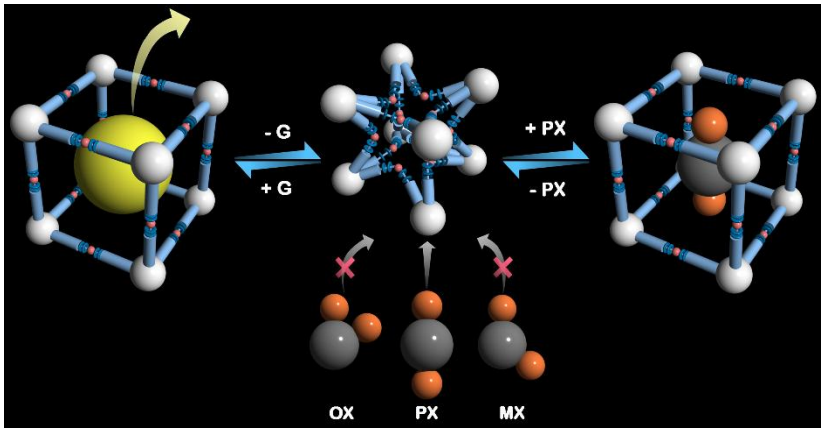

Figure 1.3: *Schematic representation of CP for separation application (adopted from ref. 74 © Nature Publishing Group).*

I.2.3. Catalysis

CPs could provide an important platform in organic catalysis **(Figure 1.4)** by utilizing uniform metal centre as an active catalytic site. There are two types of catalytic reactions namely heterogeneous and homogeneous catalysis. However, both the catalysis reactions have been benefited from the CPs. For example, Fujita *et al.* first time demonstrated catalysis reaction using a cadmium based CP and in their study, they have evident the catalysis of cyanosilylation of aldehyde.[75] Kim *et al.* showed the asymmetric catalysis reaction using a Zn(II) based CP.[76] CP based materials have successfully been investigated in catalysis of other organic reactions including Knoevenagel condensation, Friedel-Crafts alkylation, Aerobic oxidation of olefin and Suzuki-Miyaura coupling.[24]

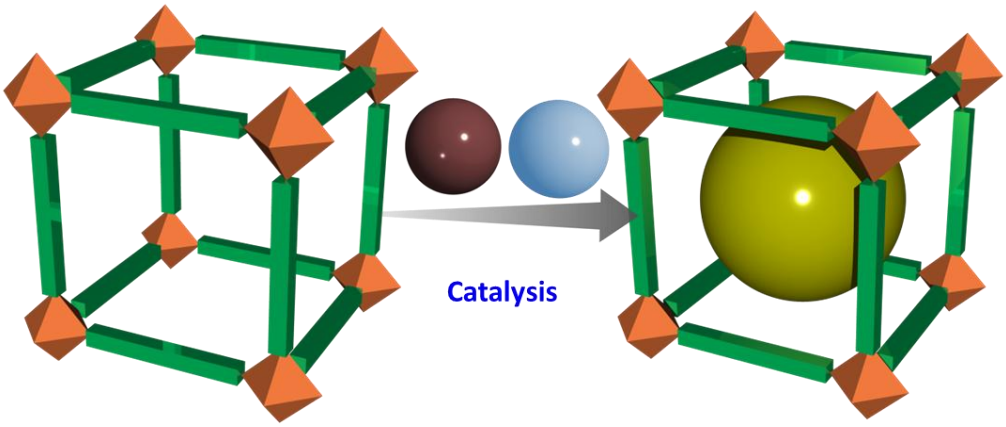

Figure 1.4: *Schematic representation of catalysis reaction performed using CP.*

I.2.4. Sensing

CP based materials are playing vital role in sensing applications[34] such as selective ion (cation/ anion) sensing,[77-78] selective explosive sensing,[35, 79] bio-sensing,[80-81] toxic chemical/ hazardous materials sensing[82-83] and toxic gas sensing[84] **(Figure 1.5)**. Such sensors are needful for several areas including environment cleanness, food industry, healthcare, medical diagnostics, security management and industrial waste management.

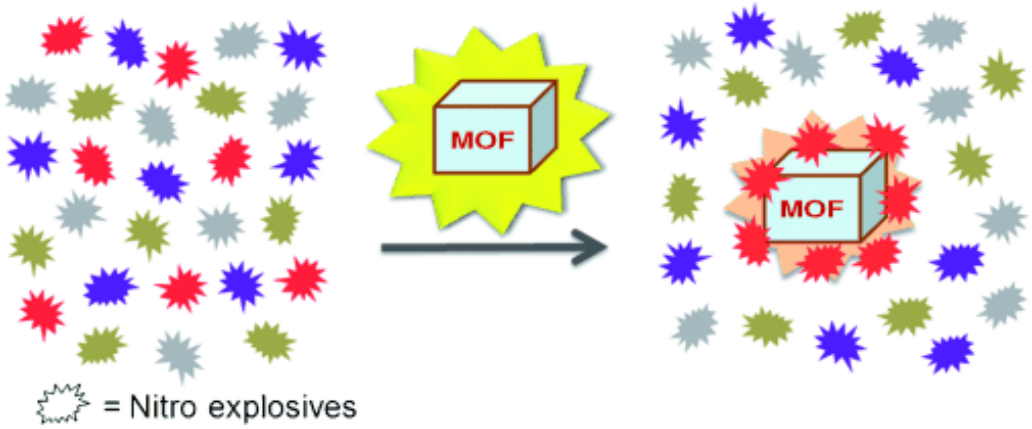

Figure 1.5: *Schematic representation of CP based nitro-sensing in aqueous medium (adopted from ref. 35 © Wiley-VCH).*

I.2.5. Magnetism

One of the fascinating properties of CPs is magnetism. Various nomenclatures of coordination networks have been proposed in the past literatures such as CPs (Coordination Polymers), PCP (Porous Coordination Polymers), MOF (Metal–Organic Framework), IRMOF (Isoreticular Metal–Organic Framework), MOP (Metal–Organic Polyhedra), MOM (Metal-Organic Material), ZIF (Zeolitic Imidazole Framework), PMOF (Porous Metal–Organic Framework), and more.[85-91] However, first time Kurmoo and co-workers came up with a new coordination polymer namely MMOF (Magnetic Metal-Organic Framework).[62] Magnetic coordination polymers are classified in the domain of molecular magnets. By arranging paramagnetic metal or introducing open-shell organic ligand or both, desired magnetic property could be easily achieved in the CPs. Since magnetism is a cooperative phenomenon, which needs exchange interaction between moment carriers, CPs are one of the best candidates due to its customizable/adjustable distance between constituents. Previously, first row transition metal ions based CPs have been heavily explored due to the existence of

their variable oxidation states which would alter paramount parameters such as spin quantum number and magnetic anisotropy. An elegant example is the co-existence of magnetism and conductivity in redox-active one-dimensional Mn-quinoid CP comprised with Mn(II) and 4,5-bis(pyridine-2-carboxamido)-1,2-catechol (redox-active ligand)[92] **(Figure 1.6)**.

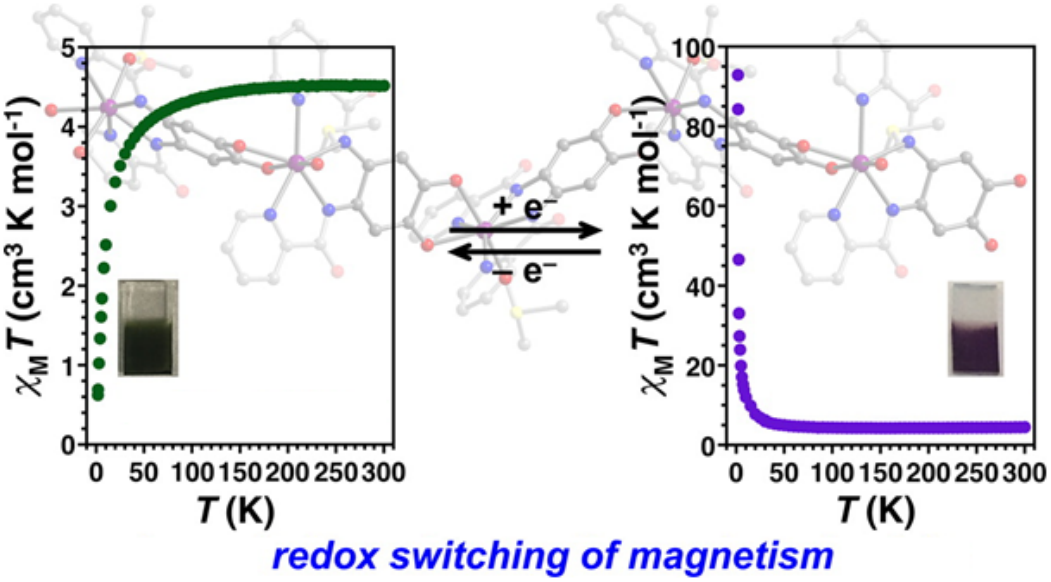

Figure 1.6: *Schematic representation magnetic CP attracted by magnet. (adopted from Ref. 92 © Journal of the American Chemical Society)*

I.2.6. Proton-Conductivity

Various proton-conducting solid state materials are explored in fuel cell applications. Nafion is one of the most widely used proton-conducting membrane. However, Nafion is a fluorinated sulfonic acid based organic polymer material where acid parts are the source of proton and it needs humid condition for conduction of protons. This criterion clearly indicates that it will work only at low-temperatures; and at high-temperatures, it will be inactive. In this context, CPs could be considered as alternative candidates due to long proton-conducting path as well as high thermal stability and could replace Nafion in the near future. It is reported that anionic CPs with protonated amine cations (extra-framework cation), and carrier molecules (such as water) are very effective in conducting proton across the material **(Figure 1.7)**. Also, various cation species such as ammonium, imidazolium, and benzimidazole hosted in CPs are observed to increase the efficiency of proton-conduction.[93]

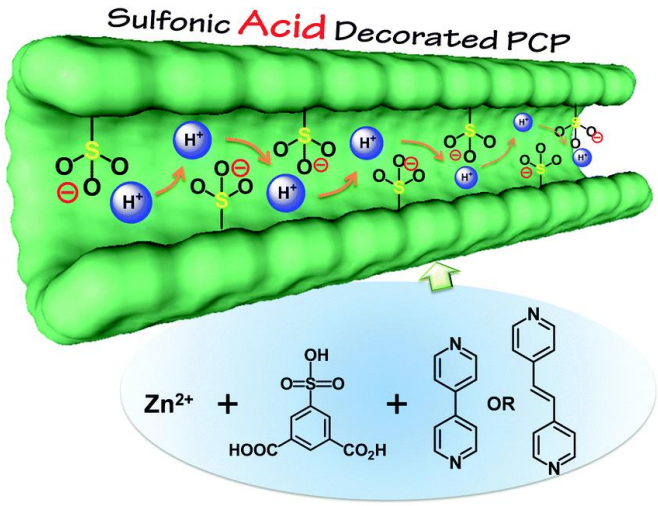

Figure 1.7: *Schematic representation of proton-conduction of CP decorated sulfonic acid in the coordination nanospace (adopted from Ref. 93 © The Royal Society of Chemistry).*

I.2.7. Supercapacitor

The global consumption of energy resources urgently demands high energy storage devices. Batteries and supercapacitors are energy storage devices. Supercapacitor realized to be very promising candidate for energy storage device which can be charged in faster rate and delivers very high power along with extremely long durability. In commercial supercapacitors, carbon analogue such as activated carbon, graphene and carbon nanotubes has been used which falls in the catagory of electrical double layer capacitors (EDLC). However, due to limited capacitance (theoretical) alternatives are required. CPs could also be an appropriate candidate.

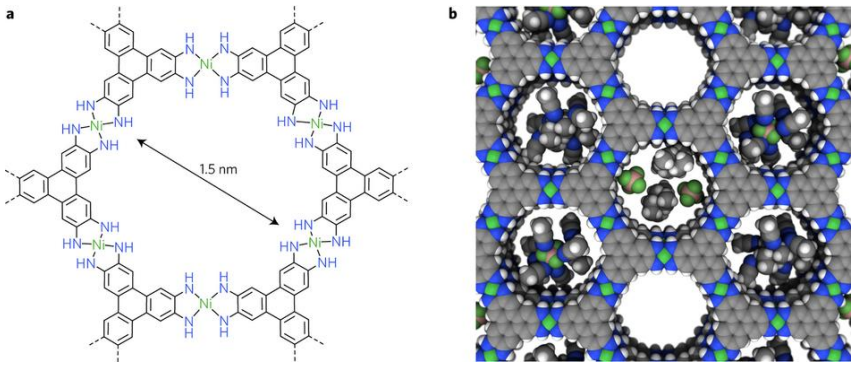

Figure 1.8: *Schematic representation of $Ni_3(HITP)_2$. CP's pores are filled with electrolytes (Et_4N^+ and BF_4^- ions), and acetonitrile solvent (adopted from ref. 94 © Nature Publishing Group).*

Recently, Dincă and co-workers have synthesized a highly conductive CP comprised with Ni(II) and 2,3,6,7,10,11-hexaiminotriphenylene (HITP) **(Figure 1.8)** and showed arial capacitance (18 μF cm^{-2} at 0.05 A g^{-1} discharge rate) with high cyclic stability (~10,000) better than carbon based material[94] as an active material for supercapacitors, because of their high surface areas, controllable pores and nanostructures.

I.2.8. Li-Ion Battery

Lithium-ion batteries (LIBs) are known for the high energy storage device. Generally, carbon based materials such as graphite is used as an anodic material for LIBs which have theoretical capacitance ~372 $mAhg^{-1}$ alongwith excellent cycling stability. However, the capacitance value of graphite is not enough to fulfill the present energy demands. Recently, CPs has been extensively explored and realized to be promising candidate in the field of LIBs. First time, Tarascon and co-workers reported Fe(III) based MIL-53 as a cathodic material, however, the capacitance (75 $mAhg^{-1}$) of the material was very low.[95] Mahanty and co-workers reported Mn-BTC (BTC= 1,3,5-benzenetricarboxylic acid) CP which in fact showed very high capacitance value (694 $mAhg^{-1}$).[96] Very recently, Wang and co-workers prepared a Cu(II) based CP with redox-active tricarboxytriphenyl amine ligand (TCA) with very high cycling stability[97] **(Figure 1.9)**.

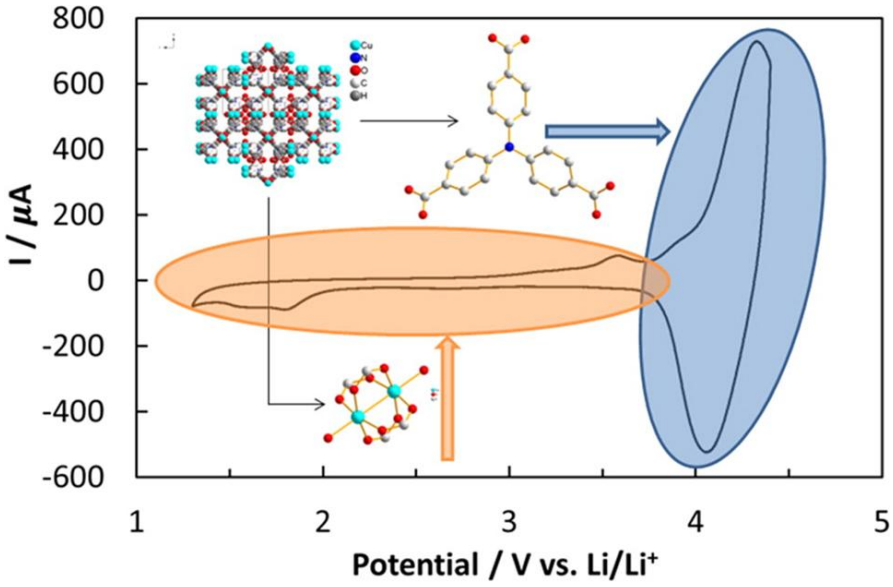

Figure 1.9: *Cu-TCA CP used as cathode material in Li-ion battery (adopted from ref. 97 © American Chemical Society).*

I.2.9. Electro-Catalysis

For any reaction, energy is required to cross the barrier and convert reactants into products.[98] In presence of catalytic material, it follows the alternative pathway and reduces the activation energy. As a result, rate of the reaction becomes faster. Likewise, chemical catalysis reaction, rate of electro-catalysis reaction also depends on the reactant/product concentration, reaction pressure and temperature. The catalytic performance of an electro-catalyst material is depending on the geometry, conductivity, oxidation state of catalytic centre and more. Various electro-catalytic reactions have been investigated in the forms of oxygen evolution reaction (OER), oxygen reduction reaction (ORR), methanol oxidation, CO_2 reduction, hydrogen evolution reaction (HER), and water-splitting. [99-101] For any electro-catalysis reaction, catalytic performance of material is defined from Tafel equation.

$$\eta = a + b\ log(J)$$

Where η is overpotential, the potential difference between thermodynamic potential (E_e) and working potential (E).

$$\eta = (E - E_e)$$

$a = -2.3(RT/\ \alpha F)log(J_0)$; b (Tafel slope)$= 2.3(RT/\ \alpha F)$; J= current density; J_0= exchange current density; α= Charge transfer coefficient that signifies the charge movement.

α is directly proportional to the charge transfer rate and inversely proportional to Tafel slope. Tafel slope can be easily calculated experimentally and lower the value better electro-catalytic performance.

From Nernst equation, the equilibrium potential (E_e) can be calculated by the following equation.

$$E_e = E^0 + \frac{RT}{nF} ln\left(\frac{[O]}{[R]}\right)$$

Where E^0 is the standard reduction potential; R and F are the ideal gas constant and Faraday constant respectively; n is the number of electron participated in redox reaction; *[O]* and *[R]* are the concentration of oxidised and reduced material respectively.

Oxygen Evolution Reaction

Oxygen evolution reaction (OER) is the half-cell reaction (anodic reaction) of water-splitting reaction. Various research groups have proposed possible mechanisms of OER. This mechanism also alters with changing the medium such as acidic, basic or neutral.[102-103] However, most of the mechanism follows the similar intermediate states. The probable mechanisms are described below

$2H_2O \rightarrow 2H_2 + O_2$

Acidic Medium

Cathode reaction: $4H^+ + 4e^- \rightarrow 2H_2$ $E^0 = 0$ V

Anode reaction: $2H_2O\ (l) \rightarrow O_2\ (g) + 4H^+ + 4e^-$ $E^0 = 1.23$ V

Probable reaction mechanism under acidic condition

$M + H_2O\ (l) \rightarrow MOH + H^+ + e^-$

$MOH + OH^- \rightarrow MO + H_2O\ (l) + e^-$

$2MO \rightarrow 2M + O_2\ (g)$

$MO + H_2O\ (l) \rightarrow MOOH + H^+ + e^-$

$MOOH + H_2O\ (l) \rightarrow M + O_2\ (g) + H^+ + e^-$

Alkaline Medium

Cathode reaction: $4H_2O\ (l) + 4e^- \rightarrow 2H_2 + 4OH^-$ $E^0 = 0.83$ V

Anode reaction: $4OH^- \rightarrow 2H_2 + 2H_2O\ (l) + 4e^-$ $E^0 = 0.40$ V

Proposed reaction mechanism under alkaline condition

$M + OH^- \rightarrow MOH$

$MOH + OH^- \rightarrow MO^- + H_2O\ (l)$

$2MO \rightarrow 2M + O_2\ (g)$

$MO + OH^- \rightarrow MOOH + e^-$

$MOOH + OH^- \rightarrow M + O_2\,(g) + H_2O\ (l)$

In current scenario, most commonly explored OER catalysts **(Figure 1.10)** are RuO_2 and IrO_2, considered as benchmark electrocatalysts[104] for OER due to their high stability in both acidic as well as alkaline solution. Unfortunately, Ir and Ru are rare elements which limit their usages. Alternatively, other metal oxides such as transition metal oxides are explored for the OER propose because they are very cheap and highly abundunt in nature. In present days, CPs are being considered as potential candidates for electro-catalysis[105] purpose due to its accessible void space which are further mutable by changing frameworks' parts. Their electrical conductivity can be modulated; also CPs could be pretty stable in both acidic and basic media **(Figure 1.10)**.

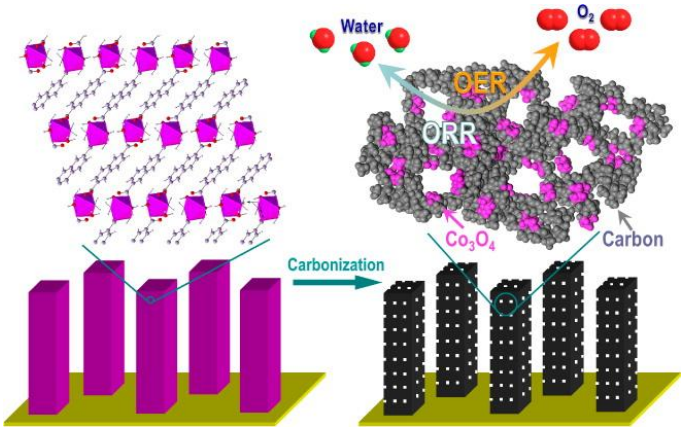

Figure 1.10: *Schematic representation of Co-NDC (NDC- 2,6-napthalenedicarboxylic acid) and utilized as OER active material after carbonization (adopted from ref. 105 © American Chemical Society).*

I.2.10. Photoluminescence Property

Photoluminescence (PL) is a physical phenomenon where a material absorb light followed by emission of energy in the form of light at different wavelengths. In general, PL has two basic forms: a) fluorescence and b) phosphorescence. In fluorescence, electronic transition occurs from singlet state to singlet state and decay time is less than 10 ns. However, in case of phosphorescence, the spin multiplicity of excited state and the ground state is different and the decay time is much more (micro to sec.). Recently, immense research effort has been

devoted for explaining the origin of PL property of CPs. Various parameters are associated for generation of PL property **(Figure 1.11)** in CPs: a) linker-based, b) metal-based, c) charge-transfer, and d) guest-induced.[41, 106-110]

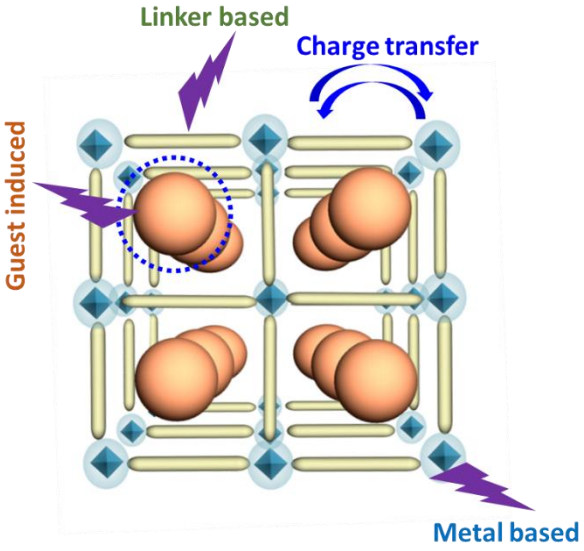

Figure 1.11: *Schematic representation of possible origin of photoluminescence from CP.*

I.2.10a. Linker-Based PL

Ligands directly coordinates with redox-inactive metal ions [Zn(II), Cd(II), Al(III), and In(III)]. For example, various isostructural Zn(II) based CPs have been prepared with various luminescent ligands such as stilbene dicarboxylic acid (1), 4,5,9,10-tetrahydropyrene 2,7-dicarboxylic acid (2), and 2,7- pyrene dicarboxylic acid (3) for tuning their emission region **(Figure 1.12)**.[111-113] Emission regions are changing due to presence of different π-conjugation of the ligands.

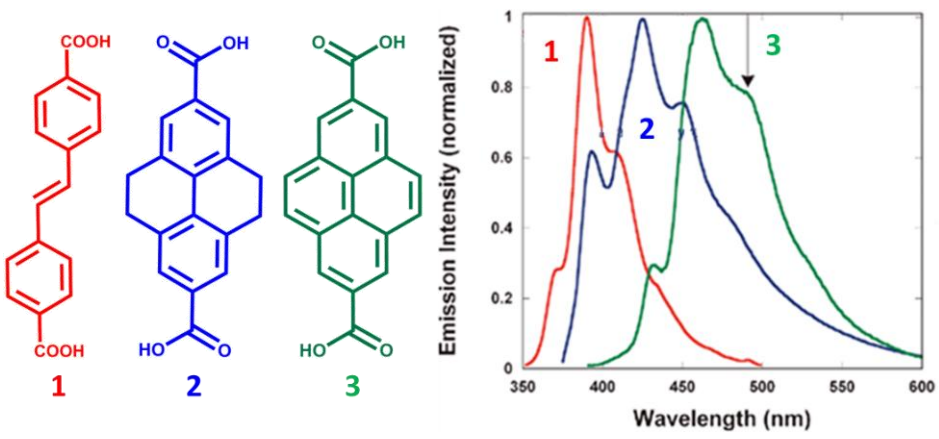

Figure 1.12: *Schematic representation of PL ligands and emission spectra of Zn(II) based CP with these ligands.(adopted from ref. 113 © Royal Society of Chemistry).*

I.2.10b. Metal-Based PL

CPs with non-luminescent linkers can also exhibit its luminescence property if the metal centres are photoluminescent. Most of the d-block metal ions except Zn(II) and Cd(II) can effectively quench the PL property, even though ligands are photoluminescent. Due to the existence of f-f transition, lanthanide based CPs have showed excellent PL property. Serre *et al.* reported MIL-78 composed with 1,3,5-benzenetricarboxylic acid (BTC) and ytterbium (Yb) **(Figure 1.13)**.[114] Also, emissions of CPs were tuned by doping with Eu (in red region), Tb (in green region), and Dy (in blue region) metal ions.

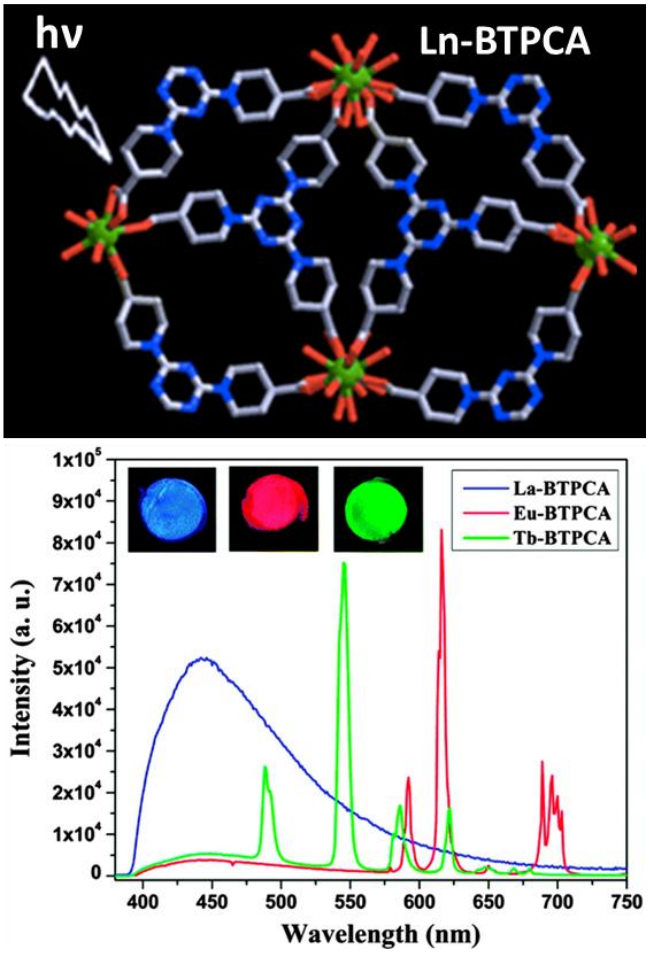

Figure 1.13: *Schematic representation of Yb based CP and photoluminescence spectra of doped CP with Eu (pink), La (blue), and Tb (green) (adopted from ref. 114 © Royal Society of Chemistry and http://pubs.rsc.org/en/content/articlehtml/2014/cc/c4cc00848k).*

I.2.10c. Charge-Transfer-Based Luminescence

Two types of charge-transfer-based luminescent namely, LMCT (ligand to metal charge transfer) and MLCT (metal to ligand charge transfer) are possible and it depends on the relative position of the energy states of both ligand and metal ions. MLCT is mainly observed in Cu(I) and Ag(I) which are d^{10} systems. These electrons are behaving as valence electrons and are responsible for MLCT pathway.

I.2.10d. Guest-Induced Luminescence

One way to make luminescent CP from a non-luminescent CP is to host appropriate luminescent guest molecules into the accessible pores. PL property of CP could be tuned by infiltration with suitable guest molecules. Kitagawa and co-workers have synthesised a Zn(II) based CP ($[Zn_2(bdc)_2(dpNDI)]_n$; bdc= 1,4-benzenedicarboxylic acid, dpNDI= *N*,*N*′-di(4-pyridyl)-1,4,5,8-naphthalenediimide) and examined the PL property by incorporating both electron rich as well as electron deficient guest molecules **(Figure 1.14)**.[110] They have found tunability of emission region over a long visible range (blue to red).

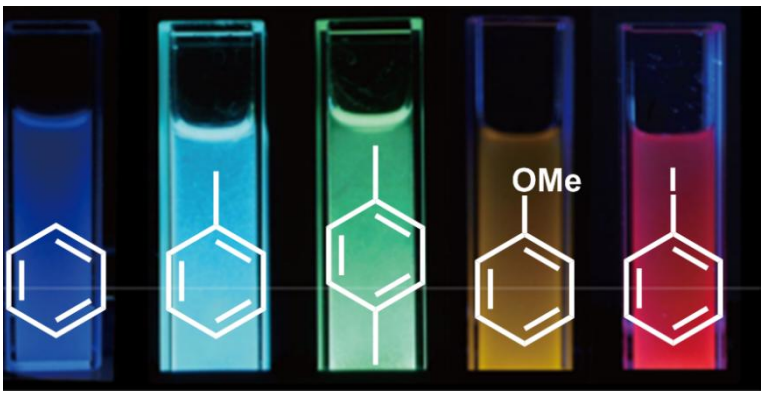

Figure 1.14: *PL property of CP incorporating various guests (adopted from ref. 110 © Nature Publishing Group).*

I.2.11. Electrical Conductivity

Usually, CPs are poor conductors of electricity[115] which limits their promise in various electronic applications such as resistive-sensors and field-effect transistors. Reason behind such poor conductivity of CPs is due to the ineffective overlap between metal ion and organic insulating ligand. Most importantly, CPs are constructed through non-covalent bonding between inorganic struts (metal ions) and organic linkers (ligands) and generate huge void

space. An important question is – how to enhance/modulate electrical conductivity in CPs? Two paramount ways have been proposed to achieve reasonable electrical conductivity in CPs: *intrinsic approach (through bond)* and *extrinsic approach (through space).*

I.2.11a. Intrinsic Approach

In this approach electrical conductivity can be modulated by changing the metal ion(s) and/or organic ligand(s). In former case, by alteration of metal ion(s) from platinum (Pt) to copper (Cu) via nickel (Ni) keeping the organic ligand (bezenehexathiol=BHT) unchanged, the electrical conductivity values varied from ~10^{-6} to ~10^{-4} to ~10^{3} S/cm, respectively. [116-117] Another interesting example was reported by Dincă and co-workers where two isostructural coordination polymers, composed of same ligand DOBDC (2,5-dioxido-1,4-benzenedicarboxylate), however changing the metal ion from Fe(II) to Mn(II), a million-fold increase in the electrical conductivity value was observed[118] **(Figure 1.15)**. In the latter case, by varying the ligand and keeping the metal ions fixed, modulation of conductivity was also achieved. For an example, ~10 times enhancement in conductivity in isostructural CPs of Fe(II) ion was achieved by simply changing the ligand from DOBDC to DSBDC (2,5-disulfhydrylbenzene-1,4-dicarboxylic acid). Theoretically, in Fe_2(DSBDC), overlap between Fe and O is found to be very weak whereas in Fe_2(DSBDC), Fe and S bond is found to be relatively stronger and charge transport can easily take place through (-Fe-S-)$_\infty$ chains. In this way energy barrier for charge hopping becomes lower and increases the conductivity.

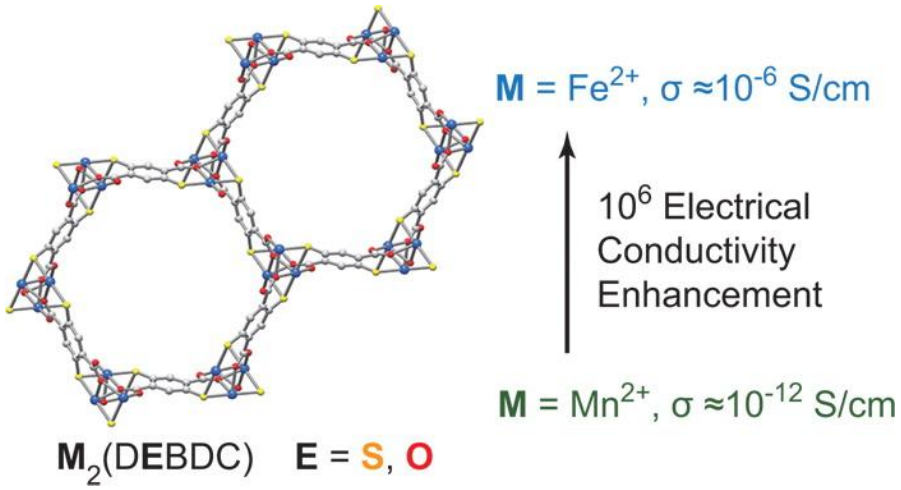

Figure 1.15: *Single crystal structures of various MOF-74 series (adopted from ref. 118 © American Chemical Society:* http://pubs.acs.org/doi/full/10.1021/jacs.5b02897*).*

I.2.11b. Extrinsic Approach

In this strategy, void space has been occupied with suitable guests and hence electrical conductivity is enhanced. Notably, small molecules as well as big molecules could execute the purpose. For example, Talin *et al.* have demonstrated an elegant approach for enhancing the electrical conductivity of CPs by introducing big molecule.[115] They synthesised a CP HKUST-1 and soaked in saturated 7,7,8,8-tetracyanoquinodimethane (TCNQ) solution **(Figure 1.16)**. As a result, they have achieved enhancement in electrical conductivity almost six orders of magnitude. Moreover, electrical conductivity of the material was tuned in that range by controlling the soaking time in TCNQ solution. After activation of HKUST-1, open metal sites of Cu are created and TCNQ molecules easily coordinated to these sites and a new pathway has been created for charge transport enhancing electrical conductivity. Another reason is the appropriate matching of redox potential and their effective orbital overlap between host and the guest molecules. From the theoretical calculation, TCNQ infiltration into HKUST-1 has been observed to lower the activation energy.

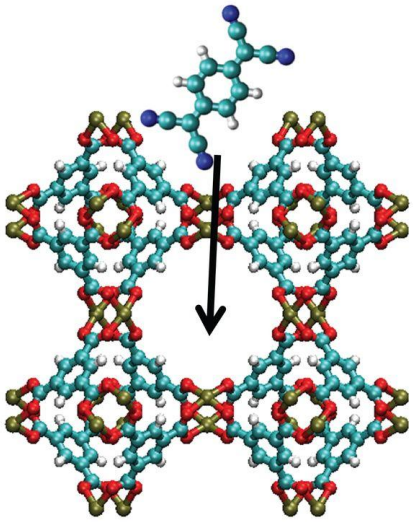

Figure 1.16: *Schematic representation of HKUST-1 filled with TCNQ molecules (adopted from ref. 115 © AAAS).*

I.2.12. Conventional Electrical Conductivity Measurement Techniques

From Ohm's law, $V=IR$; where V= voltage, I= current and R= constant which is called resistance. R depends on the geometry of the sample and it is defined as $R= \rho (l/A)$ where l= length of sample and A= cross-sectional area. ρ is the resistivity of the sample and it is

intrinsic property. It is measured in Ω cm unit. Reciprocal of resistivity is called conductivity (σ) and its unit is Ω^{-1} cm^{-1} or S cm^{-1}.

All the conducting materials do not follow the Ohm's law. Mostly, semiconductors deviate from this law except at low current range. Therefore, current and voltage range has to specify for any electrical measurement. Furthermore, electrical conductivities or resistivities are also dependent on temperature. Different methods have been proposed to measure electrical conductivity and Dincă and co-workers emphasized the importance of different measurement techniques on reporting the conductivity values of CPs.

I.2.12a. Four Contact Method

In this method four parallel line contacts are used. Current has been applied in two external contacts and subsequently voltage measurement has been measured in two internal contacts **(Figure 1.17)**. Contacts are made with very thin metallic wires such as Cu, Au, Ag etc. Here cross-sectional area of the sample $A = a \times d$ where, a and d are the length depth of cross-section respectively. Distance between two internal wires is l. Therefore, resistivity of the sample $\rho = R \times (a \times d/l)$.

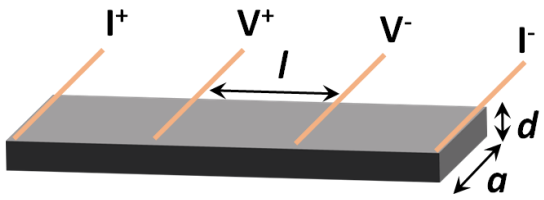

Figure 1.17: *Schematic representation four contact method for I-V measurement.*

I.2.12b. Two Contact Method

In this method, two contacts are used to measure the conductivity of a sample. One of the contacts is used to measure the voltage and other one is used to apply current **(Figure 1.18)**. In this method, conductivity of a very small sample can be measured. However, this method is useful for highly conductive samples. Resistivity of the samples has been measured by applying the equation;

$\rho = R \times (a \times d/l)$

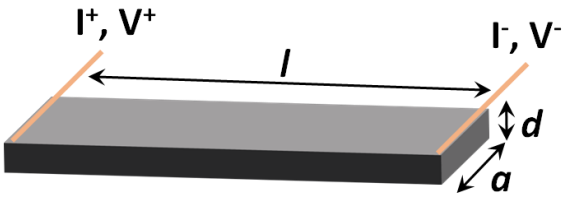

Figure 1.18: Schematic representation of two contact method for *I-V* measurement.

I.2.12c. Four-Probe Method

This is more appropriate method compared to four contact and two contact method **(Figure 1.19)**. Four points are involved in a line for measuring voltage and applying current likewise four contact method. The distance between any two adjacent points is same and the equation used to get resistivity is $\rho = 2 \times \pi \times l \times (V/I)$.

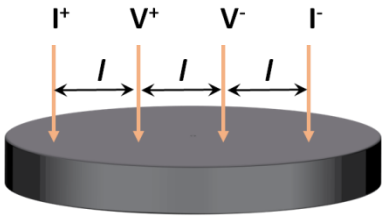

Figure 1.19: *Schematic representation of four probe method for I-V measurement.*

I.2.12d. Van der Pauw Method

In van der Pauw method[119] four contacts are placed in the periphery of the thin samples **(Figure 1.20)**. Thickness of the sample is very small. Resistance due to the contacts can be easily eliminated using this method. The formula to calculate resistivity is $\rho = \frac{\pi d}{ln2} \times \frac{R_a + R_b}{2} f(R_a/R_b)$ where, R_a is the resistances measured along one of the sides of the square and R_b is the resistance measured along the other side (orthogonal).

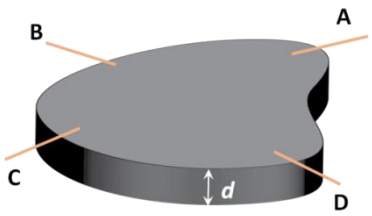

Figure 1.20: *Schematic representation of Van der Pauw method for I-V measurement.*

I.13. Brief Introduction to Conducting Polymers

In 1977, Alan J. Heeger, Alan G MacDiarmid, Hideki Shirakawa have presented remarkable conducting property of various organic polymers and changed the conventional thought about organic polymers.[120-121] Some of conducting polymers are polyphenylene, polyacetylene, polypyrrole, polythiophene and polyaniline and these conducting materials are being explored in the development of sensors, organic photovoltaics, transistors, anticorrosive coatings, batteries, supercapacitor and functional electrodes.[122-123]

These conducting polymers are easily synthesized in gram scale at reasonable cost which make more suitable for device applications. Synthesis procedure **(Figure 1.21)** for preparing conducting polymers is very simple and productive root. Monomers (aniline, pyrrole, thiophene etc) are chemically oxidized employing proper oxidizing agents or catalyst (such as ammonium persulphate and ferric chloride) to produce respective polymers.[124]

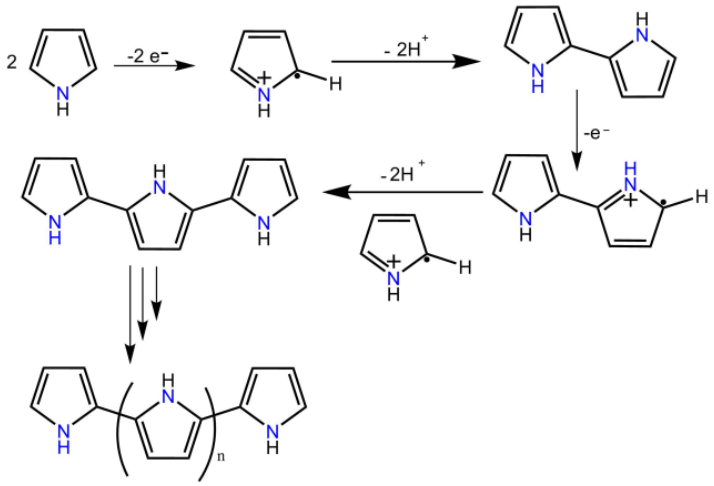

Figure 1.21: *Oxidative polymerization of Py monomers and a schematic representation of PPy.*

Conducting polymers have delocalised π-electron and their band structure configure with π-valence band and π*-conduction band. Upon doping, characteristic polaron/bipolaron bands appear in the forbidden gap, likewise donor/acceptor impurity bands in doped semiconductors, bringing the electrical conduction in conducting polymers[125] **(Figure 1.22)**. Though porous CPs have been successfully utilized as porous templates for the confined-space polymerization of various vinyl monomers (styrene, n-vinylcarbazole, methyl methacrylate, acrylonitrile). Recently, attempts are being made to incorporate conducting

polymer moieties within the pores and/or matrix of CPs which could significantly modulate the electrical conductivity in the resulted composite materials.

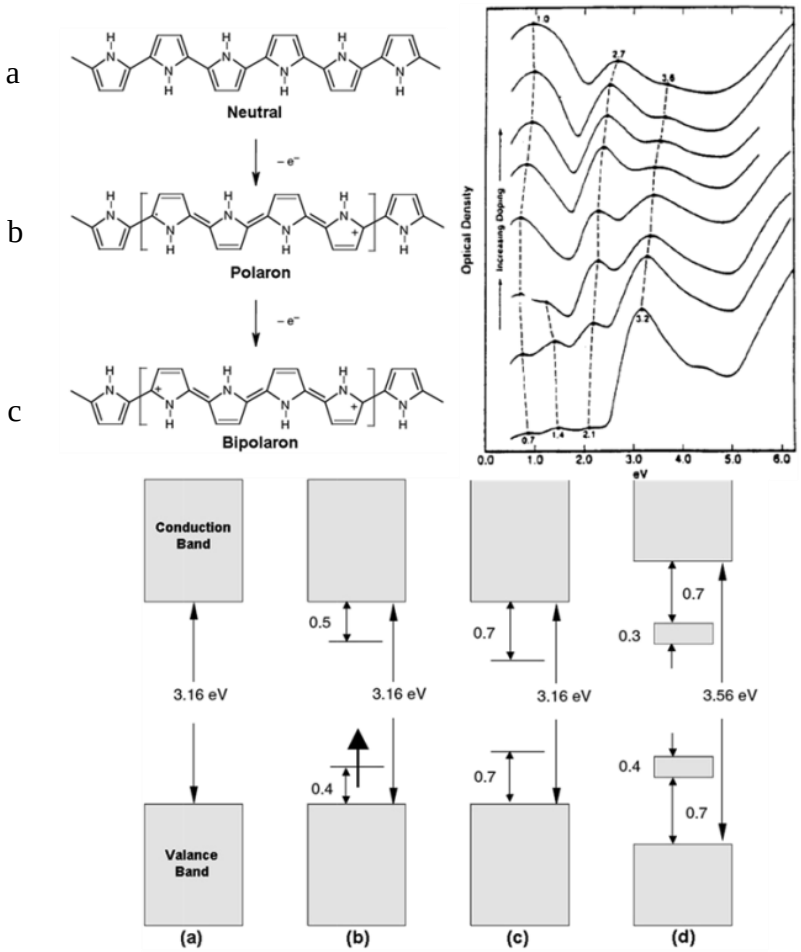

Figure 1.22: *Schematic diagram of neutral, polaron and bipolaron form of PPy.* UV-absorption spectra of PPy doped with dopant. Energy *diagrams for (a) neutral PPy, (b) polaron, (c) bipolaron, and (d) fully doped PPy (adopted from ref. 125 © 1983 AIP Publishing)*

References

1. Batten, S. R.; Champness, N. R.; Chen, X.-M.; Garcia-Martinez, J.; Kitagawa, S.; Ohrstrom, L.; O'Keeffe, M.; Suh, M. P.; Reedijk, J. Coordination polymers, metal-organic frameworks and the need for terminology guidelines. *CrystEngComm* **2012,** *14*, 3001.

2. Li, H.; Eddaoudi, M.; O'Keeffe, M.; Yaghi, O. M. Design and synthesis of an exceptionally stable and highly porous metal-organic framework. *Nature* **1999,** *402*, 276.

3. Rosi, N. L.; Eckert, J.; Eddaoudi, M.; Vodak, D. T.; Kim, J.; O'Keeffe, M.; Yaghi, O. M. Hydrogen Storage in Microporous Metal-Organic Frameworks. *Science* **2003,** *300*, 1127.

4. Millward, A. R.; Yaghi, O. M. Metal−Organic Frameworks with Exceptionally High Capacity for Storage of Carbon Dioxide at Room Temperature. *J. Am. Chem. Soc.* **2005,** *127*, 17998.

5. Rowsell, J. L. C.; Yaghi, O. M. Strategies for Hydrogen Storage in Metal–Organic Frameworks. *Angew. Chem., Int. Ed.* **2005,** *44*, 4670.

6. Ma, S.; Zhou, H.-C. Gas storage in porous metal-organic frameworks for clean energy applications. *Chem. Commun.* **2010,** *46*, 44.

7. Peng, Y.; Krungleviciute, V.; Eryazici, I.; Hupp, J. T.; Farha, O. K.; Yildirim, T. Methane Storage in Metal–Organic Frameworks: Current Records, Surprise Findings, and Challenges. *J. Am. Chem. Soc.* **2013,** *135*, 11887.

8. He, Y.; Zhou, W.; Qian, G.; Chen, B. Methane storage in metal-organic frameworks. *Chem. Soc. Rev.* **2014,** *43*, 5657.

9. Jayaramulu, K.; Datta, K. K. R.; Shiva, K.; Bhattacharyya, A. J.; Eswaramoorthy, M.; Maji, T. K. Controlled synthesis of tunable nanoporous carbons for gas storage and supercapacitor application. *Microporous Mesoporous Mater.,* **2015,** *206*, 127.

10. Roy, S.; Chakraborty, A.; Maji, T. K. Lanthanide–organic frameworks for gas storage and as magneto-luminescent materials. *Coord. Chem. Rev.* **2014,** *273–274*, 139.

11. Haldar, R.; Prasad, K.; Samanta, P. K.; Pati, S.; Maji, T. K. Luminescent Metal–Organic Complexes of Pyrene or Anthracene Chromophores: Energy Transfer Assisted Amplified Exciplex Emission and Al3+ Sensing. *Cryst. Growth Des.* **2016,** *16*, 82.

12. Li, B.; Chrzanowski, M.; Zhang, Y.; Ma, S. Applications of metal-organic frameworks featuring multi-functional sites. *Coord. Chem. Rev.* **2016,** *307, Part 2,* 106.

13. Samai, S.; Biradha, K. Chemical and Mechano Responsive Metal–Organic Gels of Bis(benzimidazole)-Based Ligands with Cd(II) and Cu(II) Halide Salts: Self Sustainability and Gas and Dye Sorptions. *Chem Mater.* **2012,** *24*, 1165.

14. Dey, A.; Mandal, S. K.; Biradha, K. Metal-organic gels and coordination networks of pyridine-3,5-bis(1-methyl-benzimidazole-2-yl) and metal halides: self sustainability, mechano, chemical responsiveness and gas and dye sorptions. *CrystEngComm* **2013,** *15*, 9769.

15. Liu, J.; Thallapally, P. K.; McGrail, B. P.; Brown, D. R.; Liu, J. Progress in adsorption-based CO_2 capture by metal-organic frameworks. *Chem. Soc. Rev.* **2012,** *41*, 2308.

16. Qiu, S.; Xue, M.; Zhu, G. Metal-organic framework membranes: from synthesis to separation application. *Chem. Soc. Rev.* **2014,** *43*, 6116.

17. Nugent, P.; Belmabkhout, Y.; Burd, S. D.; Cairns, A. J.; Luebke, R.; Forrest, K.; Pham, T.; Ma, S.; Space, B.; Wojtas, L.; Eddaoudi, M.; Zaworotko, M. J. Porous materials with optimal adsorption thermodynamics and kinetics for CO_2 separation. *Nature* **2013,** *495*, 80.

18. Li, J.-R.; Sculley, J.; Zhou, H.-C. Metal–Organic Frameworks for Separations. *Chem. Rev.* **2012,** *112*, 869.

19. Li, J.-R.; Kuppler, R. J.; Zhou, H.-C. Selective gas adsorption and separation in metal-organic frameworks. *Chem. Soc. Rev.* **2009,** *38*, 1477.

20. Huang, A.; Chen, Y.; Wang, N.; Hu, Z.; Jiang, J.; Caro, J. A highly permeable and selective zeolitic imidazolate framework ZIF-95 membrane for H_2/CO_2 separation. *Chem. Commun.* **2012,** *48*, 10981.

21. Herm, Z. R.; Wiers, B. M.; Mason, J. A.; van Baten, J. M.; Hudson, M. R.; Zajdel, P.; Brown, C. M.; Masciocchi, N.; Krishna, R.; Long, J. R. Separation of Hexane Isomers in a Metal-Organic Framework with Triangular Channels. *Science* **2013,** *340*, 960.

22. Biswal, B. P.; Bhaskar, A.; Banerjee, R.; Kharul, U. K. Selective interfacial synthesis of metal-organic frameworks on a polybenzimidazole hollow fiber membrane for gas separation. *Nanoscale* **2015,** *7*, 7291.

23. Thallapally, P. K.; Tian, J.; Radha Kishan, M.; Fernandez, C. A.; Dalgarno, S. J.; McGrail, P. B.; Warren, J. E.; Atwood, J. L. Flexible (Breathing) Interpenetrated Metal−Organic Frameworks for CO_2 Separation Applications. *J. Am. Chem. Soc.* **2008,** *130*, 16842.

24. Lee, J.; Farha, O. K.; Roberts, J.; Scheidt, K. A.; Nguyen, S. T.; Hupp, J. T. Metal-organic framework materials as catalysts. *Chem. Soc. Rev.* **2009,** *38*, 1450.

25. Liu, J.; Chen, L.; Cui, H.; Zhang, J.; Zhang, L.; Su, C.-Y. Applications of metal-organic frameworks in heterogeneous supramolecular catalysis. *Chem. Soc. Rev.* **2014,** *43*, 6011.

26. Corma, A.; García, H.; Llabrés i Xamena, F. X. Engineering Metal Organic Frameworks for Heterogeneous Catalysis. *Chem. Rev.* **2010,** *110*, 4606.

27. Yoon, M.; Srirambalaji, R.; Kim, K. Homochiral Metal–Organic Frameworks for Asymmetric Heterogeneous Catalysis. *Chem. Rev.* **2012,** *112*, 1196.

28. Mueller, U.; Schubert, M.; Teich, F.; Puetter, H.; Schierle-Arndt, K.; Pastre, J. Metal-organic frameworks-prospective industrial applications. *J. Mater. Chem.* **2006,** *16*, 626.

29. Wu, C.-D.; Lin, W. Heterogeneous Asymmetric Catalysis with Homochiral Metal–Organic Frameworks: Network-Structure-Dependent Catalytic Activity. *Angew. Chem., Int. Ed.* **2007,** *46*, 1075.

30. Dybtsev, D. N.; Nuzhdin, A. L.; Chun, H.; Bryliakov, K. P.; Talsi, E. P.; Fedin, V. P.; Kim, K. A Homochiral Metal–Organic Material with Permanent Porosity, Enantioselective Sorption Properties, and Catalytic Activity. *Angew. Chem., Int. Ed.* **2006,** *45*, 916.

31. Gao, W.-Y.; Wu, H.; Leng, K.; Sun, Y.; Ma, S. Inserting CO_2 into Aryl C−H Bonds of Metal–Organic Frameworks: CO_2 Utilization for Direct Heterogeneous C−H Activation. *Angew. Chem., Int. Ed.* **2016,** *55*, 5472.

32. Li, B.; Leng, K.; Zhang, Y.; Dynes, J. J.; Wang, J.; Hu, Y.; Ma, D.; Shi, Z.; Zhu, L.; Zhang, D.; Sun, Y.; Chrzanowski, M.; Ma, S. Metal–Organic Framework Based upon the Synergy of a Brønsted Acid Framework and Lewis Acid Centers as a Highly Efficient Heterogeneous Catalyst for Fixed-Bed Reactions. *J. Am. Chem. Soc.* **2015,** *137*, 4243.

33. Gole, B.; Bar, A. K.; Mallick, A.; Banerjee, R.; Mukherjee, P. S. An electron rich porous extended framework as a heterogeneous catalyst for Diels-Alder reactions. *Chem. Commun.* **2013,** *49*, 7439.

34. Kreno, L. E.; Leong, K.; Farha, O. K.; Allendorf, M.; Van Duyne, R. P.; Hupp, J. T. Metal–Organic Framework Materials as Chemical Sensors. *Chem. Rev.* **2012,** *112*, 1105.

35. Nagarkar, S. S.; Joarder, B.; Chaudhari, A. K.; Mukherjee, S.; Ghosh, S. K. Highly Selective Detection of Nitro Explosives by a Luminescent Metal–Organic Framework. *Angew. Chem., Int. Ed.* **2013,** *52*, 2881.

36. Chen, B.; Wang, L.; Xiao, Y.; Fronczek, F. R.; Xue, M.; Cui, Y.; Qian, G. A Luminescent Metal–Organic Framework with Lewis Basic Pyridyl Sites for the Sensing of Metal Ions. *Angew. Chem., Int. Ed.* **2009,** *48*, 500.

37. Chen, B.; Xiang, S.; Qian, G. Metal−Organic Frameworks with Functional Pores for Recognition of Small Molecules. *Acc. Chem. Res.* **2010,** *43*, 1115.

38. Lu, G.; Hupp, J. T. Metal−Organic Frameworks as Sensors: A ZIF-8 Based Fabry−Pérot Device as a Selective Sensor for Chemical Vapors and Gases. *J. Am. Chem. Soc.* **2010,** *132*, 7832.

39. Sutar, P.; Maji, T. K. Coordination polymer gels: soft metal-organic supramolecular materials and versatile applications. *Chem. Commun.* **2016,** *52*, 8055.

40. Roy, S.; Katiyar, A. K.; Mondal, S. P.; Ray, S. K.; Biradha, K. Multifunctional White-Light-Emitting Metal–Organic Gels with a Sensing Ability of Nitrobenzene. *ACS Appl. Mater. Interfaces* **2014,** *6*, 11493.

41. Cui, Y.; Yue, Y.; Qian, G.; Chen, B. Luminescent Functional Metal–Organic Frameworks. *Chem. Rev.* **2012,** *112*, 1126.

42. Kundu, T.; Mitra, S.; Díaz Díaz, D.; Banerjee, R. Gadolinium(III)-Based Porous Luminescent Metal–Organic Frameworks for Bimodal Imaging. *ChemPlusChem* **2016,** *81*, 728.

43. Banerjee, K.; Biradha, K. Two-dimensional coordination polymers and metal-organic gels of symmetrical and unsymmetrical dipyridyl [small beta]-diketones: luminescence, dye absorption and mechanical properties. *New J. Chem.* **2016,** *40*, 1997.

44. Quah, H. S.; Chen, W.; Schreyer, M. K.; Yang, H.; Wong, M. W.; Ji, W.; Vittal, J. J. Multiphoton harvesting metal–organic frameworks. *Nat. Commun.* **2015,** *6*, 7954.

45. Wang, J.-L.; Wang, C.; Lin, W. Metal–Organic Frameworks for Light Harvesting and Photocatalysis. *ACS Catal.* **2012,** *2*, 2630.

46. Lee, C. Y.; Farha, O. K.; Hong, B. J.; Sarjeant, A. A.; Nguyen, S. T.; Hupp, J. T. Light-Harvesting Metal–Organic Frameworks (MOFs): Efficient Strut-to-Strut Energy Transfer in Bodipy and Porphyrin-Based MOFs. *J. Am. Chem. Soc.* **2011,** *133*, 15858.

47. So, M. C.; Wiederrecht, G. P.; Mondloch, J. E.; Hupp, J. T.; Farha, O. K. Metal-organic framework materials for light-harvesting and energy transfer. *Chem. Commun.* **2015,** *51*, 3501.

48. Nagarkar, S. S.; Unni, S. M.; Sharma, A.; Kurungot, S.; Ghosh, S. K. Two-in-One: Inherent Anhydrous and Water-Assisted High Proton Conduction in a 3D Metal–Organic Framework. *Angew. Chem., Int. Ed.* **2014,** *53*, 2638.

49. Shimizu, G. K. H.; Taylor, J. M.; Kim, S. Proton Conduction with Metal-Organic Frameworks. *Science* **2013,** *341*, 354.

50. Saha, S.; Schön, E.-M.; Cativiela, C.; Díaz Díaz, D.; Banerjee, R. Proton-Conducting Supramolecular Metallogels from the Lowest Molecular Weight Assembler Ligand: A Quote for Simplicity. *Chem. - Eur. J.* **2013,** *19*, 9562.

51. Sikdar, N.; Dutta, D.; Haldar, R.; Ray, T.; Hazra, A.; Bhattacharyya, A. J.; Maji, T. K. Coordination-Driven Fluorescent J-Aggregates in a Perylenetetracarboxylate-Based MOF: Permanent Porosity and Proton Conductivity. *J. Phys. Chem. C* **2016,** *120*, 13622.

52. Aiyappa, H. B.; Saha, S.; Wadge, P.; Banerjee, R.; Kurungot, S. Fe(III) phytate metallogel as a prototype anhydrous, intermediate temperature proton conductor. *Chem. Sci.* **2015,** *6*, 603.

53. Jiao, Y.; Pei, J.; Yan, C.; Chen, D.; Hu, Y.; Chen, G. Layered nickel metal-organic framework for high performance alkaline battery-supercapacitor hybrid devices. *J. Mater. Chem. A* **2016,** *4*, 13344.

54. Jaouen, F.; Morozan, A. Metal-Organic Frameworks: Electrochemical Properties. In *Encyclopedia of Inorganic and Bioinorganic Chemistry*, John Wiley & Sons, Ltd: 2011.

55. Wang, L.; Han, Y.; Feng, X.; Zhou, J.; Qi, P.; Wang, B. Metal–organic frameworks for energy storage: Batteries and supercapacitors. *Coord. Chem. Rev.* **2016,** *307, Part II*, 361.

56. Sun, L.; Campbell, M. G.; Dincă, M. Electrically conductive porous metal–organic frameworks. *Angew. Chem., Int. Ed.* **2016,** *55*, 3566.

57. Givaja, G.; Amo-Ochoa, P.; Gomez-Garcia, C. J.; Zamora, F. Electrical conductive coordination polymers. *Chem. Soc. Rev.* **2012,** *41*, 115.

58. Hendon, C. H.; Tiana, D.; Walsh, A. Conductive metal-organic frameworks and networks: fact or fantasy? *Phys. Chem. Chem. Phys.* **2012,** *14*, 13120.

59. Mahmood, A.; Guo, W.; Tabassum, H.; Zou, R. Metal-Organic Framework-Based Nanomaterials for Electrocatalysis. *Adv. Energy Mater.* **2016,** *6*, 1600423.

60. Shao, M.; Chang, Q.; Dodelet, J.-P.; Chenitz, R. Recent Advances in Electrocatalysts for Oxygen Reduction Reaction. *Chem. Rev.* **2016,** *116*, 3594.

61. Ma, S.; Goenaga, G. A.; Call, A. V.; Liu, D.-J. Cobalt Imidazolate Framework as Precursor for Oxygen Reduction Reaction Electrocatalysts. *Chem. - Eur. J.* **2011,** *17*, 2063.

62. Kurmoo, M. Magnetic metal-organic frameworks. *Chem. Soc. Rev.* **2009,** *38*, 1353.

63. Chakraborty, A.; Escuer, A.; Ribas, J.; Maji, T. K. A discrete Cu^{II}_6 cluster and a 3D Mn^{II}-Cu^{II} framework based on assembly of Mn_2Cu_4 clusters: synthesis, structure and magnetic properties. *Dalton Trans* **2016,** *45*, 15523.

64. Farha, O. K.; Eryazici, I.; Jeong, N. C.; Hauser, B. G.; Wilmer, C. E.; Sarjeant, A. A.; Snurr, R. Q.; Nguyen, S. T.; Yazaydın, A. Ö.; Hupp, J. T. Metal–Organic Framework

Materials with Ultrahigh Surface Areas: Is the Sky the Limit? *J. Am. Chem. Soc.* **2012,** *134*, 15016.

65. Bruce, D. W.; O'Hare, D.; Walton, R. I. *Porous materials*. John Wiley & Sons: 2011; Vol. 13.

66. Férey, G.; Mellot-Draznieks, C.; Serre, C.; Millange, F.; Dutour, J.; Surblé, S.; Margiolaki, I. A Chromium Terephthalate-Based Solid with Unusually Large Pore Volumes and Surface Area. *Science* **2005,** *309*, 2040.

67. Koh, K.; Wong-Foy, A. G.; Matzger, A. J. A Porous Coordination Copolymer with over 5000 m2/g BET Surface Area. *J. Am. Chem. Soc.* **2009,** *131*, 4184.

68. Rollmann, L. D.; Valyocsik, E. W.; Shannon, R. D. Zeolite Molecular Sieves. In *Inorganic Syntheses*, John Wiley & Sons, Inc.: 2007; pp 61.

69. Ma, S.; Wang, X.-S.; Collier, C. D.; Manis, E. S.; Zhou, H.-C. Ultramicroporous Metal−Organic Framework Based on 9,10-Anthracenedicarboxylate for Selective Gas Adsorption. *Inorg. Chem.* **2007,** *46*, 8499.

70. Mason, J. A.; Veenstra, M.; Long, J. R. Evaluating metal-organic frameworks for natural gas storage. *Chem. Sci.* **2014,** *5*, 32.

71. Britt, D.; Furukawa, H.; Wang, B.; Glover, T. G.; Yaghi, O. M. Highly Efficient Separation of carbon dioxide by a metal-organic framework replete with open metal sites. *Proc. Natl. Acad. Sci. U.S.A.* **2009,** *106*, 20637.

72. Yazaydın, A. Ö.; Benin, A. I.; Faheem, S. A.; Jakubczak, P.; Low, J. J.; Willis, R. R.; Snurr, R. Q. Enhanced CO_2 Adsorption in Metal-Organic Frameworks via Occupation of Open-Metal Sites by Coordinated Water Molecules. *Chem. Mater.* **2009,** *21*, 1425.

73. Shimomura, S.; Horike, S.; Matsuda, R.; Kitagawa, S. Guest-Specific Function of a Flexible Undulating Channel in a 7,7,8,8-Tetracyano-p-quinodimethane Dimer-Based Porous Coordination Polymer. *J. Am. Chem. Soc.* **2007,** *129*, 10990.

74. Mukherjee, S.; Joarder, B.; Manna, B.; Desai, A. V.; Chaudhari, A. K.; Ghosh, S. K. Framework-Flexibility Driven Selective Sorption of p-Xylene over Other Isomers by a Dynamic Metal-Organic Framework. *Sci. Rep.* **2014,** *4*, 5761.

75. Fujita, M.; Kwon, Y. J.; Washizu, S.; Ogura, K. Preparation, Clathration Ability, and Catalysis of a Two-Dimensional Square Network Material Composed of Cadmium(II) and 4,4'-Bipyridine. *J. Am. Chem. Soc.* **1994,** *116*, 1151.

76. Seo, J. S.; Whang, D.; Lee, H.; Jun, S. I.; Oh, J.; Jeon, Y. J.; Kim, K. A homochiral metal-organic porous material for enantioselective separation and catalysis. *Nature* **2000,** *404*, 982.

77. Tang, Q.; Liu, S.; Liu, Y.; Miao, J.; Li, S.; Zhang, L.; Shi, Z.; Zheng, Z. Cation Sensing by a Luminescent Metal–Organic Framework with Multiple Lewis Basic Sites. *Inorg. Chem.* **2013,** *52*, 2799.

78. Beer, P. D.; Gale, P. A. Anion Recognition and Sensing: The State of the Art and Future Perspectives. *Angew. Chem., Int. Ed.* **2001,** *40*, 486.

79. Xu, H.; Liu, F.; Cui, Y.; Chen, B.; Qian, G. A luminescent nanoscale metal-organic framework for sensing of nitroaromatic explosives. *Chem. Commun.* **2011,** *47*, 3153.

80. Wu, X.-Q.; Ma, J.-G.; Li, H.; Chen, D.-M.; Gu, W.; Yang, G.-M.; Cheng, P. Metal-organic framework biosensor with high stability and selectivity in a bio-mimic environment. *Chem. Commun.* **2015,** *51*, 9161.

81. Cen, Y.; Tang, J.; Kong, X.-J.; Wu, S.; Yuan, J.; Yu, R.-Q.; Chu, X. A cobalt oxyhydroxide-modified upconversion nanosystem for sensitive fluorescence sensing of ascorbic acid in human plasma. *Nanoscale* **2015,** *7*, 13951.

82. DeCoste, J. B.; Peterson, G. W. Metal–Organic Frameworks for Air Purification of Toxic Chemicals. *Chem. Rev.* **2014,** *114*, 5695.

83. Qiao, C.; Qu, X.; Yang, Q.; Wei, Q.; Xie, G.; Chen, S.; Yang, D. Instant high-selectivity Cd-MOF chemosensor for naked-eye detection of Cu(II) confirmed using in situ microcalorimetry. *Green Chem.* **2016,** *18*, 951.

84. Barea, E.; Montoro, C.; Navarro, J. A. R. Toxic gas removal - metal-organic frameworks for the capture and degradation of toxic gases and vapours. *Chem. Soc. Rev.* **2014,** *43*, 5419.

85. Robson, R. A net-based approach to coordination polymers. *J. Chem. Soc., Dalton Trans.* **2000**, 3735.

86. Kitagawa, S.; Kitaura, R.; Noro, S.-i. Functional Porous Coordination Polymers. *Angew. Chem., Int. Ed.* **2004,** *43*, 2334.

87. Batten, S. R.; Robson, R. Interpenetrating nets: ordered, periodic entanglement. *Angew. Chem., Int. Ed.* **1998,** *37*, 1460.

88. Yaghi, O. M.; Li, H.; Davis, C.; Richardson, D.; Groy, T. L. Synthetic Strategies, Structure Patterns, and Emerging Properties in the Chemistry of Modular Porous Solids. *Acc. Chem. Res.* **1998,** *31*, 474.

89. Tranchemontagne, D. J.; Ni, Z.; O'Keeffe, M.; Yaghi, O. M. Reticular Chemistry of Metal–Organic Polyhedra. *Angew. Chem., Int. Ed.* **2008,** *47*, 5136.

90. Eddaoudi, M.; Moler, D. B.; Li, H.; Chen, B.; Reineke, T. M.; O'Keeffe, M.; Yaghi, O. M. Modular Chemistry: Secondary Building Units as a Basis for the Design of Highly Porous and Robust Metal−Organic Carboxylate Frameworks. *Acc. Chem. Res.* **2001,** *34*, 319.

91. Rosseinsky, M. J. Recent developments in metal–organic framework chemistry: design, discovery, permanent porosity and flexibility. *Microporous Mesoporous Mater.* **2004,** *73*, 15.

92. Jeon, I.-R.; Sun, L.; Negru, B.; Van Duyne, R. P.; Dincă, M.; Harris, T. D. Solid-State Redox Switching of Magnetic Exchange and Electronic Conductivity in a Benzoquinoid-Bridged Mn^{II} Chain Compound. *J. Am. Chem. Soc.* **2016,** *138*, 6583.

93. Ramaswamy, P.; Matsuda, R.; Kosaka, W.; Akiyama, G.; Jeon, H. J.; Kitagawa, S. Highly proton conductive nanoporous coordination polymers with sulfonic acid groups on the pore surface. *Chem. Commun.* **2014,** *50*, 1144.

94. Sheberla, D.; Bachman, J. C.; Elias, J. S.; Sun, C.-J.; Shao-Horn, Y.; Dinca, M. Conductive MOF electrodes for stable supercapacitors with high areal capacitance. *Nat Mater* **2017,** *16*, 220.

95. Férey, G.; Millange, F.; Morcrette, M.; Serre, C.; Doublet, M.-L.; Grenèche, J.-M.; Tarascon, J.-M. Mixed-Valence Li/Fe-Based Metal–Organic Frameworks with Both Reversible Redox and Sorption Properties. *Angew. Chem., Int. Ed.* **2007,** *46*, 3259.

96. Maiti, S.; Pramanik, A.; Manju, U.; Mahanty, S. Reversible Lithium Storage in Manganese 1,3,5-Benzenetricarboxylate Metal–Organic Framework with High Capacity and Rate Performance. *ACS Appl. Mater. Interfaces* **2015,** *7*, 16357.

97. Peng, Z.; Yi, X.; Liu, Z.; Shang, J.; Wang, D. Triphenylamine-Based Metal–Organic Frameworks as Cathode Materials in Lithium-Ion Batteries with Coexistence of Redox Active Sites, High Working Voltage, and High Rate Stability. *ACS Appl. Mater. Interfaces* **2016,** *8*, 14578.

98. Suen, N.-T.; Hung, S.-F.; Quan, Q.; Zhang, N.; Xu, Y.-J.; Chen, H. M. Electrocatalysis for the oxygen evolution reaction: recent development and future perspectives. *Chem. Soc. Rev.* **2017,** *46*, 337.

99. Zeradjanin, A. R.; Grote, J.-P.; Polymeros, G.; Mayrhofer, K. J. J. A Critical Review on Hydrogen Evolution Electrocatalysis: Re-exploring the Volcano-relationship. *Electroanalysis* **2016,** *28*, 2256.

100. Chen, Z.; Higgins, D.; Yu, A.; Zhang, L.; Zhang, J. A review on non-precious metal electrocatalysts for PEM fuel cells. *Energy Environ. Sci.* **2011,** *4*, 3167.

101. Subbaraman, R.; Tripkovic, D.; Chang, K.-C.; Strmcnik, D.; Paulikas, A. P.; Hirunsit, P.; Chan, M.; Greeley, J.; Stamenkovic, V.; Markovic, N. M. Trends in activity for the water electrolyser reactions on 3d M(Ni,Co,Fe,Mn) hydr(oxy)oxide catalysts. *Nat Mater* **2012,** *11*, 550.

102. Fabbri, E.; Habereder, A.; Waltar, K.; Kotz, R.; Schmidt, T. J. Developments and perspectives of oxide-based catalysts for the oxygen evolution reaction. *Catal. Sci. Technol.* **2014,** *4*, 3800.

103. Hong, W. T.; Risch, M.; Stoerzinger, K. A.; Grimaud, A.; Suntivich, J.; Shao-Horn, Y. Toward the rational design of non-precious transition metal oxides for oxygen electrocatalysis. *Energy Environ. Sci.* **2015,** *8*, 1404.

104. McCrory, C. C. L.; Jung, S.; Peters, J. C.; Jaramillo, T. F. Benchmarking Heterogeneous Electrocatalysts for the Oxygen Evolution Reaction. *J. Am. Chem. Soc.* **2013,** *135*, 16977.

105. Ma, T. Y.; Dai, S.; Jaroniec, M.; Qiao, S. Z. Metal–Organic Framework Derived Hybrid Co_3O_4-Carbon Porous Nanowire Arrays as Reversible Oxygen Evolution Electrodes. *J. Am. Chem. Soc.* **2014,** *136*, 13925.

106. Feng, P. L.; Leong, K.; Allendorf, M. D. Charge-transfer guest interactions in luminescent MOFs: implications for solid-state temperature and environmental sensing. *Dalton Trans.* **2012,** *41*, 8869.

107. Park, Y. K.; Choi, S. B.; Kim, H.; Kim, K.; Won, B.-H.; Choi, K.; Choi, J.-S.; Ahn, W.-S.; Won, N.; Kim, S.; Jung, D. H.; Choi, S.-H.; Kim, G.-H.; Cha, S.-S.; Jhon, Y. H.; Yang, J. K.; Kim, J. Crystal Structure and Guest Uptake of a Mesoporous Metal–Organic Framework Containing Cages of 3.9 and 4.7 nm in Diameter. *Angew. Chem., Int. Ed.* **2007,** *46*, 8230.

108. Xiang, H.-F.; Chan, S.-C.; Wu, K. K.-Y.; Che, C.-M.; Lai, P. T. High-efficiency red electrophosphorescence based on neutral bis(pyrrole)-diimine platinum(II) complex. *Chem. Commun.* **2005**, 1408.

109. Tan, X.; Chen, X.; Zhang, J.; Su, C.-Y. Luminescent coordination polymer gels based on rigid terpyridyl phosphine and Ag(I). *Dalton Trans.* **2012,** *41*, 3616.

110. Takashima, Y.; Martínez, V. M.; Furukawa, S.; Kondo, M.; Shimomura, S.; Uehara, H.; Nakahama, M.; Sugimoto, K.; Kitagawa, S. Molecular decoding using luminescence from an entangled porous framework. *Nat. Commun.* **2011,** *2*, 168.

111. Doty, F. P.; Bauer, C. A.; Skulan, A. J.; Grant, P. G.; Allendorf, M. D. Scintillating Metal-Organic Frameworks: A New Class of Radiation Detection Materials. *Adv. Mate.* **2009,** *21*, 95.

112. Bordiga, S.; Lamberti, C.; Ricchiardi, G.; Regli, L.; Bonino, F.; Damin, A.; Lillerud, K. P.; Bjorgen, M.; Zecchina, A. Electronic and vibrational properties of a MOF-5 metal-organic framework: ZnO quantum dot behaviour. *Chem. Commun.* **2004**, 2300.

113. Allendorf, M. D.; Bauer, C. A.; Bhakta, R. K.; Houk, R. J. T. Luminescent metal-organic frameworks. *Chem. Soc. Rev.* **2009,** *38*, 1330.

114. Serre, C.; Millange, F.; Thouvenot, C.; Gardant, N.; Pelle, F.; Ferey, G. Synthesis, characterisation and luminescent properties of a new three-dimensional lanthanide trimesate: M((C_6H3)-$(CO_2)_3$) (M = Y, Ln) or MIL-78. *J. Mater. Chem.* **2004,** *14*, 1540.

115. Talin, A. A.; Centrone, A.; Ford, A. C.; Foster, M. E.; Stavila, V.; Haney, P.; Kinney, R. A.; Szalai, V.; El Gabaly, F.; Yoon, H. P. Tunable Electrical Conductivity in Metal-Organic Framework Thin-Film Devices. *Science* **2014,** *343*, 66.

116. Huang, X.; Sheng, P.; Tu, Z.; Zhang, F.; Wang, J.; Geng, H.; Zou, Y.; Di, C.-a.; Yi, Y.; Sun, Y.; Xu, W.; Zhu, D. A two-dimensional π–d conjugated coordination polymer with extremely high electrical conductivity and ambipolar transport behaviour. *Nat. Commun.* **2015,** *6*, 7408.

117. Kambe, T.; Sakamoto, R.; Hoshiko, K.; Takada, K.; Miyachi, M.; Ryu, J.-H.; Sasaki, S.; Kim, J.; Nakazato, K.; Takata, M.; Nishihara, H. π-Conjugated Nickel Bis(dithiolene) Complex Nanosheet. *J. Am. Chem. Soc.* **2013,** *135*, 2462.

118. Sun, L.; Hendon, C. H.; Minier, M. A.; Walsh, A.; Dincă, M. Million-Fold Electrical Conductivity Enhancement in Fe_2(DEBDC) versus Mn_2(DEBDC) (E = S, O). *J. Am. Chem. Soc.* **2015,** *137*, 6164.

119. van der Pauw, L.; Tech, P. Rev. 1958/59, 20, 220.

120. Chiang, C. K.; Druy, M. A.; Gau, S. C.; Heeger, A. J.; Louis, E. J.; MacDiarmid, A. G.; Park, Y. W.; Shirakawa, H. Synthesis of highly conducting films of derivatives of polyacetylene, $(CH)_x$. *J. Am. Chem. Soc.* **1978,** *100*, 1013.

121. Shirakawa, H.; Louis, E. J.; MacDiarmid, A. G.; Chiang, C. K.; Heeger, A. J. Synthesis of electrically conducting organic polymers: halogen derivatives of polyacetylene, (CH). *J. Chem. Soc., Chem. Commun.* **1977**, 578.

122. Abdelhamid, M. E.; O'Mullane, A. P.; Snook, G. A. Storing Energy in Plastics: A Review on Conducting Polymers & Their Role in Electrochemical Energy Storage. *RSC Adv.* **2015,** *5*, 11611.

123. Kim, J.; Lee, J.; You, J.; Park, M.-S.; Hossain, M. S. A.; Yamauchi, Y.; Kim, J. H. Conductive polymers for next-generation energy storage systems: recent progress and new functions. *Mater. Horiz.* **2016,** *3*, 517.

124. Toshima, N.; Hara, S. Direct Synthesis of Conducting Polymers from Simple Monomers. *Prog. Polym. Sci.* **1995,** *20*, 155.

125. K. Yakushi; L. J. Lauchlan; T. C. Clarke; Street, G. B. Optical study of polypyrrole perchlorate. *The J. Chem. Phys.* **1983,** *79*, 4774.

Chapter-II

Enhancement of Conductivity in Coordination Polymers

Section-IIA

Enhancement of Conductivity in Redox-Active Coordination Polymer

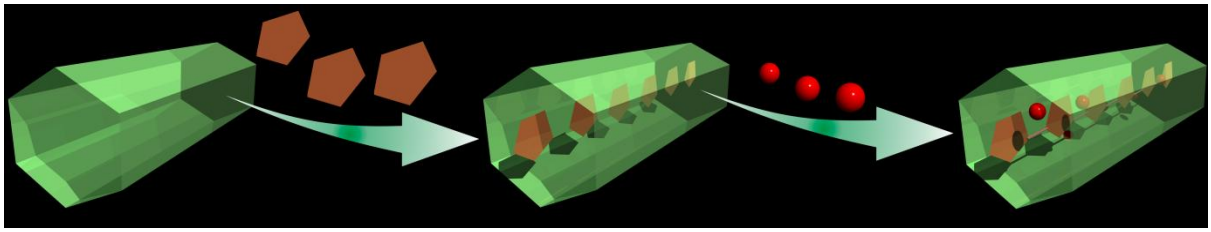

IIA.1. Introduction

Oxidizing agents are required for oxidative polymerization of organic monomers such as pyrrole (Py), aniline (Ani), and thiophene (Th). However, Kanatzidis and co-workers have illustrated an elegant approach for polymerization of these organic molecules (without using any extraneous oxidizing agents) inside redox-active inorganic layered materials such as FeOCl, V_2O_5 which is so called polymer bronze concept.[1,2] However, such concept is missing in CPs either in the form of metal–organic frameworks (MOFs) or metal–organic gels (MOGs). We wanted to explore this approach in redox-active CPs in term of conductivity enhancement. Since Fe(III) is a redox active metal ion, CP based on Fe(III) could be redox active. In this hope, we have synthesized MOG by mixing ferric nitate (Fe) and tricarboxylic acid (BTC) ligand in ethanol. Notably, Fe-BTC gel is already well characterized and it is exploited in various fields such as a) synthesis of a porous organic polymer by utilizing Fe-BTC gel as a template[3] b) heterogeneous catalysis reaction for example Friedel–Craftsbenzylation reaction[4] c) with high micro and macroporosity[5] d) CO_2 separation[6] e) removal of toxic As^{5+} ions from aqueous solutions.[6] However, redox activity of the material is unexplored, specifically for the enhancement of electrical conductivity.

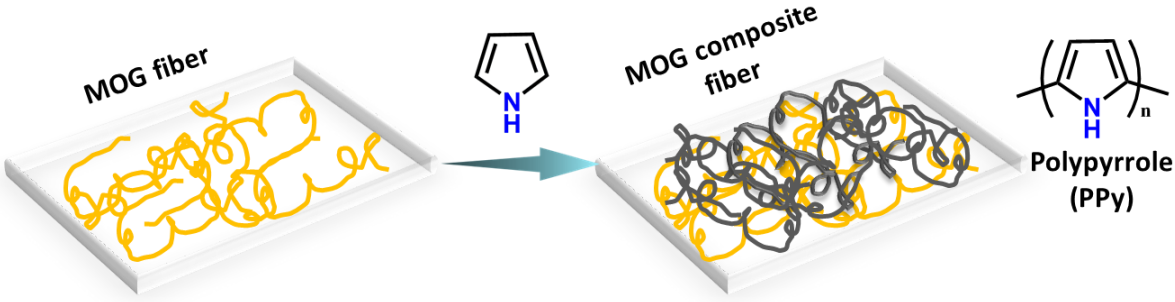

Figure 2A. 1. *Schematic illustration of conducting polymer in redox-active CP matrix.*

IIA.2. Materials and Methods

Ferric nitrate ($Fe(NO_3)_3.9H_2O$) (Fe) and 1,3,5-benzentricarboxylic acid (BTC) were purchased from Sigma Aldrich (India) and used without further purification. Py and bithiophene (BTh) were brought from Sigma Aldrich (India) and purified before use.

Fourier transform infrared (FTIR) spectra were recorded on NICOLET 6700 FTIR Spectrophotometer using KBr Pellets. Powder X-ray diffraction (PXRD) patterns were measured on Bruker D8 Advanced X-Ray diffractometer at room temperature using Cu-Kα

radiation (λ= 1.5406Å) with a tube voltage of 40 kV and current of 35 mA and scan speed of 0.5° min^{-1} and a step size of 0.01° in 2 θ. Thermal properties were analysed using Perkin-Elmer STA 6000 TGA analyser under N_2 atmosphere with heating rate of 10 ^{0}C/min. Solid and liquid state UV-vis spectra were recorded on Perkin Elmer Lambda UV/VIS spectrophotometer. Field emission scanning electron microscope (FESEM) imaging and energy-dispersive X-ray spectroscopy (EDXS) analysis were performed in a Carl-Zeiss Ultra microscope.

DC conductivity values were measured using conventional four-probe method using Keithley 2182A nanovoltmeter and 6221 DC and AC current Sourcemeter on press pallet. Optical images were taken in Labram-HR 800 Confocal microscope using different objective lenses (10× and 100×)

Fe(III) solution and BTC solution were prepared by dissolving ferric nitrate (6.06gm, 15 mmole) and BTC (2.1 gm, 10 mmole) in 80 ml ethanol separately. These two solutions were mixed together with vigorous sonication and left undisturbed for few minutes. Orange-brown gel was observed. To prepare xero-gel, wet gel was heated at 50 ^{0}C and crushed it to form orange powder (Fe-BTC).

The orange coloured xero-gel was taken in a non-reactive solvent such as hexane, chloroform and few drops of Py or BTh were added to it at room temperature. Within few minutes, orange colour turned black and after 24 hours it became dark. These dark composite materials were extracted by simple filtration method and washed heavily with $CHCl_3$ and acetone. Finally, the materials were dried at 80 ^{0}C for 24h.

Black coloured composite materials were immersed into 0.5 M ammonia solution for 24 hours and black masses were found which were washed with water, methanol and finally with acetone. These insoluble black masses were dried under vacuum.

IIA.3. Results and Discussion

Primary indication of *insitu* incorporation of the conducting polymers was the colour change of xero-gel from orange to black **(Figure 2A.2)**.[7-8] Formation of polymers was confirmed by extracting the black mass from the composite materials which was insoluble in common organic solvents such as benzene, toluene, chloroform and tetrahydrofuran. The existence of polypyrrole (PPy) in the CP was confirmed by FTIR spectra **(Figure 2A.2)**. The FTIR spectrum

of extracted PPy was almost matching with PPy which was synthesized separately outside using ferric nitrate **(Figure 2A.2b)**.[9] The peak at 1570 cm^{-1} was attributed to typical PPy ring vibration.[10-13] The observed peaks at 1382 cm^{-1} and 1184 cm^{-1} may be assigned to C-N stretching vibration and presence of C-H out of plane bending was confirmed by the peaks at 788 cm^{-1} and 673 cm^{-1}. Similarly, presence of polythiophene (PTh) was confirmed by FTIR spectra and characteristic stretching vibrations were distinguished. For example, band near 1201 cm^{-1} and 1039 cm^{-1} were assigned to C-H bending and C-H in plane deformation. C=C asymmetric and symmetric stretching vibrations were detected at 1669 cm^{-1} and 1400 cm^{-1} respectively. The presence of peaks corresponding to C-S stretching frequency at 755 cm^{-1} and 615 cm^{-1} clearly indicate the presence of PTh.

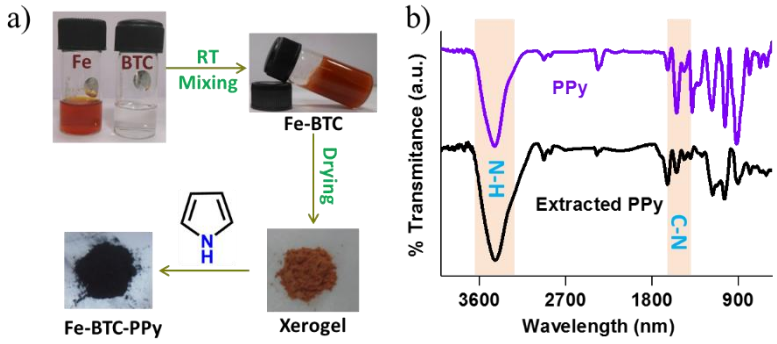

Figure 2A.2: *Synthesis of wet gel by mixing of Fe(III) (Ferric nitrate) and BTC ligand subsequent drying to make xero-gel. Polymerization of Py within xero-gel is demonstrated. Right side: FTIR spectra of extracted PPy (black) from Fe-BTC-PPy and PPy synthesized separately (violet).*

Solid state UV-vis spectra **(Figure 2A.3)** corroborated FTIR spectra. Absorption bands

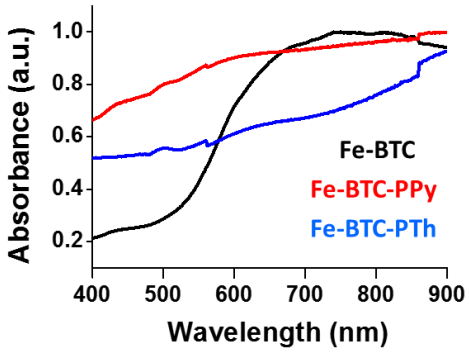

Figure 2A.3: *UV-vis spectra of Fe-BTC (black), Fe-BTC-PPy (red) and Fe-BTC-PTh (blue).*

near ~433 nm, ~500 nm and ~560 nm for Fe-BTC-PPy and ~500 nm, ~560 nm for Fe-BTC-PTh whereas these bands were absent in the parent Fe-BTC xero-gel. Formation of conducting PPy or PTh in the Fe-BTC was ensuring for the appearance of such absorption bands.[8-10, 14]

To check the structure of Fe-BTC before and after polymerization, PXRD patterns were recorded. Apparently, no change in the PXRD patterns was observed which suggested that the polymerization did not hamper the structure of CP **(Figure 2A.4a)**.[15] Even more, we have repeated the experiment many times to check the reproducibility of effect of polymerization on the CP structure. PXRD patterns indicated both composites and parent compound were amorphous in nature. PXRD patterns were directly co-related to the FESEM images. Indeed, it was found in FESEM images that xero-gel and its composite materials were fibrous in nature.[5] Fe-BTC was found to be very dense nanofiber whereas Fe-BTC-PPy was comparatively less dense **(Figure 2A.4b,c)**. Similar observation was found in case of Fe-BTC-PTh material **(Figure 2A.4d)**.

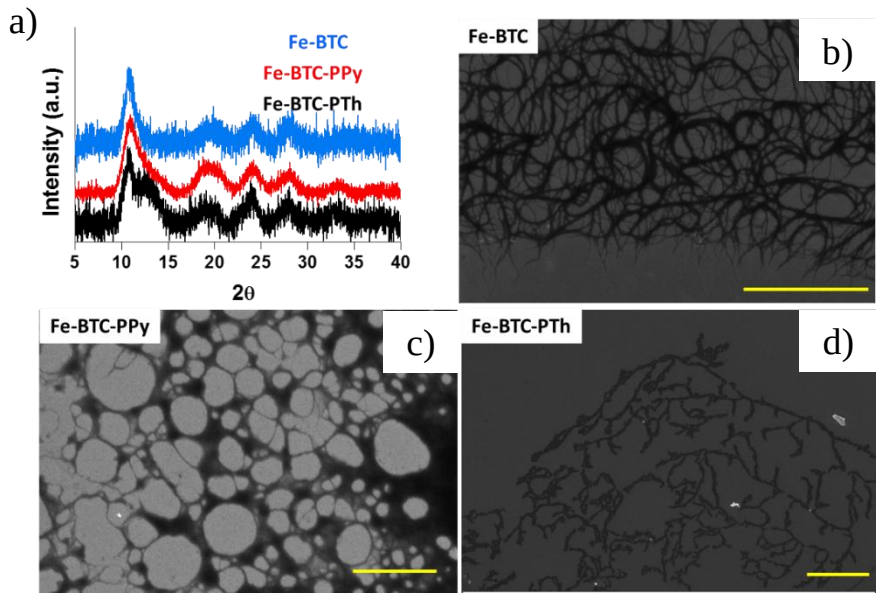

Figure 2A.4: *(a) PXRD patterns of Fe-BTC (deep sky blue), Fe-BTC-PPy (red) and Fe-BTC-PTh (black). FESEM images of Fe-BTC (b), Fe-BTC-PPy (c) and Fe-BTC-PTh (d) (Scale bar represents 2 µm).*

Magnetic measurements of Fe-BTC and its composite materials were performed to scrutinize the redox activity **(Figure 2A.5a)**.[7] Fe-BTC xero-gel material was behaving as a paramagnetic

material with critical temperature 50K. Generally, such paramagnetic behavior originates from high-spin Fe(III) states and its electronic configuration $t_{2g}^3e_g^2$ which represented the presence of five unpaired electrons **(Figure 2A.5b)**. Interestingly, upon polymerization of Py, we have observed decrease in magnetization value as well as critical temperature (~25K). Since the paramagnetic contribution of PPy is very negligible, magnetization value is originated only from metal ions (Fe). The decreased magnetization value indicated the conversion of Fe(III) to Fe(II) and at the same time Py monomer converted to PPy. The electronic configuration of high-spin Fe(II) in Fe-BTC-Py was $t_{2g}^4e_g^2$ and number of unpaired electron is 4. This was previously observed that the Fe(III) has ability to polymerize Py monomer to polymer.[9, 16] The M-H curve showed S-shape which indicated the super-paramagnetic behavior. Similarly, here also at particular field the magnetization value decreased with respect to parent compound. Magnetic measurement confirmed that the Fe-BTC xero-gel is a redox active material.

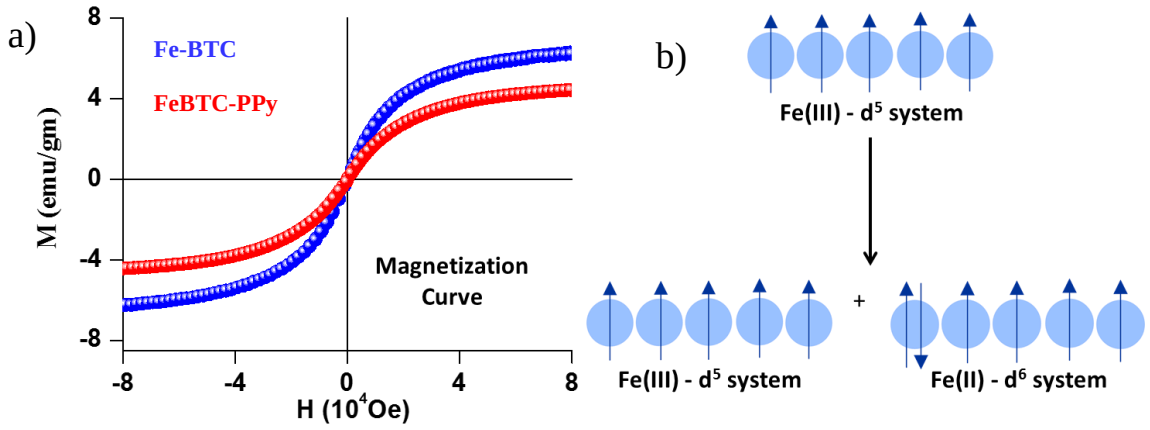

Figure 2A.5*: (a) M-H plots for Fe–BTC xerogel (blue) and Fe–BTC–PPy composite (red). (b) Schematic diagram of no. of unpaired electrons before and after oxidative polymerization.*

Since, the PPy/PTh is a conducting polymer, we wanted to check enhancement of electrical conductivity in composite materials. DC conductivities of all xero-gel materials were measured by using four probe methods on pressed pellet. *I-V* curves of all materials including Fe-BTC were straight line which supported the ohmic nature of the material **(Figure 2A.6a)**. From the *I-V* curve, the conductivity values were evaluated by applying $\rho = \rho_o/f(w/s)$ and $\rho_o = 2\pi s \times (V/I)$ where ρ is resistivity of the sample at measuring temperature, w is the thickness of the pressed pellet, s is probe spacing, V is the measured voltage, I is the applied current, $f(w/s)$ is the correction factor and Conductivity $=1/\rho$. Conductivity values of parent xero-gel is ~10^{-6} S/cm whereas for PPy and PTh loaded xero-gel materials are ~10^{-3} and ~10^{-4} S/cm

respectively **(Figure 2A.6b,c)**. ~1000 times (Fe-BTC-PPy) and ~100 times (Fe-BTC-PTh) enhancement of electrical conductivity were observed. The activation energy of Fe-BTC-PPy **(Figure 2A.6d)** was further investigated by temperature sweep conductivity measurement. This was calculated from *log(ρ)* vs *1/T* graph by applying the equation $\rho = A \exp(\frac{E_a}{KT})$ Where E_a = activation energy, *K*= Blotzmann constant, *A* = constant, *T*= temperature in Kelvin. Calculated activation energy of Fe-BTC-PPy was ~0.28 eV which was similar to organic based semiconducting material.

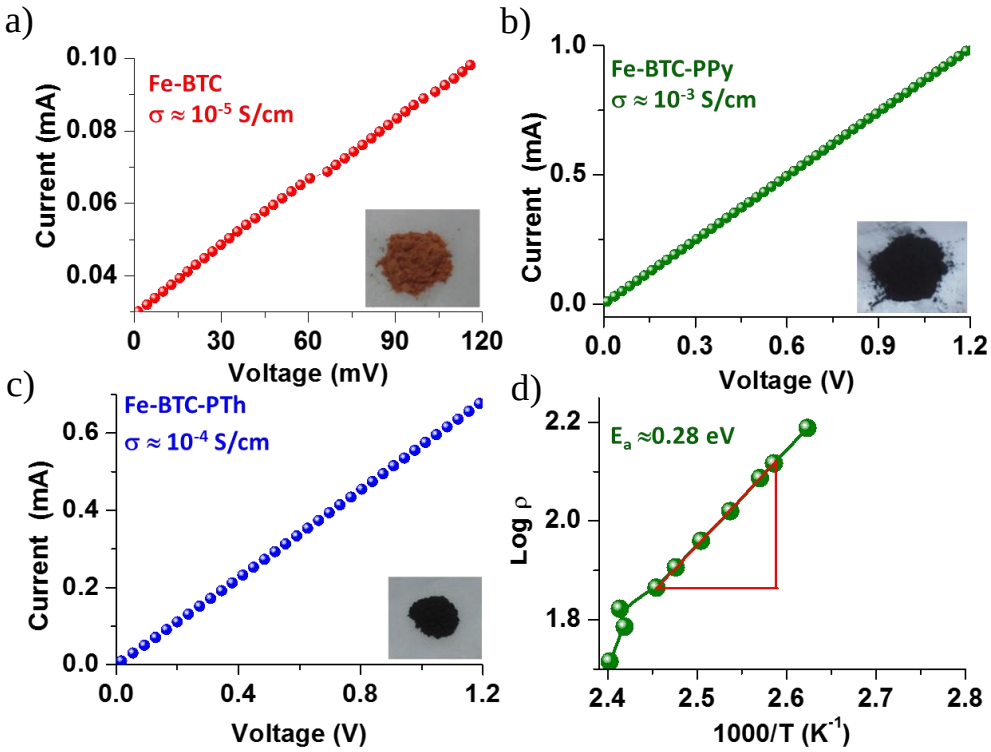

Figure 2A.6: *Room temperature I-V plots for Fe-BTC (a), Fe–BTC–PPy (b) and Fe–BTC–PTh (c). Linear curve signifies the ohmic nature. (d) Activation energy for Fe-BTC-PPy is calculated from the graph logρ Vs 1000/T.*

To check active-sites of polymerization in the gel, we have pressed it on a glass slide. Under confocal microscope brown micro-fibers were clearly visualized **(Figure 2A.7)**. Upon spraying the Py vapor, the brown fiber turned to black and it's width was increasing which indicated the formation of PPy upon gel micro-fiber.

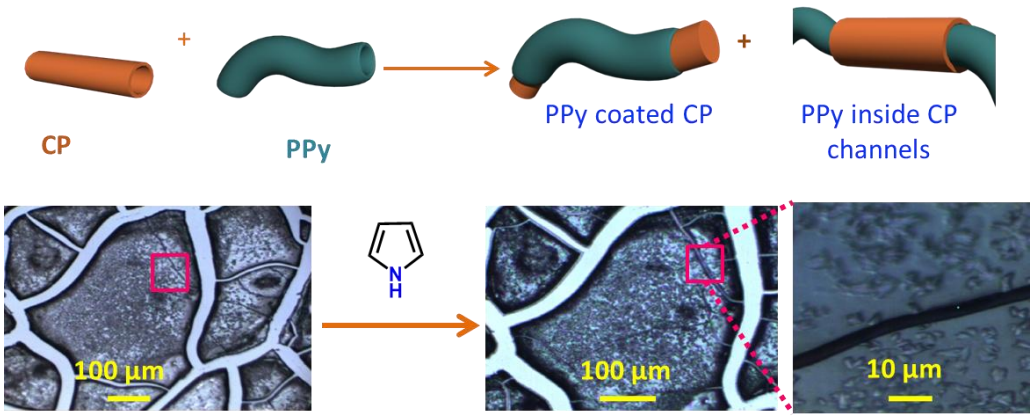

Figure 2A.7: *Schematic representation of polymerization on gel fiber (upper). Real time experiment of polymerization on gel fiber on glass slide under microscope (down).*

To check the processability of Fe-BTC wet gel, we have painted it on a filter paper for chemical lithography **(Figure 2A.8)**.[17] Noticeably, back side of the filter paper did not turn to orange which suggested, gel fibers could not penetrate through the filter paper. We have put mask on the painted filter paper and subsequently exposed with Py vapor. Interestingly, exposed area of the painted filter paper became black. Also, back side of the filter paper retained as its original colour which clearly indicated, the polymerization was taking place on only the gel micro-fiber.

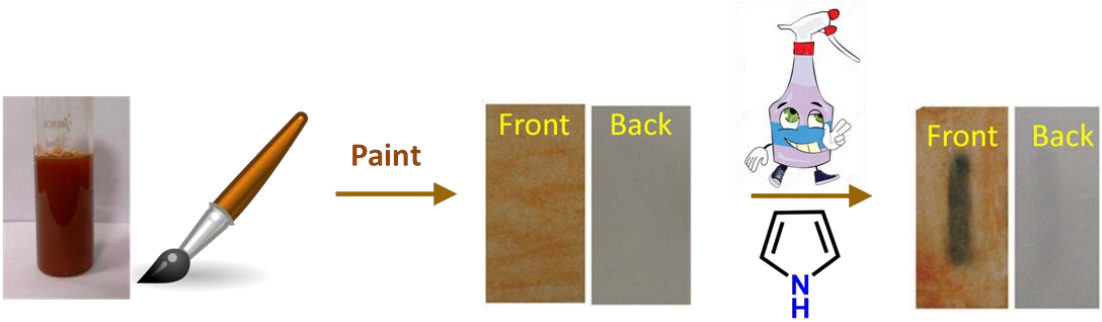

Figure 2A.8: *Chemical lithography on a filter paper coated with Fe-BTC. After exposing Py vapor exposed area became black and back side remains unchanged.*

IIA.4. Conclusions

In conclusion, we have provided evidence for the *in-situ* generation of π-conjugated polymers inside the matrix of a redox-active metal–organic gel and a hybrid composites formation thereof. Specifically, we have prepared and characterized Fe– BTC–PPy and Fe–BTC–PTh

composite systems. We anticipate that our first attempt to incorporate conducting polymers inside a metal–organic gel will open-up new possibilities and challenges to fabricate various hybrid composite materials, exploring other combinations of conducting polymers and MOGs.

References

1. Kanatzidis, M. G.; Wu, C. G.; Marcy, H. O.; Kannewurf, C. R. Conductive-polymer bronzes. Intercalated polyaniline in vanadium oxide xerogels. *J. Am. Chem. Soc.* **1989,** *111*, 4139.

2. Kanatzidis, M. G.; Tonge, L. M.; Marks, T. J.; Marcy, H. O.; Kannewurf, C. R. In situ intercalative polymerization of pyrrole in FeOCl: a new class of layered, conducting polymer-inorganic hybrid materials. *J. Am. Chem. Soc.* **1987,** *109*, 3797.

3. Wei, Q.; James, S. L. A metal-organic gel used as a template for a porous organic polymer. *Chem. Commun.* **2005**, 1555.

4. Horcajada, P.; Surble, S.; Serre, C.; Hong, D.-Y.; Seo, Y.-K.; Chang, J.-S.; Greneche, J.-M.; Margiolaki, I.; Ferey, G. Synthesis and catalytic properties of MIL-100(Fe), an iron(III) carboxylate with large pores. *Chem. Commun.* **2007**, 2820.

5. Lohe, M. R.; Rose, M.; Kaskel, S. Metal-organic framework (MOF) aerogels with high micro- and macroporosity. *Chem. Commun.* **2009**, 6056.

6. Nune, S. K.; Thallapally, P. K.; McGrail, B. P. Metal organic gels (MOGs): a new class of sorbents for CO_2 separation applications. *J. Mater. Chem.* **2010,** *20*, 7623.

7. Wu, C. G.; DeGroot, D. C.; Marcy, H. O.; Schindler, J. L.; Kannewurf, C. R.; Liu, Y. J.; Hirpo, W.; Kanatzidis, M. G. Redox Intercalative Polymerization of Aniline in V_2O_5 Xerogel. The Postintercalative Intralamellar Polymer Growth in Polyaniline/Metal Oxide Nanocomposites Is Facilitated by Molecular Oxygen. *Chem. Mater.* **1996,** *8*, 1992.

8. Yanai, N.; Uemura, T.; Ohba, M.; Kadowaki, Y.; Maesato, M.; Takenaka, M.; Nishitsuji, S.; Hasegawa, H.; Kitagawa, S. Fabrication of Two-Dimensional Polymer Arrays: Template Synthesis of Polypyrrole between Redox-Active Coordination Nanoslits. *Angew. Chem., Int. Ed.* **2008,** *47*, 9883.

9. Toshima, N.; Hara, S. Direct synthesis of conducting polymers from simple monomers. *Prog. Polym. Sci.* **1995,** *20*, 155.

10. Uemura, T.; Kadowaki, Y.; Yanai, N.; Kitagawa, S. Template Synthesis of Porous Polypyrrole in 3D Coordination Nanochannels. *Chem. Mater.* **2009,** *21*, 4096.

11. Ballav, N.; Biswas, M. High Yield Polymerisation of Aniline and Pyrrole in Presence of Montmorillonite Clay and Formation of Nanocomposites Thereof. *Polym. J.,* **2004,** *36*, 162.

12. Peng, H.; Zhang, L.; Spires, J.; Soeller, C.; Travas-Sejdic, J. Synthesis of a functionalized polythiophene as an active substrate for a label-free electrochemical genosensor. *Polymer* **2007,** *48*, 3413.

13. Ballav, N.; Biswas, M. A conducting nanocomposite via intercalative polymerisation of thiophene in montmorillonite clay. *Synth. Met.* **2004,** *142*, 309.

14. Street, G.; Clarke, T. Conducting polymers: a review of recent work. *IBM J. Res. Dev.* **1981,** *25*, 51.

15. Distefano, G.; Suzuki, H.; Tsujimoto, M.; Isoda, S.; Bracco, S.; Comotti, A.; Sozzani, P.; Uemura, T.; Kitagawa, S. Highly ordered alignment of a vinyl polymer by host–guest cross-polymerization. *Nat. Chem.* **2013,** *5*, 335.

16. Winther-Jensen, B.; Chen, J.; West, K.; Wallace, G. Vapor Phase Polymerization of Pyrrole and Thiophene Using Iron(III) Sulfonates as Oxidizing Agents. *Macromolecules* **2004,** *37*, 5930.

17. Ballav, N.; Schilp, S.; Zharnikov, M. Electron-Beam Chemical Lithography with Aliphatic Self-Assembled Monolayers. *Angew. Chem., Int. Ed.* **2008,** *47*, 1421.

Section-IIB

Enhancement of Conductivity in Redox-Inactive Coordination Polymer

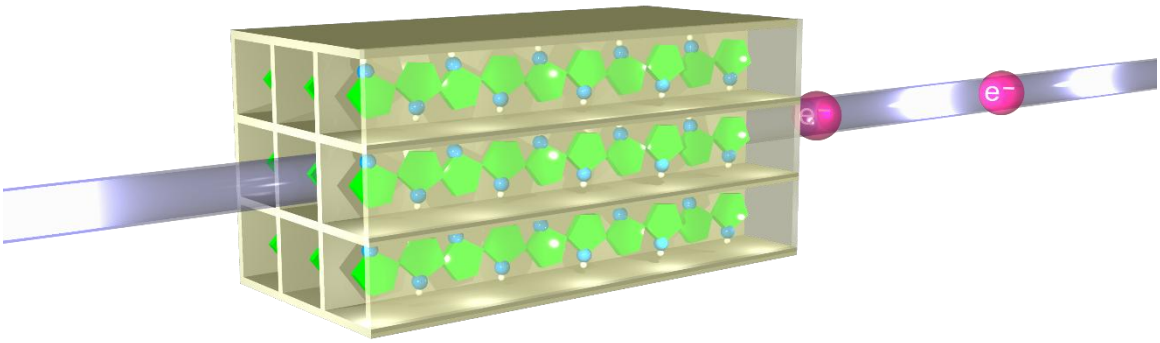

IIB.1. Introduction

In previous section, we have demonstrated formation of conducting polymers in a redox-active CP without using any external oxidizing agent and achieved ~10^3-fold enhancement of conductivity. Herein, we are motivated by the Zhang and coworker's work where they have incorporated pyrrole (Py) monomers inside 1D nanochannel of Zn-based CP first and subsequently polymerizing them using iodine (I_2) as an external oxidizing agent. Their motivation was to get highly oriented conductive and low dimensional polypyrrole (PPy) chains. Indeed, they are successful to prepare such highly conductive 1D PPy chains. By adopting this method, we thought to incorporate PPy chains in a redox-inactive CP to increase the electrical conductivity of composite material.

As a prototype, we have synthesized $[Cd(NDC)_{0.5}(PCA)]$ (NDC=2,6-napthalenedicarboxylate and PCA= 4-pyridinecarboxylate) which is 3D CP with 1D nanochannels. This CP has been explored in various applications such as specific CO_2 capture, detecting nitro explosives, OFET (organic field effect transistor) based nitro-explosive sensor due to its remarkable physical properties, such as water stability, 1D nanochannel with fluorescent behaviour. [1-3] With all these properties, it fulfilled our basic requirement i.e. channel dimension which is matching with the Py dimension (~4.3 × 3.7 $Å^2$).[4]

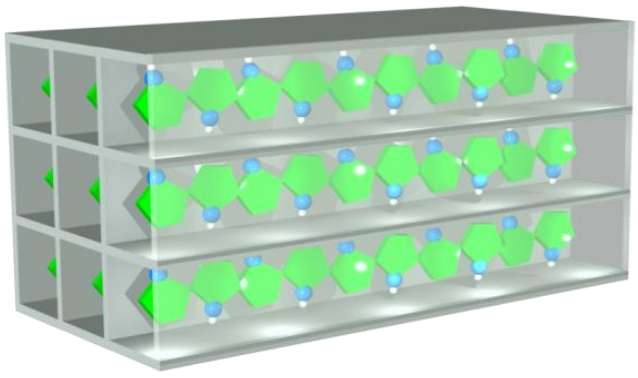

Figure 2B.1: *Schematic illustration of CP infiltrated with conducting polymers.*

IIB.2. Materials and Methods

Single crystals of $[Cd(NDC)_{0.5}(PCA)]\cdot G_x$ (CP) was prepared by reacting equal amount of $Cd(NO_3)_2\cdot 4H_2O$ (1mmole), 4-pyridinecarboxylic acid (HPCA) (1 mmole), and half molar amount of 2,6-napthalenedicarboxylic acid (H_2NDC) (0.5 mmole) in 6 ml mix-solvent of

DMF−EtOH (1:1) by the solvothermal technique, in a teflon-lined autoclave.[3] The teflon-lined autoclave was heated to 120 °C for 48h under autogenous pressure and then cooled to RT over 24 h. The peach colour block shaped single crystals were found and filtered. Since, high boiling solvents were present in the crystal as guest molecules, they were exchanged by low boiling solvent such as acetonitrile for longer periods (~1 week). Crystals were dried overnight under vacuum heating (80 ^{o}C).

The activated CP was impregnated in distilled Py under N_2 for 24 hr in a round bottom flask, followed by removal of excess Py monomers outside the host framework, under reduced pressure. The crystal structure was unchanged (confirmed from PXRD) and 10-12% Py monomer loading in this material (CP⊃Py) was determined by thermo gravimetric analysis.

CP⊃Py was immersed into 0.05 M I_2 solution in the freezer for 72 hr for complete polymerisation of Py and followed by removal of I_2 by vigorous washing with hexane. Finally, a dark green coloured product (CP⊃PPy) was collected.

The green product was crashed with 0.5 (M) NH_3 solution for 24 hr resulting in a black colour insoluble mass which dried at 80^{o}C for 24 hr.

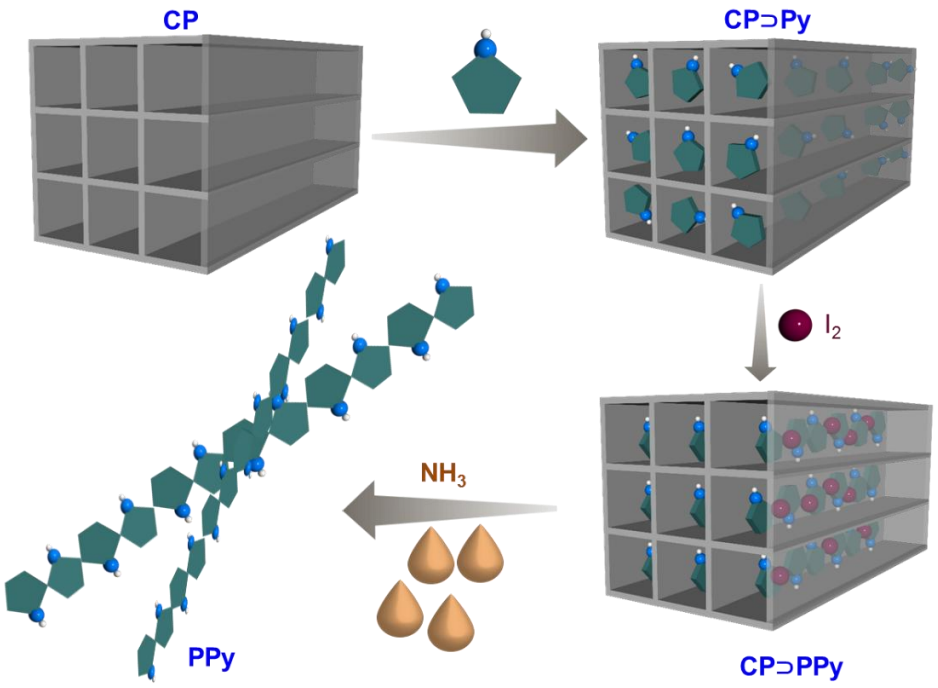

Figure 2B.2: *Schematic representation of incorporation of conducting polymer and extraction of PPy chains from CP nano-channels.*

IIB.3. Results and Discussion

$[Cd(NDC)_{0.5}(PCA)]\cdot G_x$ (CP) metal-organic 3D network is highly porous structure with 1D nanochannel in c direction. This material has channel dimension (9.5 x 7.8 $Å^2$) with 34.9% void space.[3] To prepare CP⊃Py, CP was activated under reduced pressure at 80 °C followed by immersion in distilled Py for 24 hr. The excess Py was removed under reduced pressure.

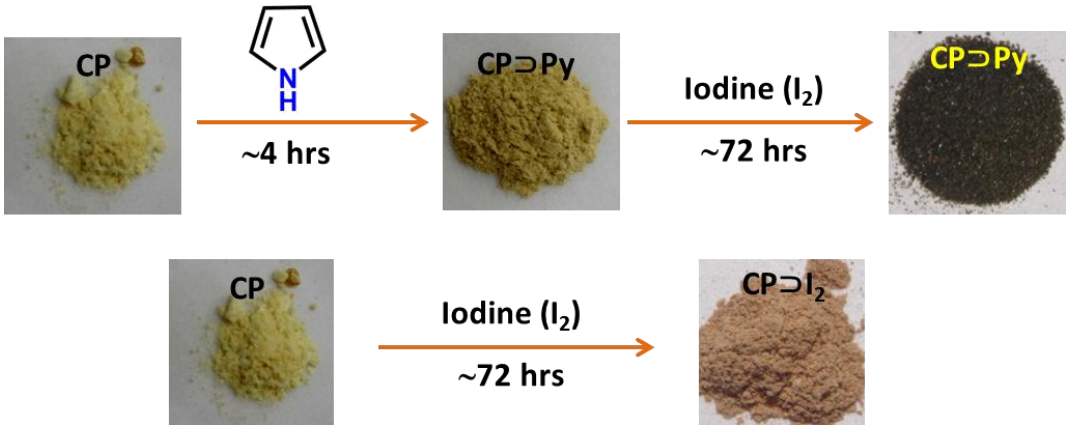

Figure 2B.3: *Peach-colored CP turned dark green upon subsequent exposure to Py, followed by I_2 solution in hexane. Colour changed from CP to CP⊃I_2 after exposing with I_2.*

However, no significant colour change was observed **(Figure 2B.3)**. Interestingly, by immersing CP⊃Py in I_2 solution at low temperature for 72 hr the colour turned to dark green from peach which indicated the polymerization of Py inside the channel.[4-6] No significant colour change was observed when CP was immersed in I_2 solution **(Figure 2B.3)**.

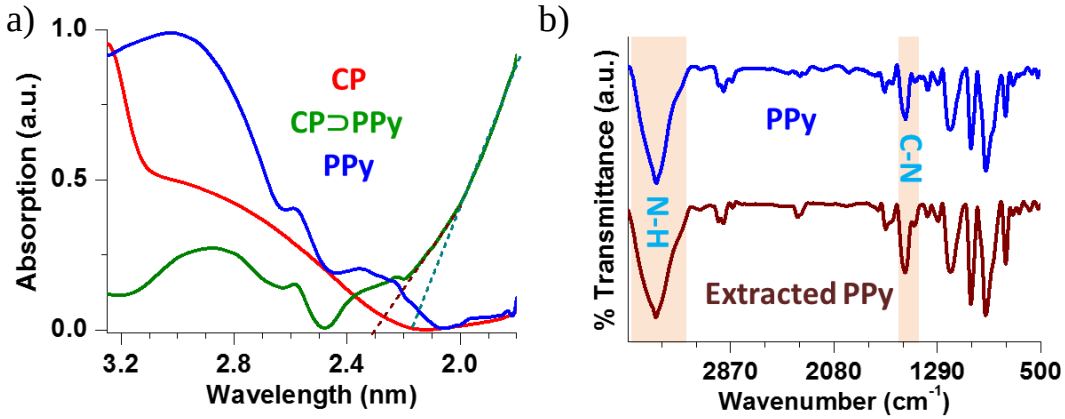

Figure 2B.4: *(a) Solid state UV-vis spectra of CP (red), CP⊃PPy (green), and extracted PPy (blue). (b) FTIR spectra of extracted PPy from CP (wine) and PPy synthesized outside using*

I_2 (blue).

Colour change was complemented by the UV-vis spectra and showed existence of PPy ~470 nm which were also present in extracted insoluble black mass from CP⊃PPy **(Figure 2B.4a)**.[5, 7-10] Interestingly, another new feature was observed in the IR region and that was probably due to formation of polaron band of PPy moiety /π-π interaction between host and guest.[19-20]

Here, PPy was extracted by dissolution of CP⊃PPy in ammonia solution and FTIR spectra were recorded of the extracted mass **(Figure 2B.4b)**. The distinctive stretching vibrations of PPy reported in the literature appeared in the extracted black mass which confirmed the existence of PPy into material. Furthermore, confinement of PPy chains were detected from nuclear magnetic resonance (NMR) (^{1}H and ^{13}C), and differential scanning calorimetry (DSC) **(Figure 2B.5)**.[4, 6, 11]

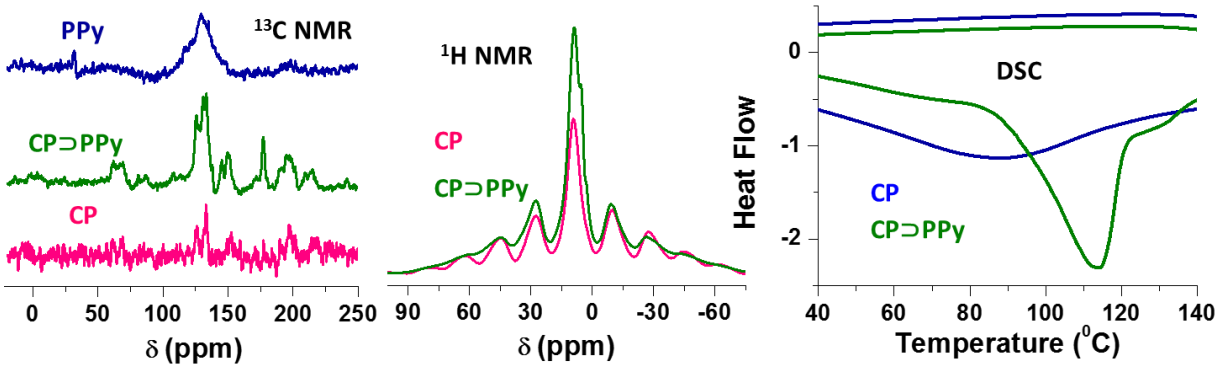

Figure 2B.5: *^{13}C and ^{1}H NMR of CP (pink) and CP⊃PPy (green) material. Differential scanning calorimetric (DSC) thermogram of CP (blue) and CP⊃PPy (green) materials indicating the crystalline nature of composite material.*

To check the crystalline nature of host framework before and after polymerization, PXRD patterns were recorded **(Figure 2B.6)**. The PXRD patterns remained the same after polymerization, indicating the structure of host framework was well preserved. However, a small change in 2θ was exhibited at 7.2°. This implied to the loading of PPy into host matrix and presumably well ordered of PPy chains were formed. Such type of observation was already established in the literatures.[12] For example, Fischer and coworkers, have demonstrated incorporation of [Ru(cod)(cot)] in the MOF-5 and showed appearance of new reflection at 13.8°.[12] They have proposed that the highly ordered packing of [Ru(cod)(cot)] molecules inside

the MOF-5 cavity generated new reflection in 2θ. On the other hand, they determined nice structure of $[(\eta^5\text{-}C_5H_5)_2Fe]_7\supset$MOF-5 by synchrotron radiation where they have observed many more weak intensity diffraction patterns due to presence of guest molecules.[13-15]

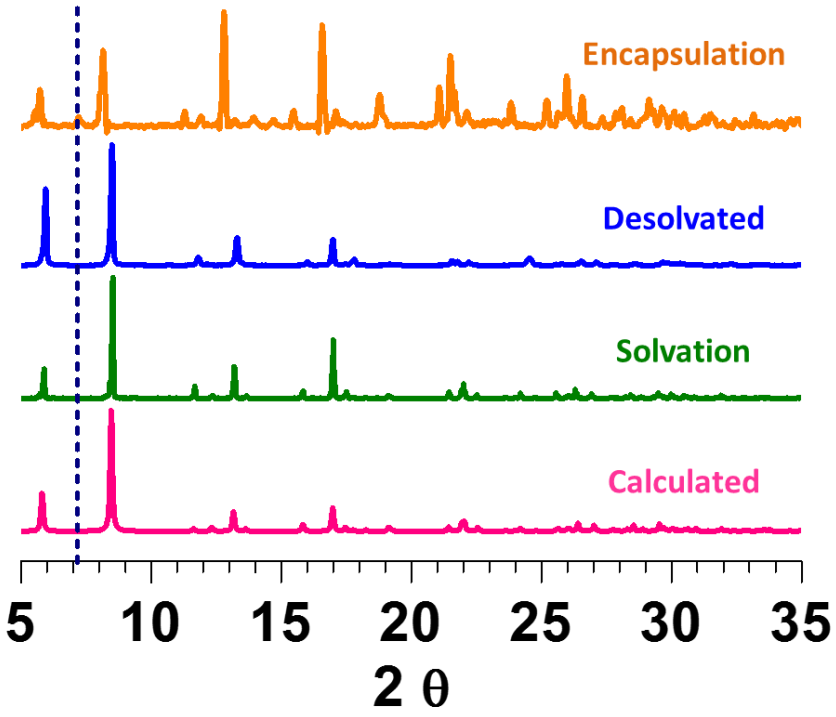

Figure 2B.6: *Powder X-ray diffraction (PXRD) patterns of CP calculated from single-crystal data (pink), as solvation(green), desolvated for activating the CP (blue); after encapsulation of PPy (orange). Blue line emphasizes the appearance of new diffraction due to incorporation of PPy chains.*

PXRD patterns are corroborated by FESEM images. Block shaped micrometer size crystal of CP was clearly visualized under FESEM which retained similar morphology **(Figure 2B.7)** after polymerization with I_2, indicating polymerization did not hamper its structure.[4, 16] Surprisingly, negligible amount of I_2 was detected from EDXS (energy dispersive X-ray spectroscopy), indicating I_2 here acted as an oxidizing agent to polymerize Py monomer to PPy.

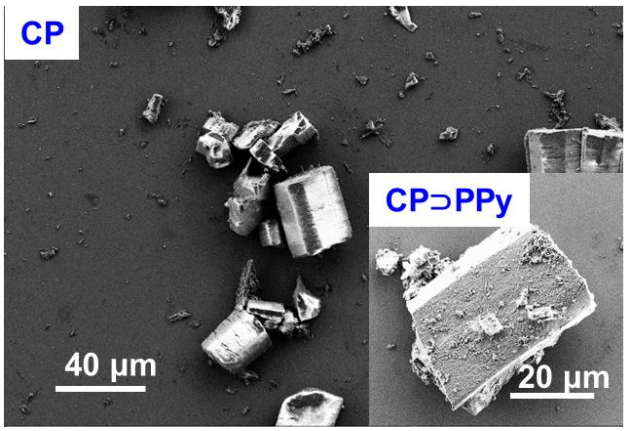

Figure 2B.7: *FESEM images of CP and CP⊃PPy (inset) with scale bar 40 μm and 20 μm; both are identical in morphology.*

To check the habitat where the particular polymerization of Py is taking place (inside or outside of the nanochannel of the framework), gas adsorption measurements were carried out at 195 K for both CP and CP⊃PPy. CO_2 gas adsorption of activated CP was exhibited reversible Type-I adsorption isotherm like microporous materials and the dimension of CP was ~9.5 × 7.8 $Å^2$, indicating the presence of good accessible pores for guest molecules.[3] Whereas dramatic decrease of CO_2 adsorption of (CP⊃PPy) was observed which confirmed that PPy chains were encapsulated in CP **(Figure 2B.8)** and there was no vacant space for CO_2 to sit into the CP nanochannels implying that the pores were blocked by the polymers.[4]

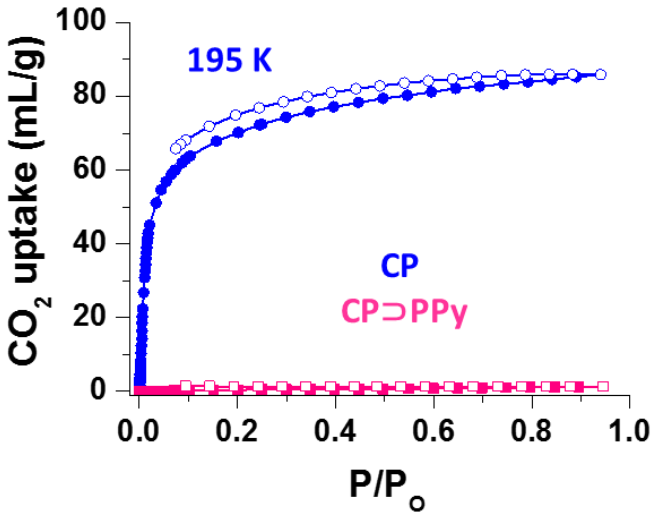

Figure 2B.8: *CO_2 gas adsorption study on CP (blue) and CP⊃PPy (pink) at 195 K. CP was porous in nature whereas CP⊃PPy behaved as non-porous material.*

Various instruments were utilized to measure electrical conductivity of parent and composite materials such as, two-probe, dielectric, and four-probe measurements **(Figure 2B.9)**. Electrical conductivity of CP was found to be ~10^{-12} S/cm by two-probe method **(Figure 2B.10a)**. To check reliability of two-probe conductivity data, dielectric measurement was performed with temperature as well as AC frequency variation **(Figure 2B.10b)**.

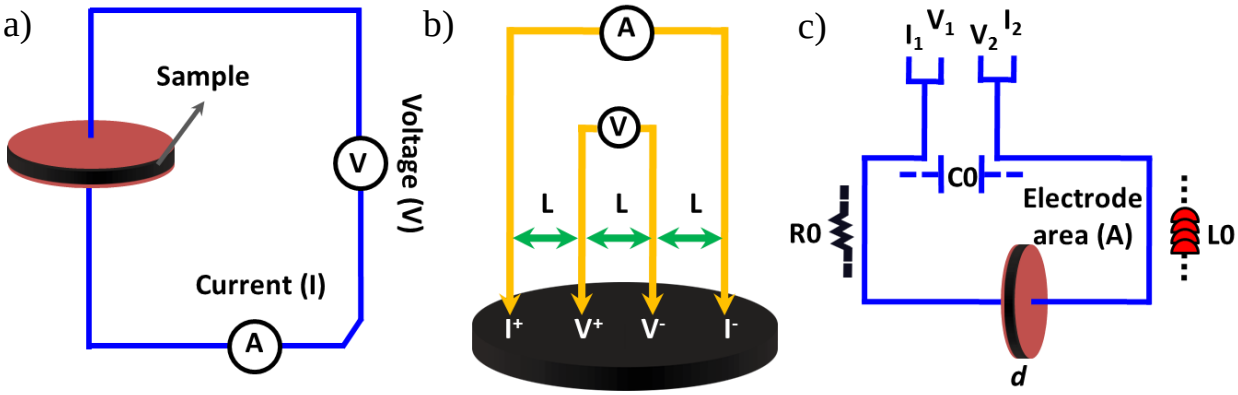

Figure 2B.9: *Schematic representations of dielectric measurement (a), four-probe measurement (b), and two-probe measurement (c).*

In fact, the conductivity value at room temperature with lower frequency was equivalent to two-probe measurement.[17] The conductivity value was extracted by applying the equation:

σ *(conductivity)* $= (2\pi \times f \times C_p \times D \times t)/A$ *(S/m)*

Where f is the frequency, C_p is the capacitance, D is dielectric loss, and t and A are the thickness of the sample and cross-sectional area of the electrode, respectively. Interestingly, with changing temperature the conductivity value remained almost unaltered whereas on varying the AC frequency the conductivity value changed.[18] By increasing frequency, the conductivity value reached ~10^{-10} S/cm which could have been due to heterogeneous interfacial polarization of CP made of organic linkers which have their intrinsic conductivity. Both two-probe and dielectric showed similar conductivity value ~10^{-12} S/cm which confirmed the material to be insulator. The electrical conductivity of CP⊃PPy was recorded in conventional four-probe method and drastic improvement of electrical conductivity was observed and the value reached upto ~10^{-3} S/cm **(Figure 2B.10b)**. Almost billion times enhancement of conductivity have been achieved. Such improvement may be due to the insertion of conducting polymer. It is not expected every time that if conducting polymer is inside a porous material, it will increase

conductivity. For example, by incorporation of conducting polyaniline filament in the salt form inside the MCM host could not enhance its conductivity.[19] The conductivity value of PANI-MCM was ~10^{-8} S/cm comparable with bare MCM material.

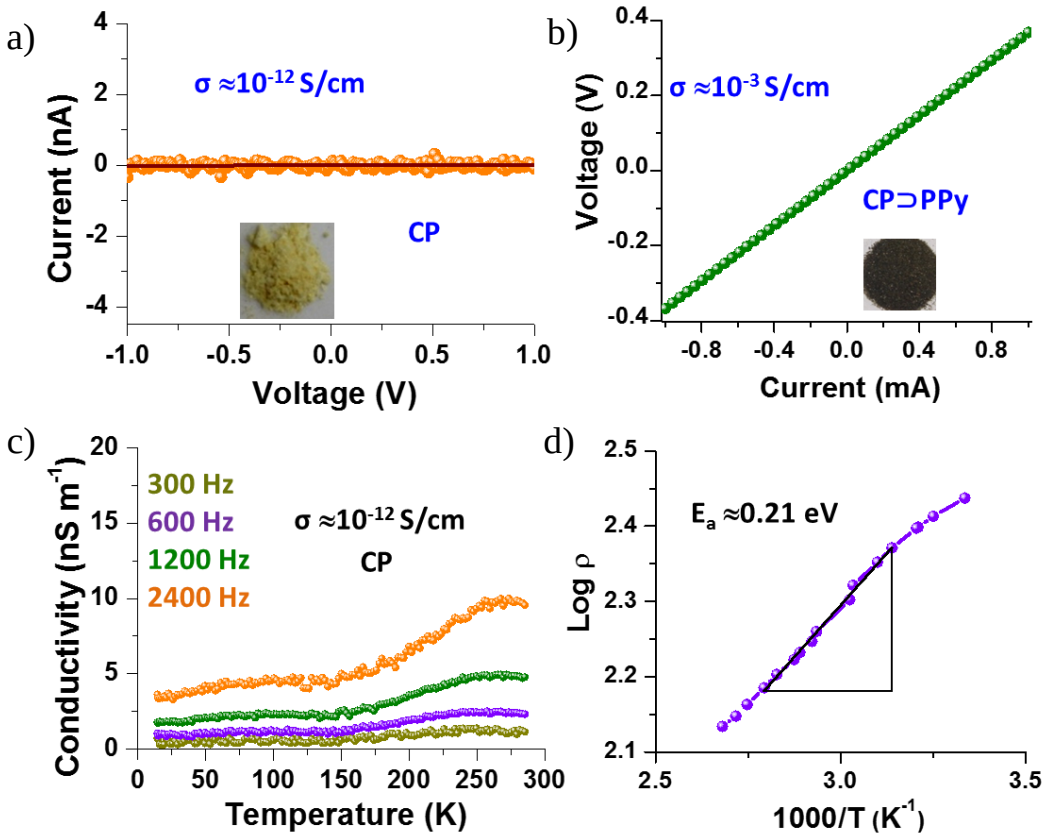

Figure 2B.10: *(a) Two probe I-V measurement of CP(inset powder CP); (b) Conductivity versus temperature plots acquired from frequency-dependent dielectric measurements of CP. (c) Four probe I-V measurement of CP⊃PPy (inset powder CP⊃PPy) (d) linear fit of log ρ Vs. 1000/T plot and extraction of activation energy of CP⊃PPy.*

However, the extracted polyaniline was highly conducting (~10^{-2} S/cm) and very thin filament like. So, conducting polymer loading into any cavity is not the primary criteria for enhancement of electrical conductivity. Furthermore, an optimal condition has to be applied for polymerization. Time is one of the parameter and for complete polymerization in the CP nanochannels, it requires ~ 36 h **(Figure 2B.11b)**. The temperature dependent conductivity measurement was done from room temperature to 100 ^{o}C and conductivity increased with temperature. The CP⊃PPy material was observed to be of semiconducting nature from temperature dependent I-V measurement with activation energy ~0.2 eV like organic based

semiconducting materials **(Figure 2B.10d, 11a)**. Electrical conductivity and activation energy of material from four-probe instrument was calculated by applying the following equations.

$$\rho = \rho_o / G$$

$\rho_0 = 2\pi S.(V/I)$; where S= probe distance, V= potential difference between two probes, I= applied current and G is the constant. Conductivity $(\sigma) = (1/\rho)$. Activation energy $(E_a) = 2.303 \times 10^3 \times 2k \times (slope)$. The slope between log of resistivity $(log\rho)$ and reciprocal of the temperature $(10^3/T)$.

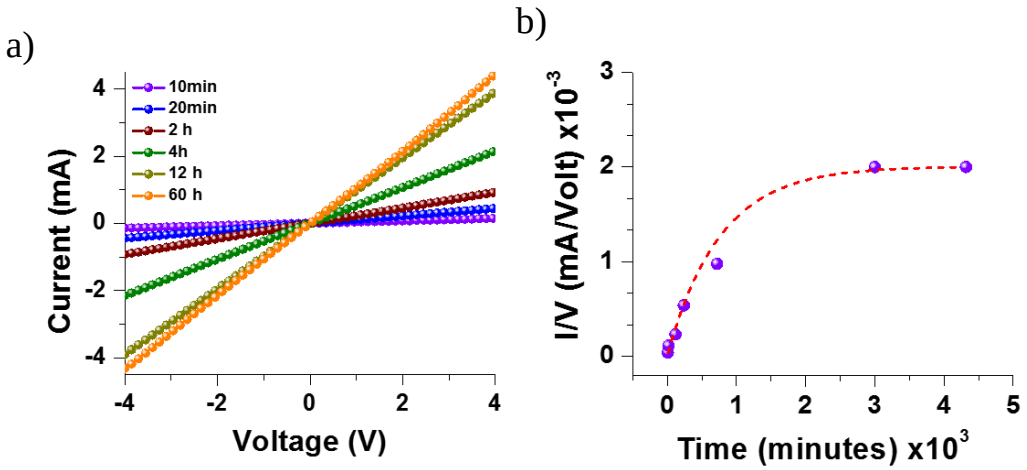

Figure 2B.11: *Time dependent (a) I* Vs *V measurements and I/V* Vs *time (b) plots.*

For the processability of CP⊃PPy, a thin film was fabricated on a flexible substrate and it also exhibited the equivalent electrical identity with bulk material **(Figure 2B.12).**

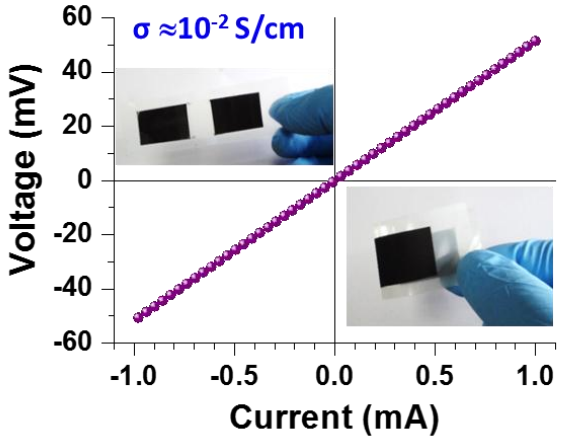

Figure 2B. 12: *I-V measurement of CP⊃PPy on flexible substrate (inset: flexibility of the material).*

The electronic and semiconducting properties were further investigated by Hall-effect measurement **(Figure 2B.13)**. Various parameters were extracted from this measurement such as Hall coefficient (R_H), high-carrier density (η), Hall mobility (μ) and carrier type.

B = magnetic field, l = length of the sample, t = thickness of the sample, w = width, I_x = current V_H =Hall voltage = ($R_H \cdot I \cdot B/t$), R_H = Hall coefficient, carrier density (η) = $1/(R_H \cdot e)$, Hall mobility (μ) = (R_H/ρ), and ρ = resistivity.

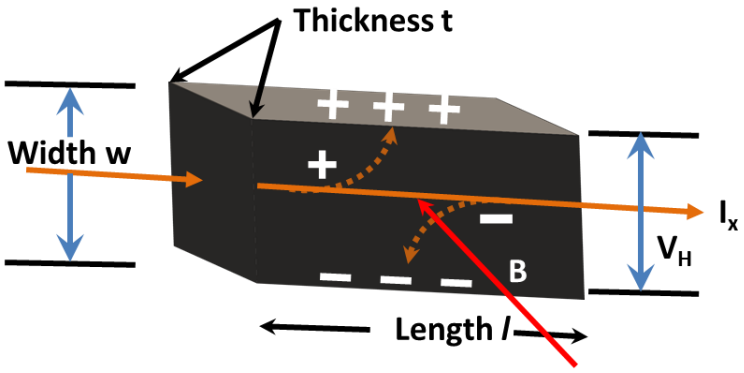

Figure 2B.13: *Schematic representation of Hall effect measurement.*

The Hall coefficient value of CP⊃PPy was ~− 42.0 cm^3C^{-1} and negative sign of R_H indicated that the material was n-type semiconductor and electrons are the majority of carrier. Carrier density of CP⊃PPy is very high and its value is ~1.5×10^{17} cm^{-3}. Furthermore, the Hall mobility (μ) and resistivity (ρ) were found to be ~8.15 cm^2 V^{-1} s^{-1} and ~5.15 Ohm cm, respectively. However, such types of measurement mainly for CP based materials are very rare. One of the examples was transformation of insulating p-type Co-NDC to n-type conducting material by doping with I_2.[20-21] Still their carrier density (~5×10^{11} cm^{-3}) value is very much less compared to our. Our results from Hall Effect measurements were quite comparable with inorganic based classical semiconductor like doped GaAs and conducting PPy based materials.[22]

Now the question that arises is why such remarkable enhancement in conductivity? To get possible mechanism for electrical enhancement, various control experiments were performed such as conductivity and fluorescent measurement. Conductivity value of PPy synthesised using I_2 in cyclohexane was estimated to be ~10^{-7} S/cm **(Figure 2B.14)** and bare CP was exhibited ~10^{-12} S/cm.[4] Notably, if it was additive phenomena, conductivity value should have appeared in between 10^{-12} S/cm and 10^{-6} S/cm. However, such expectation was not fulfilled; it

is neither 10^{-12} S/cm nor 10^{-6} S/cm. On the other hand, conductivity of I_2 incorporated CP found to be ~10^{-7} S/cm although very negligible amount of I_2 in CP was noticed. These control experiments clearly signified that there must be some another reason for such unusual enhancement of conductivity.

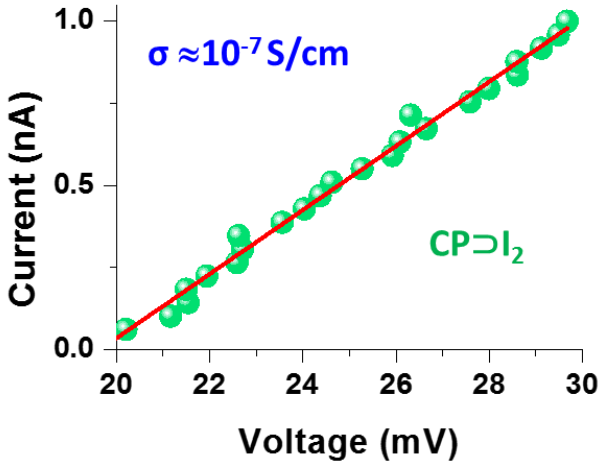

Figure 2B. 14: *Four probe I-V measurement of CP⊃I_2.*

This CP is very much fluorescent in nature and this is mainly ligand based fluorescence.[3, 23] Upon exciting CP with 300 nm, various emissions were appeared below 450 nm which were mainly generated from ligand itself in solid state **(Figure 2B.15a)**. Surprisingly, significant retention in fluorescence intensity in the same emission range of CP⊃PPy was exhibited upon exciting with same wavelength (300 nm). In addition, new emission band appeared at ~520 nm which could be due to formation of exciplex between NDC moiety (ligand) and PPy chain or π–π interaction involving ligand and PPy. In fact, this interaction could provide another path for electronic interaction.[24] Notably, no such interaction was found when the solution state fluorescence spectra of H_2NDC and H_2NDC+Py were recorded **(Figure 2B.15b)** which clearly suggested that the confinement effect was possible only in presence of CP. Host-guest interaction and as well as confinement effect could be elaborated from the solid-state UV−vis spectra.[25] CP⊃PPy material exhibited a new band, which appeared at the IR region and went upward higher from ~620 nm, possibly due to the formation of typically polaron/bipolaron band in PPy indicating that PPy became highly doped state. This phenomenon would decrease the overall E_a value of the system. Interestingly, such type of band was not present in externally polymerized Py. Overall, the possible reasons for incredible enhancement of electrical conductivity by almost billion times were; i) formation of filament (1D) like highly order thin

PPy nanofiber, detected from FESEM image likewise previous work by Chun-Yang Zhang group and also Thomas Bein group,[4, 19] ii) confinement effect of the PPy chain,[26-27] and iii) electronic interaction between host and the guest chain.[28]

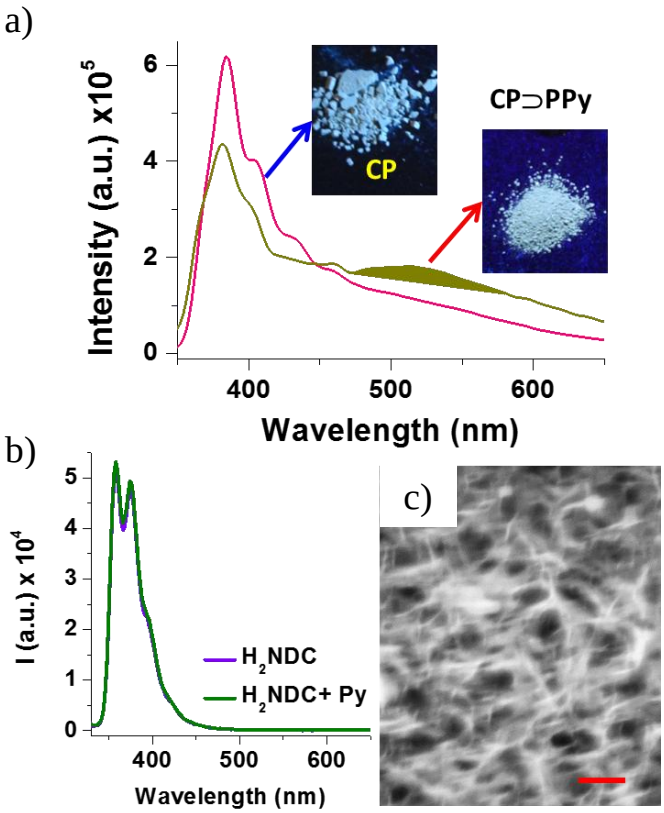

Figure 2B.15: *(a) Solid state fluorescence spectra of CP (pink) and CP⊃PPy (yellow) with λ_{ex}= 300 nm; inset, fluorescence images of their respective under commercial UV lamp with λ_{ex}= 265 nm, (b) liquid state UV-vis spectra of H_2NDC and H_2NDC+Py. (c) FESEM image of extracted PPy, showing thin fibrous nature (Scale bar 200 nm).*

IIB.3. Conclusions

In a nutshell, we have validated the billion fold (~10^9) improvement of electrical conductivity of an insulating redox-inactive cadmium based CP by infiltration of conducting PPy in its 1D nanochannel. Insulator material to semiconducting material transformation was achieved and I_2 was used as extraneous oxidising agent for oxidative polymerisation of Py. Finally, such incredibly high conductivity enhancement in redox-inactive coordination polymer system is due to the formation of exciplex/ π–π interaction/ N-H–π interaction, confinement effect allowing percolating conducting paths for electron hopping.

References

1. Nagarkar, S. S.; Joarder, B.; Chaudhari, A. K.; Mukherjee, S.; Ghosh, S. K. Highly Selective Detection of Nitro Explosives by a Luminescent Metal–Organic Framework. *Angew. Chem., Int. Ed.* **2013,** *52*, 2881.

2. Surya, S. G.; Nagarkar, S. S.; Ghosh, S. K.; Sonar, P.; Ramgopal Rao, V. OFET based explosive sensors using diketopyrrolopyrrole and metal organic framework composite active channel material. *Sensors and Actuators B: Chemical* **2016,** *223*, 114.

3. Nagarkar, S. S.; Chaudhari, A. K.; Ghosh, S. K. Selective CO_2 Adsorption in a Robust and Water-Stable Porous Coordination Polymer with New Network Topology. *Inorg. Chem.* **2012,** *51*, 572.

4. Wang, Q.-X.; Zhang, C.-Y. Oriented Synthesis of One-Dimensional Polypyrrole Molecule Chains in a Metal-Organic Framework. *Macromol. Rapid Commun.* **2011,** *32*, 1610.

5. Yanai, N.; Uemura, T.; Ohba, M.; Kadowaki, Y.; Maesato, M.; Takenaka, M.; Nishitsuji, S.; Hasegawa, H.; Kitagawa, S. Fabrication of Two-Dimensional Polymer Arrays: Template Synthesis of Polypyrrole between Redox-Active Coordination Nanoslits. *Angew. Chem., Int. Ed.* **2008,** *47*, 9883.

6. Dhara, B.; Ballav, N. In situ generation of conducting polymer in a redox-active metal-organic gel. *RSC Adv.* **2013,** *3*, 4909.

7. Patil, A. O.; Heeger, A. J.; Wudl, F. Optical properties of conducting polymers. *Chem. Rev.* **1988,** *88*, 183.

8. Wang, L.; Schindler, J.; Thomas, J. A.; Kannewurf, C. R.; Kanatzidis, M. G. Entrapment of Polypyrrole Chains between MoS_2 Layers via an in Situ Oxidative Polymerization Encapsulation Reaction. *Chem. Mater.* **1995,** *7*, 1753.

9. Udum, Y. A.; Pekmez, K.; Yıldız, A. Electropolymerization of self-doped polythiophene in acetonitrile containing FSO_3H. *Synth. Met.* **2004,** *142*, 7.

10. Uemura, T.; Kadowaki, Y.; Yanai, N.; Kitagawa, S. Template Synthesis of Porous Polypyrrole in 3D Coordination Nanochannels. *Chem. Mater.* **2009,** *21*, 4096.

11. Toshima, N.; Hara, S. Direct Synthesis of Conducting Polymers from Simple Monomers. *Prog. Polym. Sci.* **1995,** *20*, 155.

12. Schröder, F.; Esken, D.; Cokoja, M.; van den Berg, M. W. E.; Lebedev, O. I.; Van Tendeloo, G.; Walaszek, B.; Buntkowsky, G.; Limbach, H.-H.; Chaudret, B.; Fischer, R. A. Ruthenium Nanoparticles inside Porous $[Zn_4O(bdc)_3]$ by Hydrogenolysis of Adsorbed

[Ru(cod)(cot)]: A Solid-State Reference System for Surfactant-Stabilized Ruthenium Colloids. *J. Am. Chem. Soc.* **2008,** *130*, 6119.

13. Rosler, C.; Fischer, R. A. Metal-organic frameworks as hosts for nanoparticles. *CrystEngComm* **2015,** *17*, 199.

14. Kim, H.; Chun, H.; Kim, G.-H.; Lee, H.-S.; Kim, K. Vapor phase inclusion of ferrocene and its derivative in a microporous metal-organic porous material and its structural characterization by single crystal X-ray diffraction. *Chem. Commun.* **2006**, 2759.

15. Meilikhov, M.; Yusenko, K.; Fischer, R. A. The adsorbate structure of ferrocene inside $[Al(OH)(bdc)]_X$ (MIL-53): a powder X-ray diffraction study. *Dalton Trans.* **2009**, 600.

16. Chaudhari, A. K.; Mukherjee, S.; Nagarkar, S. S.; Joarder, B.; Ghosh, S. K. Bi-porous metal-organic framework with hydrophilic and hydrophobic channels: selective gas sorption and reversible iodine uptake studies. *CrystEngComm* **2013,** *15*, 9465.

17. Singh, D.; Singh, N. L.; Qureshi, A.; Kulriya, P.; Tripathi, A.; Avasthi, D. K.; Gulluoglu, A. N. Radiation induced modification of dielectric and structural properties of Cu/PMMA polymer composites. *J. Non-Cryst. Solids* **2010,** *356*, 856.

18. Joo, J.; Lee, J. K.; Lee, S. Y.; Jang, K. S.; Oh, E. J.; Epstein, A. J. Physical Characterization of Electrochemically and Chemically Synthesized Polypyrroles. *Macromolecules* **2000,** *33*, 5131.

19. Wu, C.-G.; Bein, T. Conducting Polyaniline Filaments in a Mesoporous Channel Host. *Science* **1994,** *264*, 1757.

20. Lee, D. Y.; Lim, I.; Shin, C. Y.; Patil, S. A.; Lee, W.; Shrestha, N. K.; Lee, J. K.; Han, S.-H. Facile interfacial charge transfer across hole doped cobalt-based MOFs/TiO_2 nano-hybrids making MOFs light harvesting active layers in solar cells. *J. Mater. Chem. A* **2015,** *3*, 22669.

21. Lee, D. Y.; Kim, E.-K.; Shrestha, N. K.; Boukhvalov, D. W.; Lee, J. K.; Han, S.-H. Charge Transfer-Induced Molecular Hole Doping into Thin Film of Metal–Organic Frameworks. *ACS Appl. Mater. Interfaces* **2015,** *7*, 18501.

22. Shinohara, K.; Motokawa, T.; Kasahara, K.; Shimomura, S.; Sano, N.; Adachi, A.; Hiyamizu, S. Electrical properties of Si-doped GaAs layers grown on (411) A GaAs substrates by molecular beam epitaxy. *Semicond. Sci. Technol.* **1996,** *11*, L125.

23. Kreno, L. E.; Leong, K.; Farha, O. K.; Allendorf, M.; Van Duyne, R. P.; Hupp, J. T. Metal–Organic Framework Materials as Chemical Sensors. *Chem. Rev.* **2012,** *112*, 1105.

24. Gould, I. R.; Young, R. H.; Mueller, L. J.; Farid, S. Mechanisms of Exciplex Formation. Roles of Superexchange, Solvent Polarity, and Driving Force for Electron Transfer. *J. Am. Chem. Soc.* **1994,** *116*, 8176.

25. Uemura, T.; Uchida, N.; Asano, A.; Saeki, A.; Seki, S.; Tsujimoto, M.; Isoda, S.; Kitagawa, S. Highly Photoconducting π-Stacked Polymer Accommodated in Coordination Nanochannels. *J. Am. Chem. Soc.* **2012,** *134*, 8360.

26. Bein, T.; Enzel, P. Encapsulation of Polypyrrole Chains in Zeolite Channels. *Angew. Chem., Int. Ed.* **1989,** *28*, 1692.

27. Yamamoto, J.; Furukawa, Y. Electronic and Vibrational Spectra of Positive Polarons and Bipolarons in Regioregular Poly(3-hexylthiophene) Doped with Ferric Chloride. *J. Phys. Chem. B* **2015,** *119*, 4788.

28. MacLean, M. W. A.; Kitao, T.; Suga, T.; Mizuno, M.; Seki, S.; Uemura, T.; Kitagawa, S. Unraveling Inter- and Intrachain Electronics in Polythiophene Assemblies Mediated by Coordination Nanospaces. *Angew. Chem., Int. Ed.* **2016,** *55*, 708.

Section-IIC

Modulation of Conductivity in Bimetallic Coordination Polymer

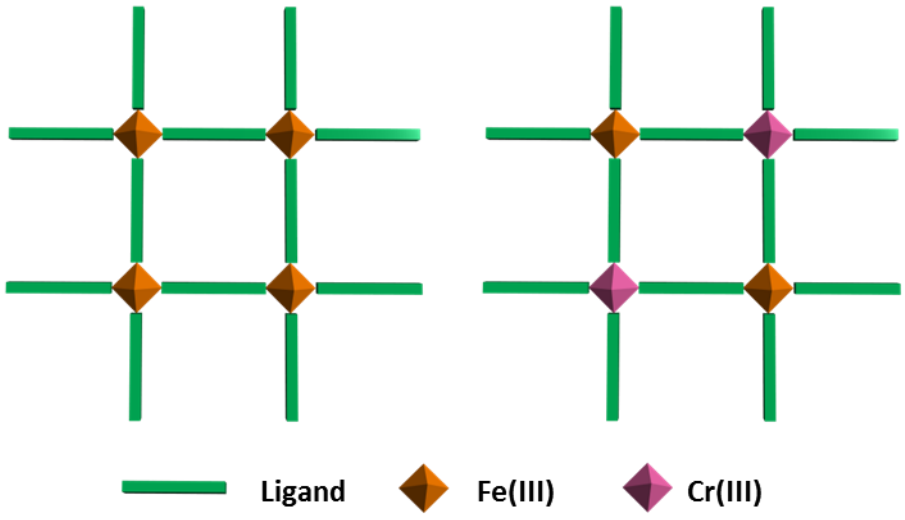

IIC.1. Introduction

In previous sections (Section-IIA and IIB), electrical conductivity of coordination polymers (CPs) were enhanced via incorporation of conducting polymers such as polypyrrole (PPy) and polythiophene (PTh) so called an extrinsic approach. Dincă and coworkers have shown million-fold enhancement of electrical conductivity of CPs by only modifying the coordination metal center from Mn(II) to Fe(II) (intrinsic approach). Herein, we are motivated by this work. Instead of changing metal ion, we are rather interested in bimetallic CPs for tuning the electrical conductivity.

As a prototype, we have prepared bimetallic CPs with Fe(III) and Cr(III) metal ions and 1,3,5 benzenetricarboxylic acid ligand (BTC) and examine the electrical properties.

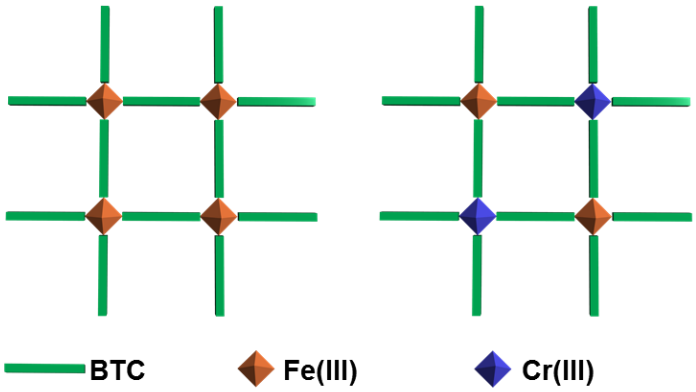

Figure 2C.1: *Schematic representations of Fe-BTC (monometallic) and Fe -BTC-Cr (bimetallic). Brown and blue polyhedrons represent the iron and chromium metal ions respectively. Green rod represents the BTC ligand.*

IIC.2. Materials and Methods

Ferric nitrate, chromium nitrate and 1,3,5-benzenetricarboxylic acid were purchased from Sigma Aldrich.

Fourier transform infrared (FTIR) spectra were recorded in a NICOLET 6700 spectrophotometer using KBr pellet. Solid-state UV-Vis spectra were measured with a Perkin–Elmer Lambda 900 spectrophotometer equipped with an integrating sphere in the 250–800 nm range. Kubelka–Munk function was applied to convert reflectance spectra into equivalent absorption spectra using the reflectance of $BaSO_4$ as reference. Field emission scanning

electron microscope (FESEM) imaging and energy-dispersive X-ray spectroscopy (EDXS) analysis were performed in a Carl-Zeiss Ultra microscope. Transmission electron microscopy (TEM) images were recorded in Philips CM200 instrument. X-ray photoelectron spectra (XPS) of powder sample was obtained in Phi 5000 Versa Probe-2 instrument equipped with a monochromatic Al Kα (1486.6 eV) X-ray source and a hemispherical electron analyzer. The DC conductivity values were measured by Four-probe technique using Keithley 6221 AC and DC current sourcemeter and 2182A Nanovoltmeter. The powder X-ray diffraction (PXRD) patterns of all xero-gels were recorded from 2θ = 5 to 35 degree at room-temperature in Bruker D8 advanced diffractometer. The Hall-effect measurements were performed using five-probe method in Quantum Design-PPMS-Evercool II instrument at room-temperature.

Monometallic CPs were prepared by mixing metal ions (iron/chromium) with BTC ligand in ethanol in accordance with previously reported literature.[1] In brief, to synthesize Fe-BTC gel, equal amount (mole) of ferric nitrate (0.6 mmole; 242.4 mg) and BTC (0.6 mmole; 126.0 mg) were dissolved in 4 ml ethanol and subsequently, mixed together with sonication **(Figure 2C.2)**. Similarly, Cr-BTC gel was synthesized by dissolving BTC (42.4 mg, 0.2 mmole) and chromium nitrate (80.0 mg, 0.2 mmole) in 5 ml ethanol separately. Both solutions were mixed together with sonication and kept at 80 ^{0}C for 4 hr for gelation **(Figure 2C.2)**. Both the gels were dried to form xero-gels under vacuum at room temperature.

Bimetallic gel was prepared with similar procedure, 0.6 mmole of mixed metal (ferric nitrate : chromium nitrate = 1:1) and 0.6 mmole of BTC were dissolved in 4 ml ethanol solvent each and both the solutions were rapidly mixed together and kept at room temperature. To prepare xero-gel, wet gel was dried under vacuum at room temperature. Different ratios of iron and chromium bimetallic gels were prepared by similar procedure **(Figure 2C.2)**.

IIC.3. Results and Discussion

Gelation was firstly confirmed by the vial inversion method. Gel formation indicated the coordination between metal ion (Fe(III)/Cr(III)) and organic ligand **(Figure 2C.2)**. The colour of pure Cr-BTC and Fe-BTC was green and orange respectively whereas Fe-BTC-Cr was wine in colour **(Figure 2C.2; inset)**. Such colour change was due to ligand to metal charge transfer (LMCT) interaction, suggesting the substitution of metal ion in xero-gels.[2]

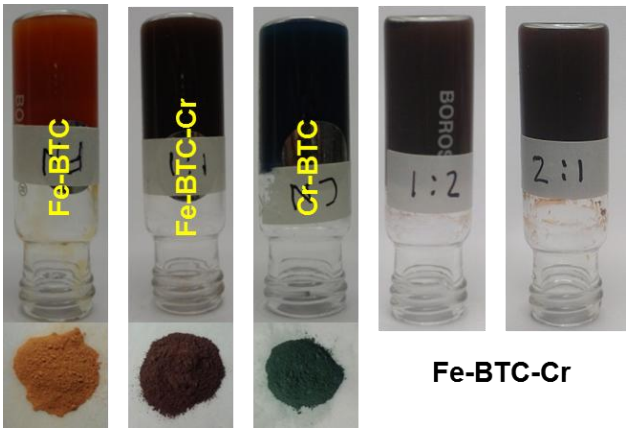

Figure 2C.2: *Preparation of monometallic and Fe-BTC-Cr (1:1) bimetallic gels. Inset: xero-gels of Fe-BTC (orange), Fe-BTC-Cr (wine) and Cr-BTC (green); Photograph of different wet gels with various iron, chromium ratios 1:2 and 2:1 (from left to right).*

Formation of Fe-BTC and Cr-BTC was confirmed by FTIR and Raman spectroscopy **(Figure 2C.3)**. In FTIR spectra, C=O stretching vibration of BTC at ~1730 cm^{-1} was clearly shifted to 1630 cm^{-1} indicating the formation of metal-oxygen bond in CP.[1, 3] Moreover, stretching vibrations at ~470 cm^{-1} and ~525 cm^{-1} were detected which represents Fe-O and Cr-O bonds, respectively. Similar observation was found in Raman spectra. Overall, the formation of metal-oxygen bonds was proved.

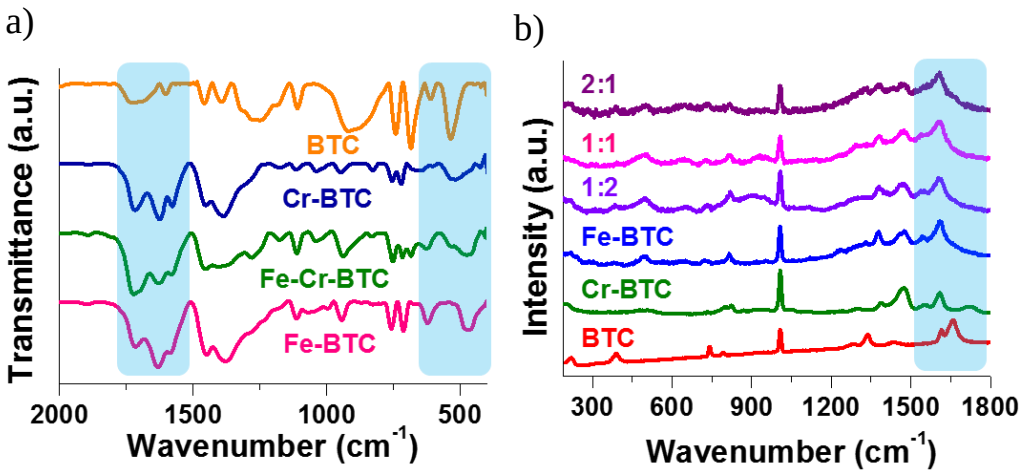

Figure 2C.3: *(a) FTIR spectra of BTC (orange), Cr-BTC (blue), Fe -BTC-Cr (green) and Fe-BTC (pink) clearly indicate the bond formation between metal ion and BTC ligand. (b) Raman spectra of BTC (red), Cr-BTC (green), Fe-BTC (blue), 1:2 (violet), 1:1(pink), and 2:1(violet).*

Earlier, Dinca and coworkers have shown electrical conductivity to be highly dependent on central metal ions.[4] Indeed, similar observation was found and the electrical conductivity values of Fe-BTC and Cr-BTC were found to be ~10^{-5} S/cm and ~10^{-8} S/cm respectively **(Figure 2C.4)**. In fact, with this observation, one can easily speculate the manipulation of conductivity in between the two values by taking together (Fe(III) and Cr(III)) in single platform with different ratios. However, two metal ions in one CP is very difficult. It needs to satisfy following criteria, i) both metal ions coordinate with ligand and ii) homogeneous distribution of both metal ions throughout the samples. With the hope of synthesizing bimetallic CPs, different stoichiometric ratios of metal ions Fe(III) and Cr(III) were mixed together with BTC ligand. Surprisingly, different bimetallic CPs were distinguished and their colour was entirely different from original one which was the primary indication of hybrid CPs (Fe-BTC-Cr).

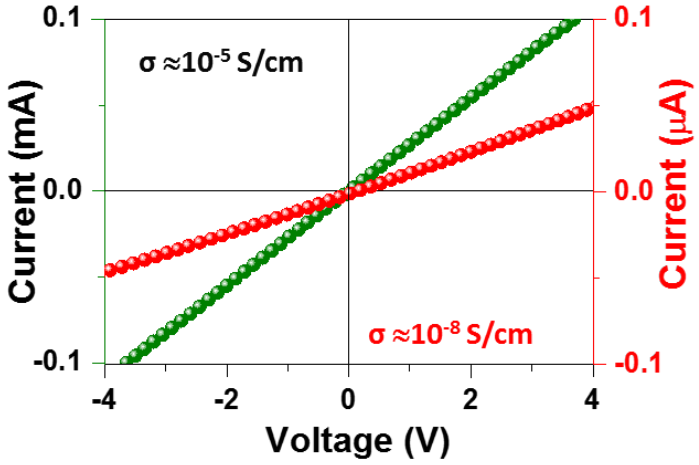

Figure 2C.4: *Four-probe conductivity of Fe-BTC (green) and Cr-BTC (red).*

Morphology of xero-gels was examined based on various microscopic techniques such as FESEM and TEM. As shown in **Figure 2C.5a** Fe-BTC sample consisted of micrometre sized irregular crystalline blocks, whereas Cr-BTC exhibited globular/fibrous morphology **(Figure 2C.5b)**. Regular cuboids morphology **(Figure 2C.5c)** was noticed in bimetallic Fe-BTC-Cr (1:1) system thereby, indicating Fe-BTC-Cr adopting the Fe-BTC structure. Similar observation was found in the TEM image and selected-area electron diffraction (SAED) pattern revealed the crystalline nature **(Figure 2C.5d; inset)**.

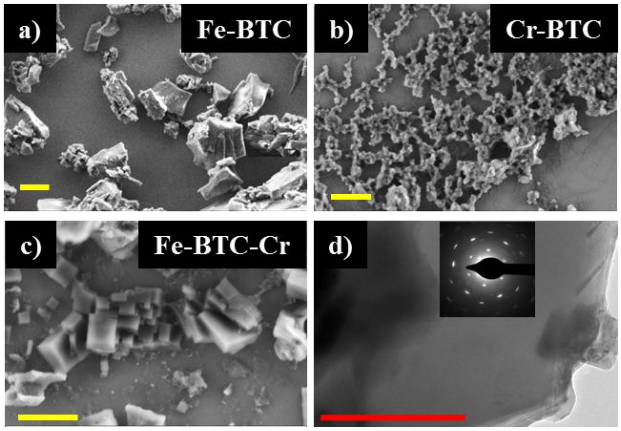

Figure 2C.5: *FESEM images of Fe-BTC, Cr-BTC and Fe-BTC-Cr (a, b, and c) with scale bar of 2μm. (d) TEM image of Fe-BTC-Cr (1:1) sample (inset: SAED pattern) with scale bar 200nm.*

Distribution of the metal ions was scrutinized by using energy-dispersive X-ray spectroscopy (EDXS) analysis attached with FESEM instrument. Interestingly, homogeneous distribution of both the metal ions was found in Fe-BTC-Cr sample **(Figure 2C.6)**. Metal ions' ratios were also examined which were matching with our feeding moles **(Figure 2C.6)**. This phenomenon was well in agreement with synthesizing of desired bimetallic CPs.

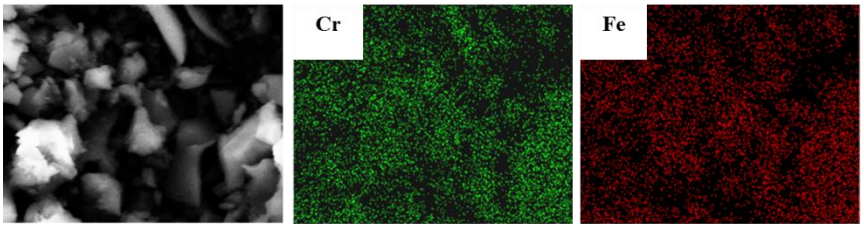

Sample	Fe	Cr
1:1	1.59	1.48
1:1	0.20	0.21
2:1	4.63	1.98
2:1	0.59	0.25
1:2	0.12	0.21
1:2	0.24	0.52

Figure 2C.6: *Elemental mapping of elements; Cr, Fe, C and O from FESEM and EDXS analysis of bimetallic analogues.*

PXRD patterns of xero-gels were corroborating the electron microscopic images. Monometallic analogues Cr-BTC and Fe-BTC were observed to be amorphous and crystalline in nature respectively. Moreover, PXRD pattern of Fe-BTC-Cr was similar to Fe-BTC, suggesting Fe-BTC-Cr was adopting the Fe-BTC structure **(Figure 2C.7)**.

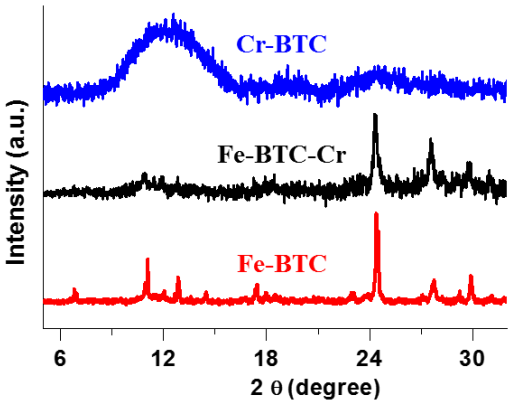

Figure 2C.7: *PXRD patterns of Fe-BTC (red), Fe-BTC-Cr (1:1) (black) and Cr-BTC (blue).*

If these two monometallic systems were finely mixed mechanically, conductivity value is expected to lie in between their individual values. Indeed, the conductivity value was observed to be ~10^{-6} S/cm-an intermediate value of their monometallic analogues **(Figure 2C.8a)**. Surprisingly, the conductivity value of bimetallic system was remarkably enhanced which was neither comparable of their individual values nor intermediate value **(Figure 2C.8b)**. Conductivity of Fe-BTC-Cr (1:1) was estimated to be in the range of 10^{-4} to 10^{-3} S/cm which was of ~10^{2} fold higher than that of Fe-BTC and ~10^{4} fold higher than that of Cr-BTC.

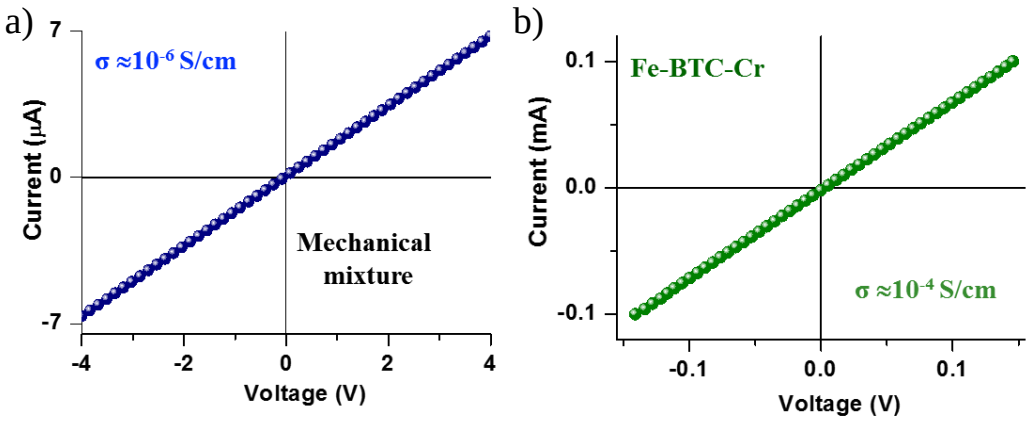

Figure 2C.8: *Four-probe I-V measurements of Fe-BTC+Cr-BTC mechanical mixture (a) and Fe-BTC-Cr (1:1) (b).*

The electrical conductivity of the xero-gels with possible combinations of Fe(III) and Cr(III): 1:1, 2:1 and 1:2 were found to be ~10^{-3}, ~10^{-5}, and ~10^{-5} S/cm respectively, which is quite exciting and perhaps, showing the high level tunability in the valence and conduction bands (VB and CB). Notably, highest conductivity was observed in the 1:1 Fe-BTC-Cr **(Figure 2C.9)**. The *I-V* curve of Fe-BTC-Cr was ohmic in nature **(Figure 2C.8)**, suggesting the probable molecular arrangement in the system was D-A-D-A type.

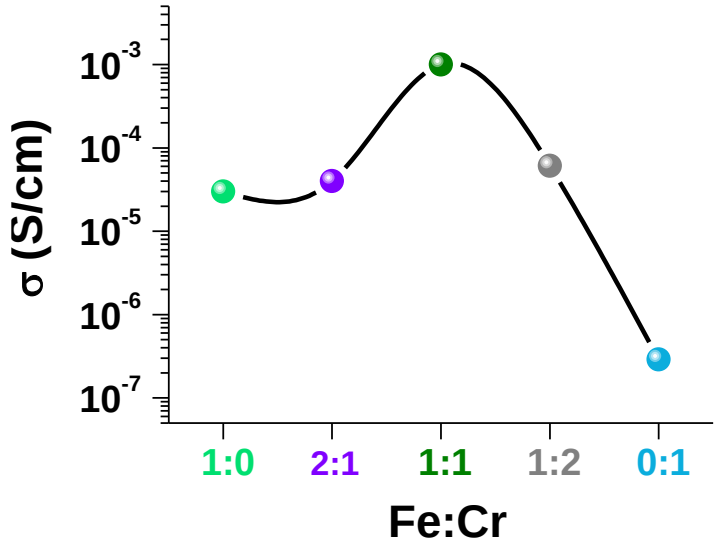

Figure 2C.9: *Four-probe conductivity values of different ratios of iron and chromium.*

To further investigate the possible reasons behind the unprecedented enhancement of electrical conductivity for bimetallic CPs, solid-state UV-Vis measurement was performed for all the xero-gels **(Figure 2C.10)**. The major bands such as ~430 nm (Cr-BTC) and ~466 nm (Fe-BTC) appeared due to ligand to metal charge transfer state alongwith an extra peak at ~700 nm was observed for the bimetallic analogues which could be attributed to the formation of new hybrid charge transfer state **(Figure 2C.10; inset)**.

Optical band gaps were calculated by applying Kubelka-Munk theory in the order; Cr-BTC < Fe-BTC < Fe-BTC-Cr was observed. As a result conductivity enhancement was found in bimetallic analogues.

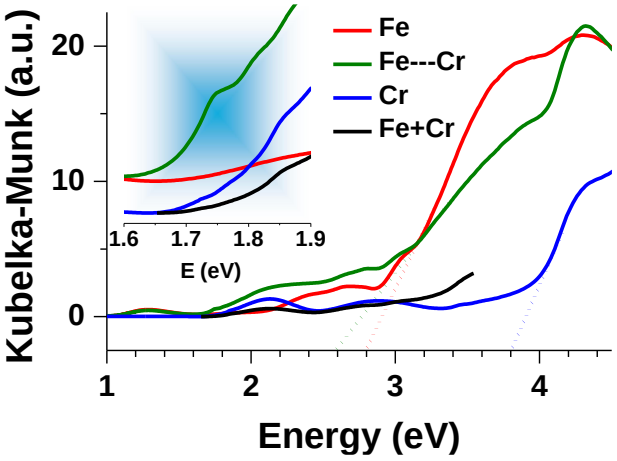

Figure 2C.10: *Solid-state UV-Vis spectra of all xero-gels; Fe-BTC (red), Fe-BTC-Cr (green), Cr-BTC (blue) and mechanical mixture (black). Inset; zoom-in part of the spectra (1.6-1.9 eV).*

To verify, the oxidation state of iron in Fe-BTC and bimetallic analogues colorimetric tests were performed. After addition of ammonium acetate in acidified Fe-BTC and bimetallic analogues **(Figure 2C.11)**, the solution colour turned to red, indicating the presence of Fe(III). Furthermore, Ferroin test was performed to detect Fe(II) in xero-gels and no colour change was observed which indicated the absence of Fe(II).[5]

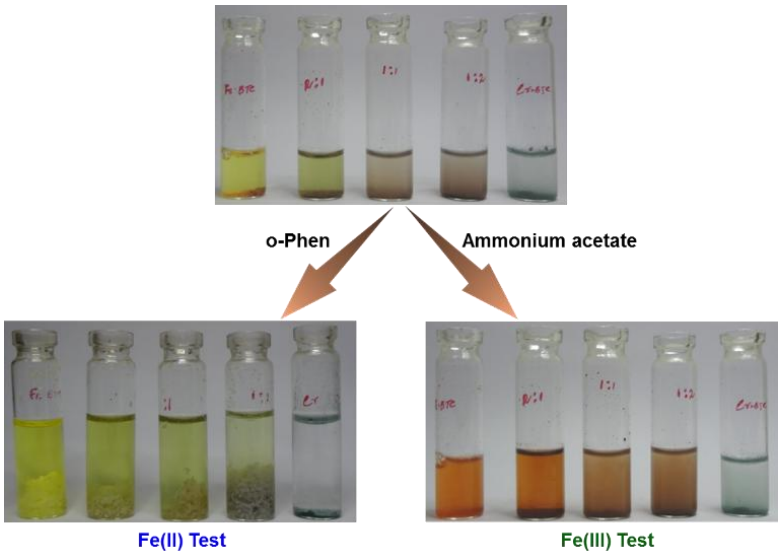

Figure 2C.11: *Chemical test for existence of Fe(II)/Fe(III).*

Colorimetric test was supported by XPS data **(Figure 2C.12)** which revealed the existence of Fe(III) and Cr(III) and no signatures of Fe(II) or Cr(II) was observed. [6-7]

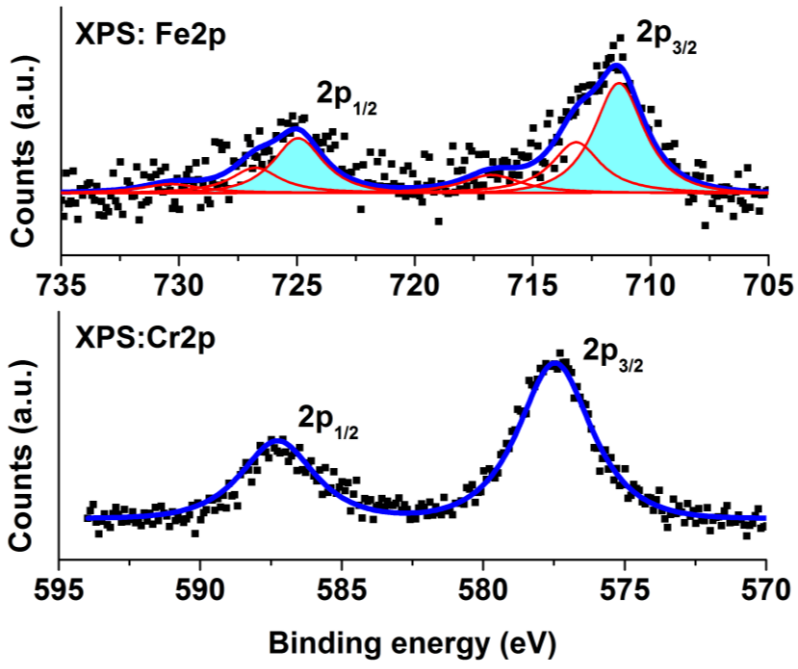

Figure 2C.12: *XPS data of Fe 2p and Cr 2p represented the presence of Fe(III) and Cr(III) in Fe-BTC-Cr (1:1) sample.*

Hall-effect measurement of xero-gels was performed to investigate the possible reason for the unusual enhancement in electrical conductivity. Generally, conductivity of a material depends on two factors; carrier density and carrier mobility. Carrier concentration was found to be similar in all the xero-gels **(Table 1)**. However, carrier mobility is enhanced heavily for Fe-BTC-Cr in comparison to monometallic analogues. This tremendous increase in the mobility

Table 1. Calculated various parameters from Hall-Effect measurement of CPs

Parameters	Fe-BTC	Cr-BTC	Fe-BTC-Cr (1:1)	1:2	2:1
Semiconductor	P-type	n-type	n-type	n-type	P-type
Hall coefficient (R_H)($cm^3\ C^{-1}$)	≈1 x 10^3	≈-8.2 x 10^4	≈-1.5 x 10^4	≈-2.2 x 10^5	≈2.5 x 10^4
Resistivity (ρ) (Ohm cm)	≈3.33 x 10^4	≈3.45 x 10^6	≈1 x 10^3	≈4.0 x 10^4	≈3.95 x 10^4
Carrier density (η) (cm^{-3})	≈6.24x 10^{15}	≈7.61 x 10^{13}	≈4.2 x 10^{14}	≈2.8x 10^{13}	≈2.5 x 10^{14}
Carrier mobility (μ) ($cm^2\ V^{-1}\ s^{-1}$)	≈0.03	≈0.0024	≈15	≈5.5	≈0.63
Conductivity (σ) ($S\ cm^{-1}$)	≈3 x 10^{-5}	≈2.9 x 10^{-7}	≈1x10^{-3}	≈2.5x10^{-5}	≈2.53 x 10^{-5}

for bimetallic analogues is proffered to reduction of energy barrier for hopping of ‘‘Coulomb holes’’ by Coulomb attraction. Such high mobility could be the main origin of high conductivity value of the bimetallic analogues and these systems could be highly ordered arrangements of Fe and Cr in alternative fashion. It stands out that mobility value of our Fe-BTC-Cr bimetallic CP is one of the best amongst the reported mobility values of various CPs, metal-organics and organic-based semiconductors.[8-11]

IIC.4. Conclusions

A new strategy has been developed to enhance the electrical conductivity of CPs. Unusual enhancement of carrier moblility is the probable reason behind such phenomenon. Further, this elevated value of conductivity and mobility has been assigned to the donor-acceptor assembly and high order of crystallinity. Picking and choosing the appropriate combinations of metal ions, this strategy can be applied to a broad class of CPs.

References

1. Xiang, S.; Li, L.; Zhang, J.; Tan, X.; Cui, H.; Shi, J.; Hu, Y.; Chen, L.; Su, C.-Y.; James, S. L. Porous organic-inorganic hybrid aerogels based on Cr^{3+}/Fe^{3+} and rigid bridging carboxylates. *J. Mater. Chem.* **2012,** *22*, 1862.

2. Cui, Y.; Yue, Y.; Qian, G.; Chen, B. Luminescent Functional Metal–Organic Frameworks. *Chem. Rev.* **2012,** *112*, 1126.

3. Mahmood, A.; Xia, W.; Mahmood, N.; Wang, Q.; Zou, R. Hierarchical Heteroaggregation of Binary Metal-Organic Gels with Tunable Porosity and Mixed Valence Metal Sites for Removal of Dyes in Water. *Sci. Rep.* **2015,** *5*, 10556.

4. Sun, L.; Hendon, C. H.; Minier, M. A.; Walsh, A.; Dincă, M. Million-Fold Electrical Conductivity Enhancement in Fe_2(DEBDC) versus Mn_2(DEBDC) (E = S, O). *J. Am. Chem. Soc.* **2015,** *137*, 6164.

5. Dhara, B.; Patra, P. P.; Jha, P. K.; Jadhav, S. V.; Pavan Kumar, G. V.; Ballav, N. Redox-Induced Photoluminescence of Metal–Organic Coordination Polymer Gel. *J. Phys. Chem. C* **2014,** *118*, 19287.

6. Liu, R.; Zhu, X.; Chen, B. A New Insight of Graphene oxide-Fe(III) Complex Photochemical Behaviors under Visible Light Irradiation. *Sci. Rep.* **2017,** *7*, 40711.

7. Manning, B. A.; Kiser, J. R.; Kwon, H.; Kanel, S. R. Spectroscopic Investigation of Cr(III)- and Cr(VI)-Treated Nanoscale Zerovalent Iron. *Environ. Sci. Technol.* **2007,** *41*, 586.

8. Nikitenko, V. R.; Tameev, A. R.; Vannikov, A. V. Mechanism of enhanced mobility and conductivity at donor–acceptor organic interfaces. *Organic Electronics* **2011,** *12*, 589.

9. Alves, H.; Pinto, R. M.; Maçôas, E. S. Photoconductive response in organic charge transfer interfaces with high quantum efficiency. *Nat. Commun.* **2013,** *4*, 1842.

10. Fu, B.; Baltazar, J.; Hu, Z.; Chien, A.-T.; Kumar, S.; Henderson, C. L.; Collard, D. M.; Reichmanis, E. High Charge Carrier Mobility, Low Band Gap Donor–Acceptor Benzothiadiazole-oligothiophene Based Polymeric Semiconductors. *Chem. Mater.* **2012,** *24*, 4123.

11. Kraus, M.; Richler, S.; Opitz, A.; Brütting, W.; Haas, S.; Hasegawa, T.; Hinderhofer, A.; Schreiber, F. High-mobility copper-phthalocyanine field-effect transistors with tetratetracontane passivation layer and organic metal contacts. *J. Appl. Phys.*, **2010,** *107*, 094503.

Chapter-III

Photoluminescence Property of Redox-Active Coordination Polymer

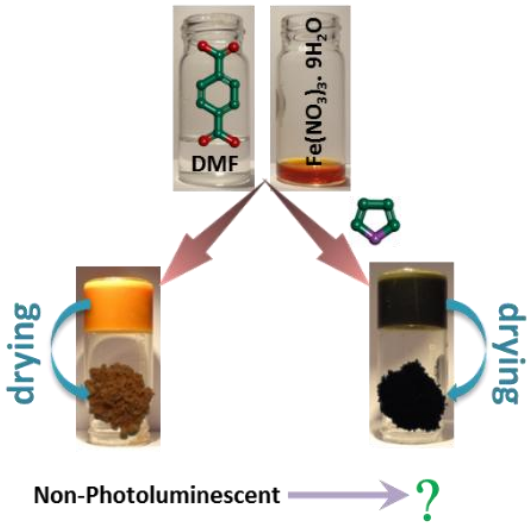

III.1. Introduction

In previous chapter (Section-IIA), we have demonstrated the redox-property of CPs in terms of electrical conductivity enhancement. Redox-active CPs are reported to be non-photoluminescent whereas, redox-inactive CPs with metal ions such as, Zn(II), Cd(II), Al(III), In(III) etc. are found to be photoluminescent (PL). Even if a PL active ligand was deliberately taken during the synthesis of CPs with redox-active metal-ions such as Fe(III), its PL activity will be quenched eventually. Therefore, it is really a challenging task to bring PL into a redox-active system, which motivates us to enter into this work.

As a prototype, we have synthesized redox-active Fe(III) based CP with 1,4-benzenedicarboxylic acid (TPA) ligand and investigated the PL property by incorporating various small molecules such as aniline (Ani), pyrrole (Py), thiophene (Th), bithiophene (BTh), cylopentadiene (CPD) and toluene (Tol).

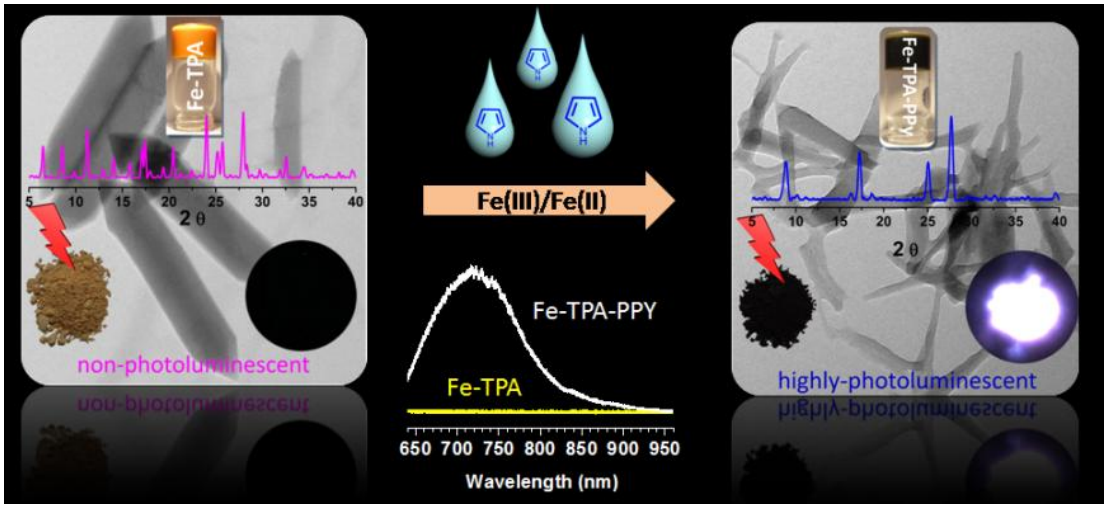

Figure 3.1: *Schematic illustration of turn on photoluminescence in redox-active CP.*

III.2. Materials and Methods

Ferric nitrate ($Fe(NO_3)_3.9H_2O$) (Fe), 1,4-benzenedicarboxylic acid (TPA) and various monomers like aniline (Ani), pyrrole (Py), thiophene (Th), bithiophene (BTh), toluene (Tol), p-xylene (p-Xy) and cylopentadiene (CPD) were purchased from Sigma Aldrich (India) and used after necessary purifications.

Fourier transform infrared (FTIR) spectra were measured on NICOLET 6700 FTIR Spectrophotometer using KBr Pellets. The morphological features of the gel and its hybrid materials were recorded in Zeiss Ultra Plus field-emission scanning electron microscopy (FESEM) (3kV). TEM images were obtained in a Philips CM200 machine (200kV). Powder X-ray diffraction patterns (PXRD) were recorded on Bruker D8 Advanced X-Ray diffractometer at room temperature using Cu-Kα radiation (λ= 1.5406Å) with tube voltage of 40 kV and current of 35 mA and scan speed of 0.5° $min^{-1}$and a step size of 0.01° in 2θ. Solid and liquid state UV-Vis spectra were recorded on Perkin Elmer Lambda UV/Vis spectrophotometer. DC conductivity was measured using conventional four-probe method using Keithley 2182A nanovoltmeter and 6221 DC and AC current sourcemeter on pressed pellets. PL spectra of xero-gels and wet gels were recorded on an ultraclean glass slide with use of a high-resolution confocal Raman microscope (Lab RAMHR, Horbia Jobin Yvon) with a 60X objective lens. Here both 532 nm and 633 nm LASERs were used to record PL spectra. Gas adsorption measurements were performed with a BELSORP max instrument.

In a typical synthesis process, 6 mmole of ferric nitrate and 6 mmole TPA were dissolved in 3mL ethanol and 18 mL dimethyl formamide (DMF) respectively. These two solutions were mixed together with vigorous sonication. After 7-8 h, an orange colored Fe-TPA gel was found and gelation was confirmed by inversion vial test method **(Figure 3.2)**. Following the same procedure, composite materials like Fe-TPA-Py, Fe-TPA-Ani, Fe-TPA-BTh, Fe-TPA-Tol, Fe-TPA-Th, Fe-TPA-p-Xyand Fe-TPA-CPD were prepared by using various monomers such as Py, Ani, BTh, Tol, Th and CPD respectively (monomers are added in TPA solution and monomer: TPA=1:1). Importantly, the gelation process was not hampered in the presence of the monomers. Wet gels were dried under vacuum heating to form xero-gels **(Figure 3.2; inset)**. In case of Fe-TPA-Py, Fe-TPA-Ani, Fe-TPA-BTh xero-gels were immersed in 0.5 M aqueous NH_3 solution and subsequently, washed with water and methanol to remove TPA and metal ions. Finally, extracted dark materials were isolated and dried under vacuum.

III.3. Results and discussion

Significant colour change from brown to black was observed as we dried composite wet-gels, indicating the formation of polymers/oligomers into the matrix. However, colour change was not observed in other systems, Fe-TPA-Th, Fe-TPA-Tol and Fe-TPA-CPD, suggesting no such type of polymerization/oligomerization was taking place.[1]

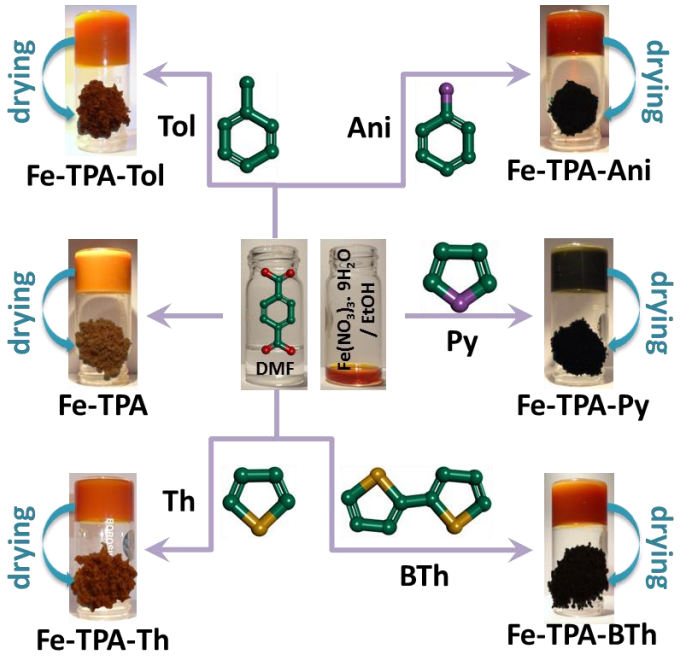

Figure 3.2: *Synthesis of gels in presence of small molecules and their respective xero-gel colour (down to the vial).*

FESEM images of Fe-TPA showed spindle like structure **(Figure 3.3a)** which was complemented by TEM image **(Figure 3.3d)**. Such spindle like structures were previously reported in the literature for Fe(III) and TPA based material namely MIL-88 (Fe).[2-6] Interestingly, in the present case the spindle like structures were transformed to fibrous networks for all black composite materials **(Figure 3.3; inset)**.

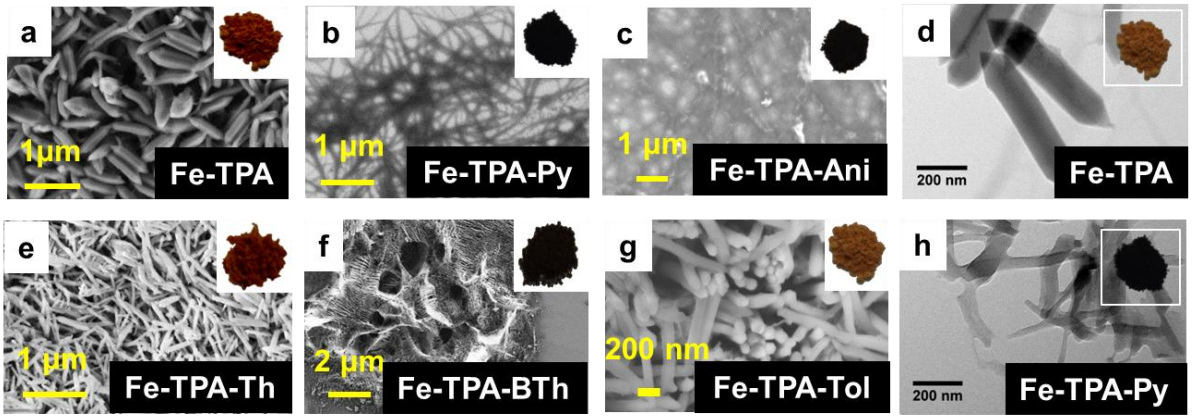

Figure 3.3: *FESEM images of Fe-TPA (a), Fe-TPA-Py (b), Fe-TPA-Ani (c), Fe-TPA-Th (e), Fe-TPA-BTh (f) and Fe-TPA-Tol (g). TEM images of Fe-TPA (d), Fe-TPA-Py (h).*

Such a remarkable structural transformation from spindle to nano-fiber clearly indicated the reactivity of small molecules. Notably, this transformation was also observed from TEM images **(Figure 3.3d, h)**. On the other hand, morphological features of Fe-TPA-Th, Fe-TPA-Tol, Fe-TPA-p-Xy and Fe-TPA-CPD systems **(Figure 3.4 and Figure 3.3g)** were similar to that of Fe-TPA. Overall, retention or changing morphology is directly correlated with colour change of the xero-gels.

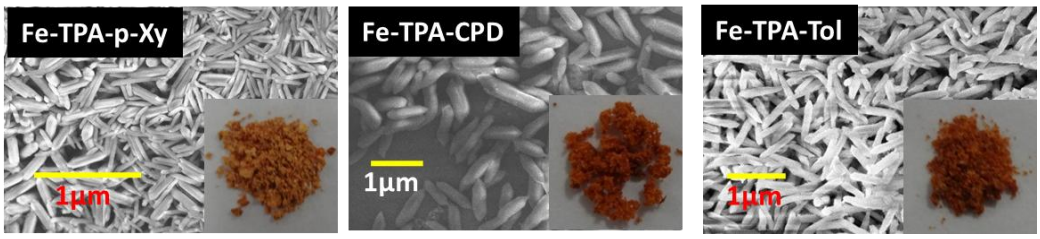

Figure 3.4: *FESEM images of Fe-TPA-p-Xy, Fe-TPA-CPD and Fe-TPA-Tol.*

The SEM/TEM data are complemented by the PXRD patterns **(Figure 3.5)**. The PXRD pattern of Fe-TPA showed various diffraction peaks indicating crystalline nature. Similar PXRD patterns were observed in case of orange xero-gels (Fe-TPA-Th, Fe-TPA-Tol, and Fe-TPA-CPD), suggesting small molecules such as Th, Tol and CPD were not hampering the crystal structure **(Figure 3.5)**. However, significant changes in PXRD patterns were observed in the black xero-gels, indicating the higher activity of Py, Ani and BTh compared to other monomers (Th,CPD, p-Xy and Tol) **(Figure 3.5)**.

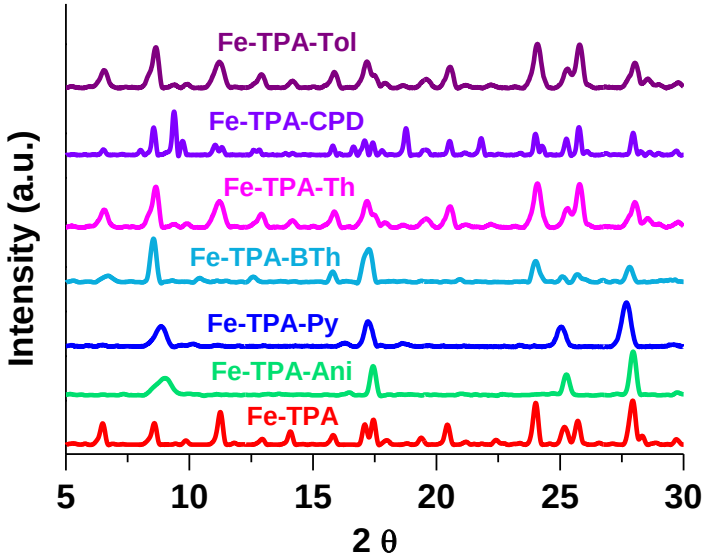

Figure 3.5: *PXRD patterns of Fe-TPA (red), Fe-TPA-Ani (green), Fe-TPA-Py (blue), Fe-TPA-BTh (cyan), Fe-TPA-Th (pink), Fe-TPA-CPD (violet) and Fe-TPA-Tol (purple).*

PL spectra of all the xero-gels were investigated using optical setup as shown in **Figure 3.6a** attached with both green (532 nm) and red (633 nm) LASERs having 1 milli-watt power and acquisition time for each spectrum was 2 sec. When xero-gels were excited with green laser (532 nm) or red laser (633 nm), xero-gels appeared to be green or red respectively **(Figure 3.6b)**.[7,8]

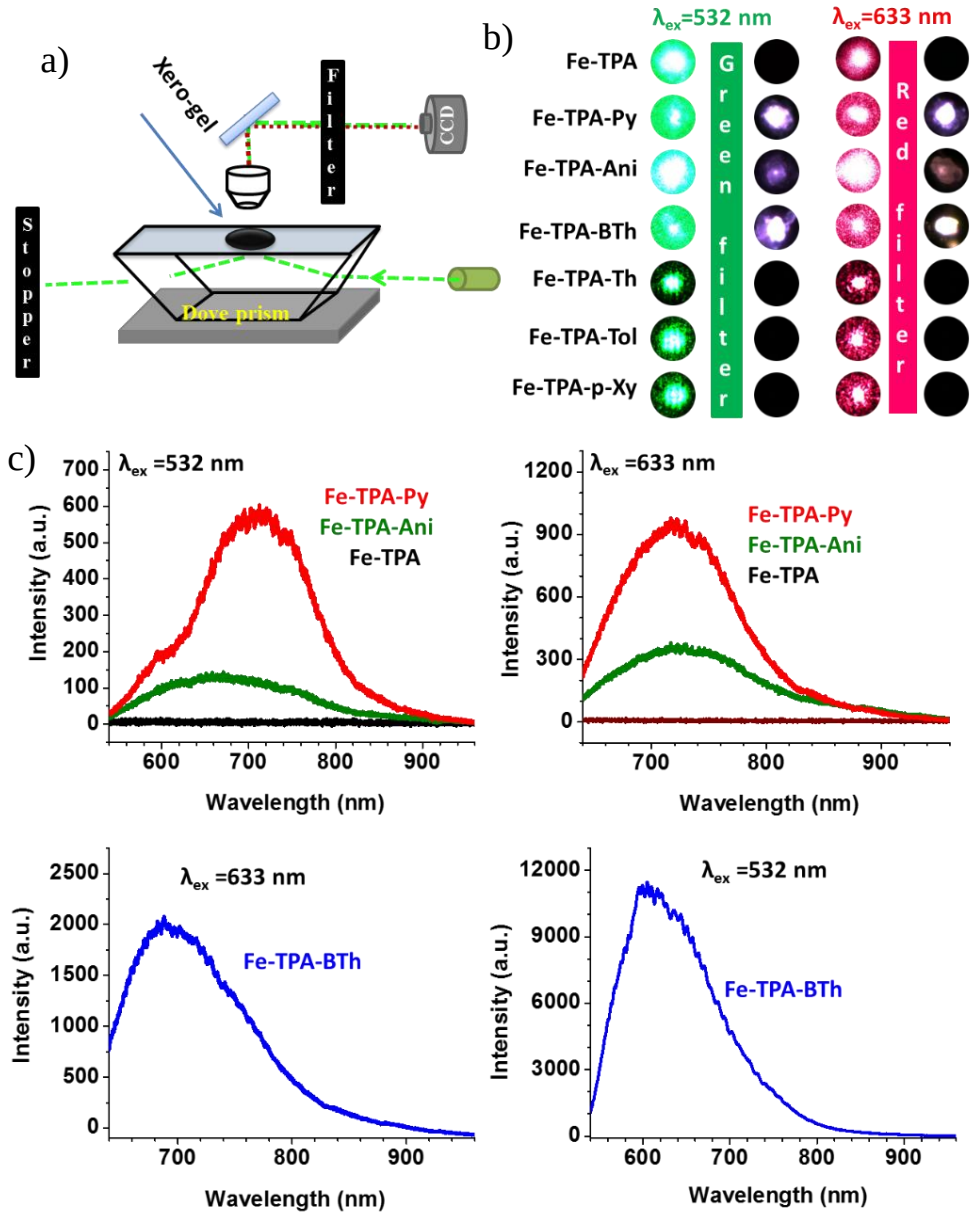

Figure 3.6: *(a) Schematic illustration of the optical setup for an evanescent-field imaging. High-intensity green (λ_{ex} = 532 nm) and red (λ_{ex} = 633 nm) LASER sources and respective filters were used to record the PL images (b) and spectra (c).*

However, these colours appeared from the primary laser sources. To avoid the interference of primary light, respective green and red edge-filters were applied and only black hybrid xero-gels (Fe-TPA-Py, Fe-TPA-Ani and Fe-TPA-BTh) were appeared to be PL. Orange coloured xero-gels (Fe-TPA-Th, Fe-TPA-Tol and Fe-TPA-CPD) including Fe-TPA were found to be PL inactive under either of the LASERs. However, black hybrid xero-gels showed PL maximum between 500 nm to 800 nm regions with intensity order Fe-TPA-BTh⟩ Fe-TPA-Py⟩ Fe-TPA-Ani **(Figure 3.6c)**. In summary, such small reactive molecules (Ani, Py and BTh) could generate PL within redox-active CPs.

To check the origin of PL, we performed i) colorimetric test (Ferroin test), and ii) magnetic measurement. In Ferroin test, o-phenanthroline (o-phen) was used to detect the presence of Fe(II) ions in samples. When o-phen was added in the acidic solutions of composite materials (Fe-TPA-BTh, Fe-TPA-Py, Fe-TPA-Ani), the colors were found to be red, indicating the presence of Fe(II). However, Fe-TPA remained inert, indicating the existence of Fe(III) instead of Fe(II) **(Figure 3.7)**.

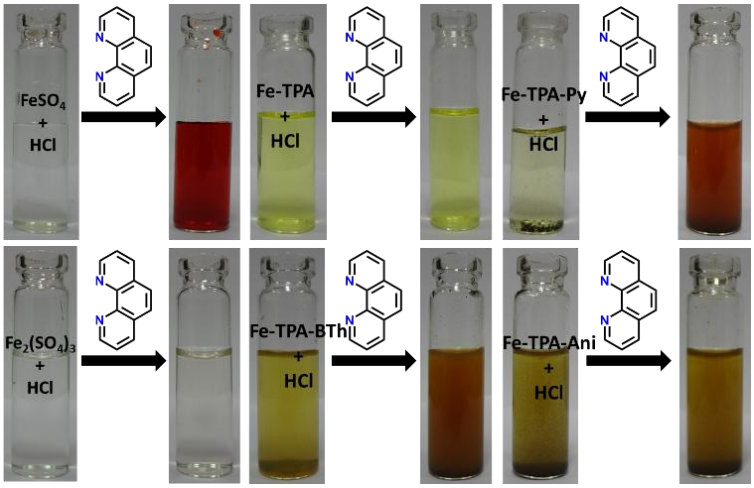

Figure 3.7: *Presence of Fe(II) ions in the Fe-TPA-Py, Fe-TPA-Ani and Fe-TPA-BTh hybrid xero-gels were chemically identified by Ferroin-test. $Fe_2(SO_4)_3$ and $FeSO_4$ were used as standard samples.*

To further support our observation, magnetic measurements **(Figure 3.8)** of xero-gels were performed likewise previous chapter (chapter-IIA).[1] In the present scenario, we have observed the magnetization value increased in case of black hybrid material (Fe-TPA-Ani) compared to Fe-TPA, possibly due to a change in the oxidation-state of Fe ion.

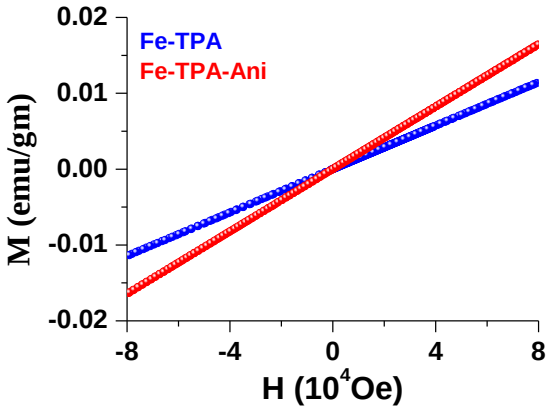

Figure 3.8: *Room temperature magnetization vs applied field (M-H) plot of Fe-TPA (blue) and Fe-TPA-ani (red).*

We have successfully demonstrated the PL activity in a redox-active CP. Furthermore, to check its origin, the PL activity of gel ingredients (Fe, TPA and polypyrrole (PPy)) and mechanical mixture of Fe(III) and TPA were recorded using 532 nm (green) laser excitation.[26, 31 9,104] Interestingly, gel ingredients as well as mechanical mixture (Fe+TPA) remained inactive **(Figure 3.9)**.

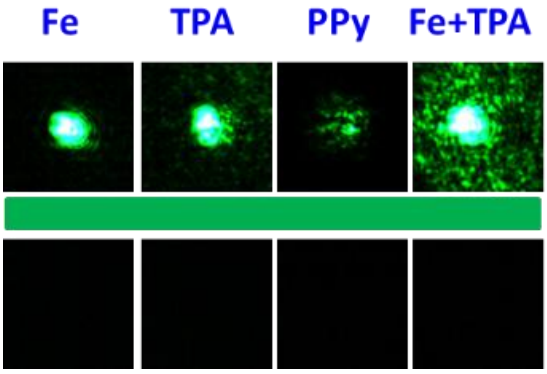

Figure 3.9: *PL images of xero-gel ingredients and mechanical mixture with green LASER excitation.*

Moreover, PL spectra of all small molecules (Py, Ani and BTh) were recorded with the same laser excitation and found to be PL inactive. To clarify the origin of PL, various indirect experiments were performed. For example, PL spectra were recorded for all possible combinations of TPA, Fe, polyaniline (PANI), polypyrrole (PPy), polythiophene (PTh). No PL was observed from any of the combinations, indicating mechanical mixtures are not responsible for turn-on PL **(Figure 3.10)**. Furthermore, when we deliberately combine Fe(III) with a highly fluorescent ligand (TCA), that PL was totally quenched due to the d-orbital participation of

metal ion.[11] Overall, the controlled experiments, made us realize that ligand, metal ions or polymers were not responsible for turn-on PL responses **(Figure 3.10)**.

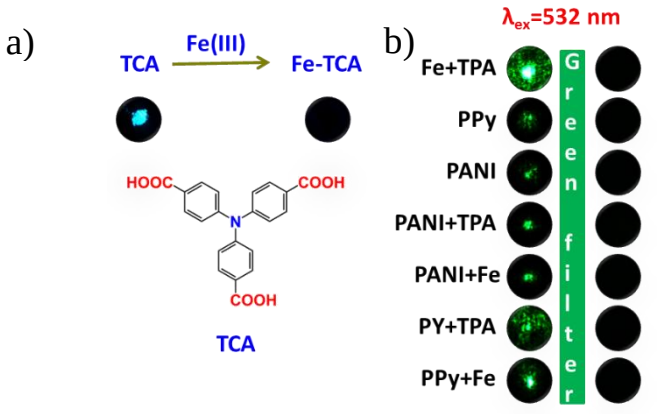

Figure 3.10: *(a) Photoluminescence is quenched in presence of Fe(III) ions. (b) Photoluminescence images of mechanical mixtures of various combinations.*

Moreover, *insitu* incorporation of conducting polymers in Fe-TPA was checked likewise section-IIA. Both parent Fe-TPA and monomer (Py/BTh) were taken in $CHCl_3$ and refluxed

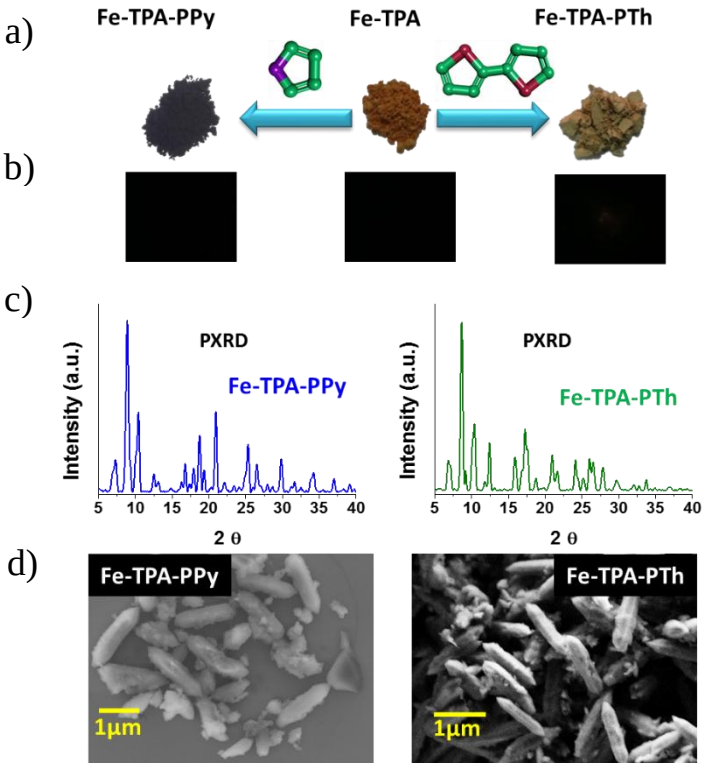

Figure 3.11: *Insitu polymerization of Py and BTh (a). PL images (b) PXRD patterns (c) and morphology (d) of composite materials.*

for ~24 hours. The orange coloured Fe-TPA turned to black indicating the loading of polymers was successful and conductivity enhancement was observed to be ~10 times in comparison to Fe-TPA likewise previous chapter.[1] Moreover, its PXRD pattern and morphology remain same, indicating polymerization could not hamper its structure **(Figure 3.11)**. However, PL was not found in the isolated black composite material in such procedure, explaining confinement effect as well as polymer effect was absent.

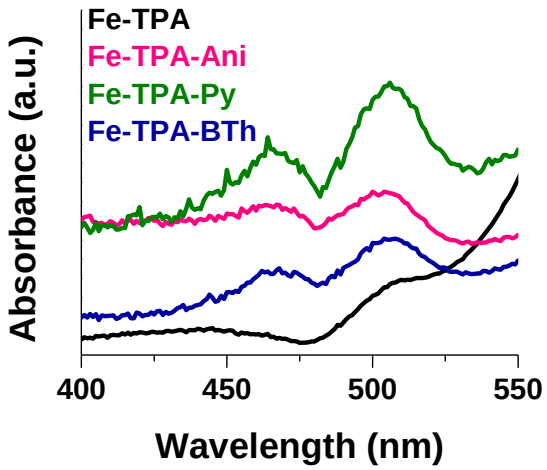

Figure 3.12: *Solid-state UV-Vis spectra of Fe-TPA (black), Fe-TPA-Ani (gray), Fe-TPA-Py (green), and Fe-TPA-BTh (blue).*

To scrutinize the existence of the oxidized polymeric/oligomeric moiety of reactive monomers, solid-state UV−Vis spectra **(Figure 3.12)** were recorded and new absorption band was observed at ~470 nm for all black composite systems, which is the characteristic signature of π−π* transition in oligomers.

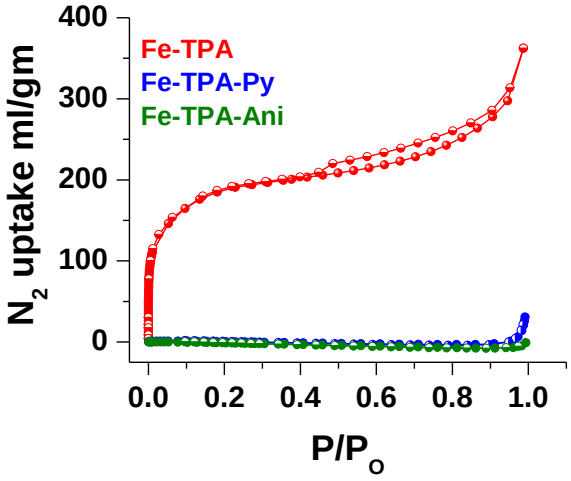

Figure 3.13: *N_2 adsorption isotherm of Fe-TPA (red), Fe-TPA-Ani (green), and Fe-TPA-Py (blue) at 77K.*

In N_2 adsorption and desorption experiment, Fe-TPA adsorbed huge amount of N_2 gas at 77 K indicating highly porous nature compound however, drastically reduced N_2 uptake for the composite materials was observed as the pores were blocked after polymerization **(Figure 3.13)**.

To investigate more, we have extracted some black masses from Fe-TPA-Ani, Fe-TPA-Py, Fe-TPA-BTh by dissolving in NH_3 and also removing TPA and Fe ion by washing with water as well as ethanol. We have recorded FTIR spectra of the extracted materials **(Figure 3.14)**. Notably, extracted masses were observed not to be simple polymers. In fact, these are oxidized polymers having keto, sulfoxo and nitro groups. Oxidized polymers could be PL active materials, which are already reported in various literatures.[12-14] To crosscheck, we have performed PL experiment of the extracted materials and have found the existence of PL. Overall, oxidized polymers were key materials for generation of PL responses.

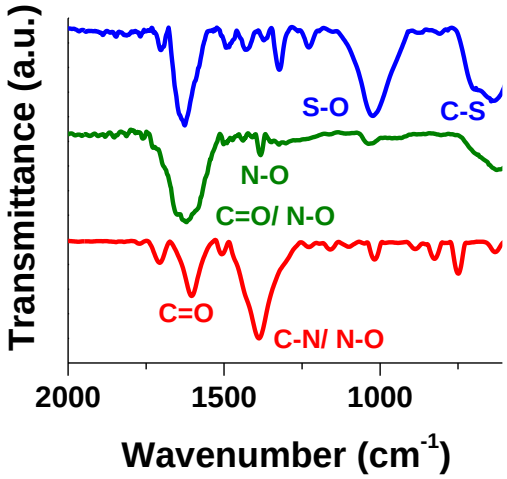

Figure 3.14: *FTIR spectra of the extracted materials from Fe-TPA-Ani (red), Fe-TPA-Py (green), and Fe-TPA-BTh (blue). Specific stretching frequencies are marked (1382 cm^{-1} (N-O), 1622 cm^{-1} (C=O/ N-O), 1388 cm^{-1} (N-O/ C-N) and 1024 cm^{-1} (S-O).*

III.4. Conclusions

In conclusion, we have demonstrated a novel strategy for turn-on PL in a redox-active CP. Intrinsically, non-photoluminescent monomers such as Py, Ani, BTh have been converted to PL active oxidized polymers which was the key reason behind the turn-on PL response of the

materials. With this excellent and cleaver strategy, many other redox-active CPs could be further explored to oxidize other reactive monomers/activation of small molecules to achieve interesting PL and/or other optical properties. This kind of smart and novel materials could be used in lasing applications, optical amplifiers, nonlinear optical switches, and photovoltaics in future.

References

1. Dhara, B.; Ballav, N. *In situ* generation of conducting polymer in a redox-active metal-organic gel. *RSC Adv.* **2013,** *3*, 4909.

2. Ramsahye, N. A.; Trung, T. K.; Scott, L.; Nouar, F.; Devic, T.; Horcajada, P.; Magnier, E.; David, O.; Serre, C.; Trens, P. Impact of the Flexible Character of MIL-88 Iron(III) Dicarboxylates on the Adsorption of n-Alkanes. *Chem. Mater.* **2013,** *25*, 479.

3. Surble, S.; Serre, C.; Mellot-Draznieks, C.; Millange, F.; Ferey, G. A new isoreticular class of metal-organic-frameworks with the MIL-88 topology. *Chem. Commun.* **2006**, 284.

4. Cho, W.; Park, S.; Oh, M. Coordination polymer nanorods of Fe-MIL-88B and their utilization for selective preparation of hematite and magnetite nanorods. *Chem. Commun.* **2011,** *47*, 4138.

5. Pham, M.-H.; Vuong, G.-T.; Vu, A.-T.; Do, T.-O. Novel Route to Size-Controlled Fe–MIL-88B–NH_2 Metal–Organic Framework Nanocrystals. *Langmuir* **2011,** *27*, 15261.

6. Paseta, L.; Seoane, B.; Julve, D.; Sebastián, V.; Téllez, C.; Coronas, J. Accelerating the Controlled Synthesis of Metal–Organic Frameworks by a Microfluidic Approach: A Nanoliter Continuous Reactor. *ACS Appl. Mater. Interfaces* **2013,** *5*, 9405.

7. Sruthi, P.; Danveer, S.; Kumar, G. V. P. Evanescent field-assisted intensity modulation of surface-enhanced Raman scattering from a single plasmonic nanowire. *J. Phys. D: Appl. Phys.* **2013,** *46*, 195107.

8. Patra, P. P.; Chikkaraddy, R.; Tripathi, R. P. N.; Dasgupta, A.; Kumar, G. V. P. Plasmofluidic single-molecule surface-enhanced Raman scattering from dynamic assembly of plasmonic nanoparticles. *Nat. Commun.* **2014,** *5*, 4357.

9. Cui, Y.; Yue, Y.; Qian, G.; Chen, B. Luminescent Functional Metal–Organic Frameworks. *Chem. Rev.* **2012,** *112*, 1126.

10. Allendorf, M. D.; Bauer, C. A.; Bhakta, R. K.; Houk, R. J. T. Luminescent metal-organic frameworks. *Chem. Soc. Rev.* **2009,** *38*, 1330.

11. Dhara, B.; Sappati, S.; Singh, S. K.; Kurungot, S.; Ghosh, P.; Ballav, N. Coordination Polymers of Fe(III) and Al(III) Ions with TCA Ligand: Distinctive Fluorescence, CO_2 Uptake, Redox-Activity and Oxygen Evolution reaction. *Dalton Trans.* **2016,** *45*, 6901.

12. Abdou, M. S. A.; Holdcroft, S. Mechanisms of photodegradation of poly(3-alkylthiophenes) in solution. *Macromolecules* **1993,** *26*, 2954.

13. Ezumi, K.; Miyazaki, H.; Kubota, T. Stretching vibration of nitro and N-oxide groups of the anion radicals of 4-nitropyridine N-oxide and related nitro compounds. *J. Phys. Chem.* **1970,** *74*, 2397.

14. Cativo, M. H. M.; Kamps, A. C.; Gao, J.; Grey, J. K.; Hutchison, G. R.; Park, S.-J. Oxidation-Induced Photoluminescence of Conjugated Polymers. *J. Phys. Chem. B* **2013,** *117*, 4528.

Chapter-IV

Electro-catalytic Activity of Redox-Active Coordination Polymer

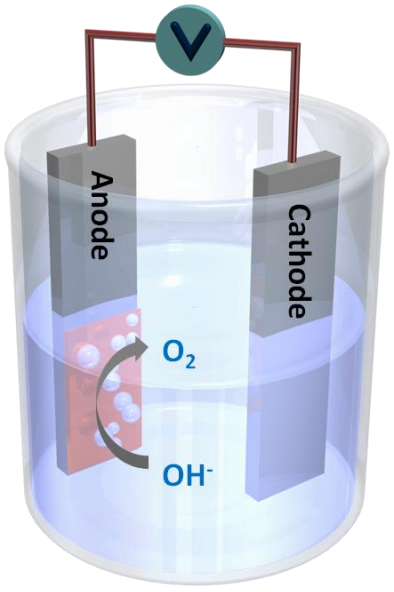

IV.1. Introduction

In the current scenario of electro-catalysis, such as, OER, and HER, various metal oxides (mostly transition metals) has been extensively explored and preferred because of their excellent performance, high abundance and low cost. However, the low surface area and poor electrical conductivity of metal oxides limits their use as such (pure) for the electro-catalysis. Therefore, other materials such as, coordination polymers (CPs), which evolved in the recent past, can be considered as alternatives for such a valuable field. CPs has very high intrinsic surface area, but the low conducting nature can decrease the overall performance. In order to increase the conductivity cum catalytic performance, recently Ma *et al.* calcined the cobalt based CP and used for OER.[1] Furthermore, such calcination hampers the integrity of CPs, therefore by bringing intrinsic electrical conductivity in CPs, such practice can be avoided. Herein, we have synthesized Fe(III) 4,4′,4″-tricarboxyphenylamine (Fe-TCA), redox-active CP and used it as such (without any calcination or treatment) for the OER activity **(Figure 4.1)**.

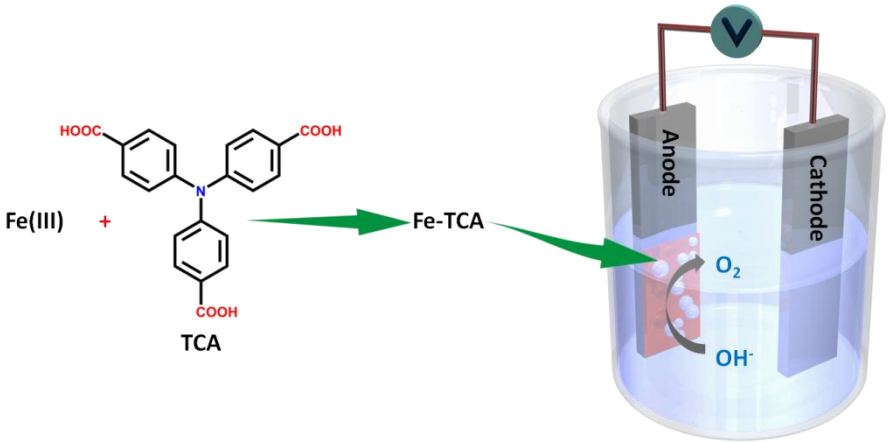

Figure 4.1. *Schematic illustration of OER by employing redox-active CP as electro-catalyst.*

IV.2. Materials and Methods

4-cyanobenzonitrile, 4-fluorobenzonitrile, cesium fluoride, sodium hydroxide, ferric nitrate were purchased from Sigma Aldrich.

Fourier transform infrared (FTIR) spectra were recorded in a NICOLET 6700 spectrophotometer using KBr pellet. Field emission scanning electron microscope (FESEM) imaging and energy-dispersive X-ray spectroscopy (EDXS) analysis were performed in a Carl-Zeiss Ultra microscope. Atomic force microscope (AFM) images were recorded using Veeco

Nanoscope IV instrument. The DC conductivity values were measured by four-probe technique using Keithely 6221 AC and DC current sourcemeter and 2182A Nanovoltmeter. The powder X-ray diffraction (PXRD) patterns of all xero-gels were recorded from 2θ = 5 to 35° at room-temperature in Bruker D8 advanced diffractometer.

All the electrochemical analyses have been performed in VMP-3 model Biologic potentiostat. A conventional three electrode cell setup containing glassy carbon (GC) coated with catalyst, graphite rod and Hg/HgO as a working electrode (WE), counter electrode (CE) and reference electrodes (RE) respectively and 1M KOH was used as electrolyte. The potentials obtained using Hg/HgO RE during catalysis, were converted with respect to RHE. The GC electrode was polished by 0.3 µm alumina slurry and cleaned properly before coating the active catalyst on it. For the electrochemical performance, active material slurry was prepared by mixing 90% active material, 10% acetylene black and 40 µL 5% Nafion, in 1 mL 3:2 (IPA:water) solution followed by vigorous sonication for 1h. Furthermore, 10 µL of the prepared slurry was coated and kept under IR lamp for drying. To check the electro-catalytic activity, cyclic voltammetry (CV), and linear sweep voltammery (LSV) have been performed.

A mixture of 4-cyanobenzonitrile (1 mmole) and 4-fluorobenzonitrile (2 mmole) were refluxed (160 °C) for 48 hours, in DMF (60 ml) solvent in presence of cesium fluoride (2 mmole) as a base **(Figure 4.2)**. Reaction mixture was cooled down upto room temperature, and ice cold water was added,[2-4] a pale yellowish white precipitate was filtered, vigorous washed with cold water and dried under vacuum. About 4 gm product was added in water ethanol mixture (1:1; 120 ml) and allowed to reflux with sodium hydroxide for 2 days to hydrolyze the cyano group. Furthermore, the solution was neutralized using hydrochloric acid and the pH was maintained at 7. Light yellow precipitate was filtered and washed with water. Finally, the 4,4′,4″-tricarboxyphenylamine (TCA) was obtained and characterized using various techniques.

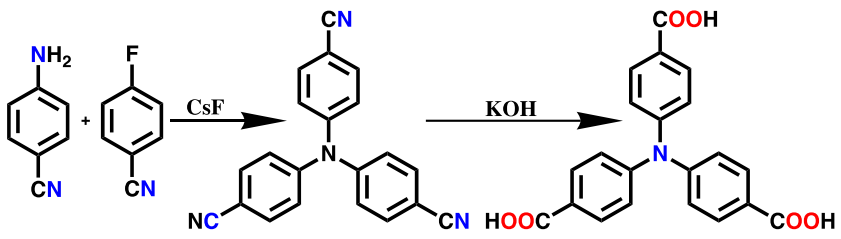

Figure 4.2: *Schematic presentation of ligand (TCA) synthesis.*

Ethanolic solutions of TCA (37.5 mg in 0.5 ml ethanol) and ferric nitrate (40.4 mg in 0.5 ml ethanol) were prepared separately and mixed together with sonication.[5] Within few seconds a brown coloured gel (Fe-TCA) was formed **(Figure 4.3)** which was further dried under vacuum at room temperature to get xero-gel.

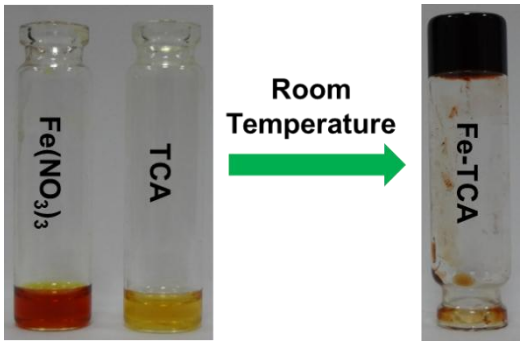

Figure 4.3: *Gelation test between TCA ligand with ferric nitrate.*

IV.3. Results and Discussion

FESEM images of Fe-TCA revealed the fibrous network with high degree of macro-porosity **(Figure 4.4a)** likewise other metallogel materials,[5] and the observation was supported by AFM **(Figure 4.4b)**. Such fibrous nature of gel clearly indicates the formation of homogeneous polymeric network throughout the sample.

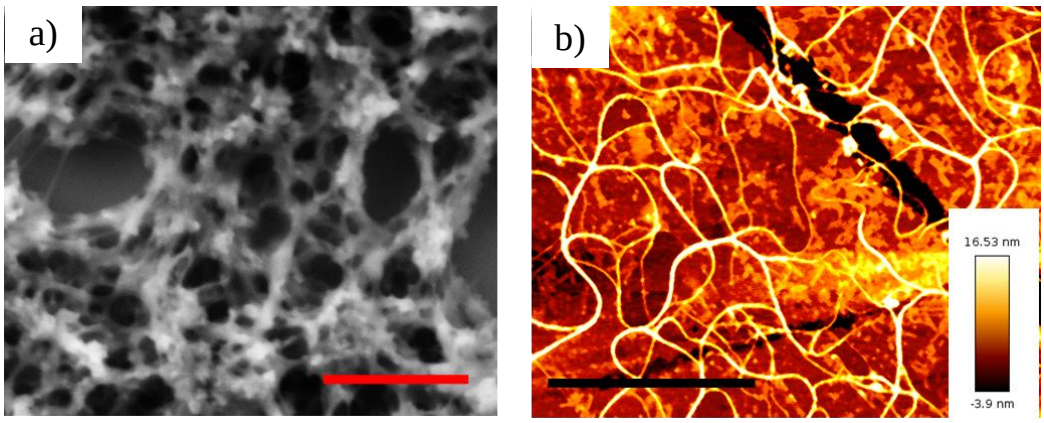

Figure 4.4: *FESEM (a) and AFM (b) images of Fe–TCA xero-gel of 2 µm, and 500 nm respectively.*

Interestingly, from the PXRD analysis, Fe-TCA was found to be semi-crystalline material **(Figure 4.5)** which complemented by the microscopic images (FESEM and AFM images).

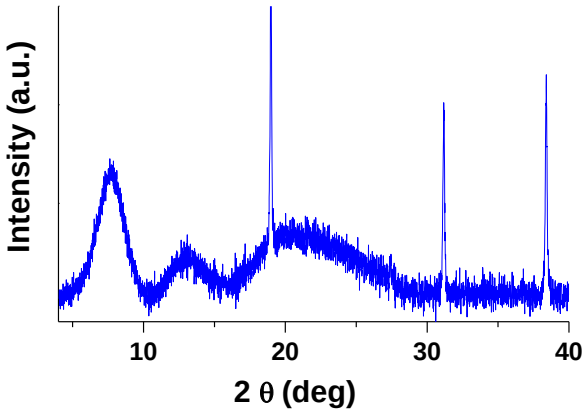

Figure 4.5: *PXRD patterns of Fe-TCA xero-gel indicating the semi-crystalline nature.*

Gas adsorption-desorption isotherm was performed to check the potential void space in the material. Distinctive CO_2 uptake was observed in Fe-TCA at room temperature **(Figure 4.6)** which was similar to the previously reported Zn-TCA CP.[4] Such hysteresis behaviour of Fe-TCA xero-gel is mainly because of the interaction between the host (N atoms of the TCA ligand) and guest CO_2 molecules. Overall, porous Fe-TCA CP could be very crucial material to accommodate the suitable molecule and use for potential applications.

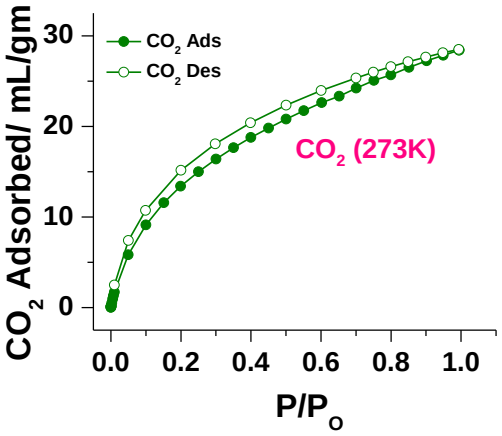

Figure 4.6: *Room temperature CO_2 adsorption isotherm of Fe-TCA xero-gel.*

To test the redox-activity of the xero-gel, oxidative polymerization technique (likewise previous chapters, section-IIA and chapter-III) has been employed. In short, xero-gel was taken in a non-reactive solvent such as hexane or chloroform and few drops of pyrrole (Py) monomers was added.[6-7] Interestingly, in few hours, colour change of xero-gel from brown to black was observed **(Figure 4.7a),** which clearly indicates the redox-activity of the material.[8-9] Further,

the above obtained black material was dissolved in 0.5 M HCl solution and extracted the insoluble black mass, which again vigorously washed with water, acetone and methanol. Finally, the black insoluble mass was characterized by FTIR spectroscopy and assigned as polypyrrole (PPy) by matching it with directly synthesized PPy. DC electrical conductivity of Fe-TCA and Fe-TCA-PPy were recorded on pressed pellet. The electrical conductivity value of Fe-TCA was found to be ~10^{-6} S/cm. Interestingly, electrical conductivity of Fe-TCA-PPy found to be ~10^{-3} S/cm **(Figure 4.7b)** and such remarkable enhancement of conductivity could be due to the formation of PPy moiety in the Fe-TCA cavity.

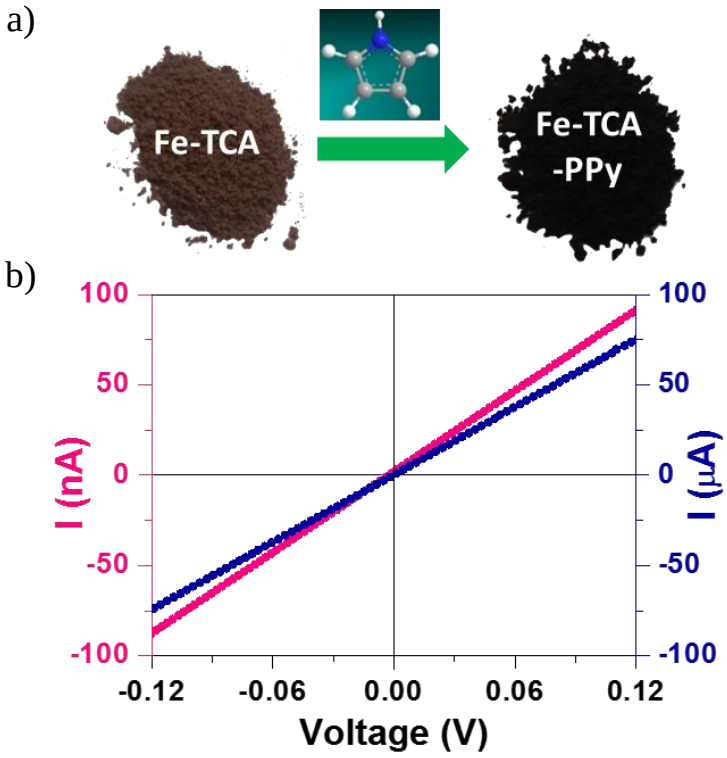

Figure 4.7: *(a) Redox-active behavior of Fe-TCA. (b) Room temperature I–V curves for Fe-TCA (pink), Fe-TCA-Py (blue).*

The OER is an anodic reaction where hydroxide ions convert to oxygen and water. The OER activity was done by using linear scan voltammetry (LSV) technique at 10 mV/s. LSV plot revealed the onset potential of the material ~1.58V whereas bare GC was inactive for OER **(Figure 4.8)**. The overpotential value of xero-gel material was found to be ~458 mVat 10 mA cm^{-2}, which is comparably better than those well-established iron-oxyhydroxide materials.[10-11] Remarkable overpotential value is perhaps due to the presence of redox-active iron center

and reasonable porosity, which could be easily accessible by ions present in the electrolyte. Further to test the importance of redox-active Fe-TCA CP for OER activity another Al(III) based Al-TCA redox-inactive CP has been synthesized **(Figure 4.8).** However, Al-TCA xero-gel did not show any activity towards the OER.

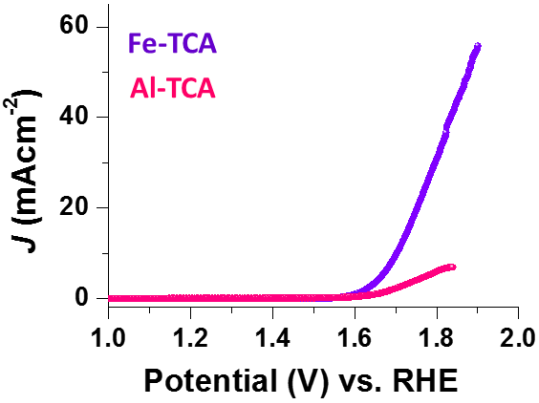

Figure 4.8: *LSV plots of Fe-TCA (violet) and Al-TCA (pink).*

To understand the OER kinetics, Prof. Tafel gave an equation where log of the current density (log *J*) can be plotted against potential and the slope value at low potential range can be obtained. The lower overpotential value is the signature of higher OER activity; faster adsorption of the reactant (OH^-) and desorption of O_2 from the catalytic site. The Tafel slope of here made Fe- TCA xero-gel was found to be ~87 mV per decade **(Figure 4.9b)** which is comparably better than iron based material.[12] Reasonable value of the low Tafel slope can be well explained in terms of high porosity and easy percolation of the electrolyte to the active sites. Moreover, to investigate the long-term stability of the material, 500 catalytic cycles were

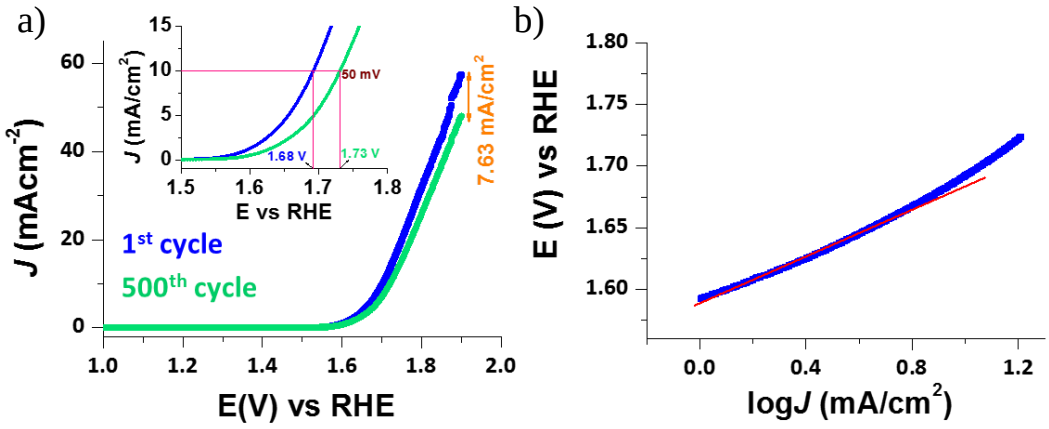

Figure 4.9: *(a) comparative LSV plots of the Fe–TCA xero-gel before (blue) and after (green) the durability test. (b)Tafel Plot of Fe-TCA (blue) and red line is the fitted graph.*

performed **(Figure 4.9a)**. Interestingly, at 10 mA cm^{-2} current density, only ~11% overpotential (from 458-508 mV) value has been increased. Overall, Fe-TCA material as such showed remarkable OER activity alongwith long term cycling stability.[13-14]

IV.4. Conclusions

First time we have successfully prepared Fe-TCA coordination polymer with specific physicochemical properties, such as reasonable surface area, electrical conductivity, and redox-activity. The as synthesised Fe-TCA xero-gel was used for OER activity and the overpotential (~450 mV) value was realized to be comparable/higher than most of the reported Fe-based standard oxyhydroxide material. The cycling stability was also noteworthy. Result could be useful to design other CPs with better catalytic performance and further use in fuel cell applications.

References

1. Ma, T. Y.; Dai, S.; Jaroniec, M.; Qiao, S. Z. Metal–Organic Framework Derived Hybrid Co_3O_4-Carbon Porous Nanowire Arrays as Reversible Oxygen Evolution Electrodes. *J. Am. Chem. Soc.* **2014,** *136*, 13925.

2. Dapperheld, S.; Steckhan, E.; Brinkhaus, K.-H. G.; Esch, T. Organic Electron Transfer Systems, II Substituted Triarylamine Cation-Radical Redox Systems – Synthesis, Electrochemical and Spectroscopic Properties, Hammet Behavior, and Suitability as Redox Catalysts. *Chemische Berichte* **1991,** *124*, 2557.

3. Lee, E. Y.; Jang, S. Y.; Suh, M. P. Multifunctionality and Crystal Dynamics of a Highly Stable, Porous Metal−Organic Framework $[Zn_4O(NTB)_2]$. *J. Am. Chem. Soc.* **2005,** *127*, 6374.

4. Suh, M. P.; Cheon, Y. E.; Lee, E. Y. Reversible Transformation of Zn(II) Coordination Geometry in a Single Crystal of Porous Metal-Organic Framework $[Zn_3(ntb)_2(EtOH)_2]\cdot 4$ EtOH. *Chem. – Eur. J.* **2007,** *13*, 4208.

5. Lohe, M. R.; Rose, M.; Kaskel, S. Metal-Organic Framework (MOF) Aerogels With High Micro- and Macroporosity. *Chem. Commun.* **2009**, 6056.

6. Dhara, B.; Ballav, N. In situ generation of conducting polymer in a redox-active metal-organic gel. *RSC Adv.* **2013,** *3*, 4909.

7. Dhara, B.; Patra, P. P.; Jha, P. K.; Jadhav, S. V.; Pavan Kumar, G. V.; Ballav, N. Redox-Induced Photoluminescence of Metal–Organic Coordination Polymer Gel. *J. Phys. Chem. C* **2014,** *118*, 19287.

8. Kanatzidis, M. G.; Wu, C. G.; Marcy, H. O.; Kannewurf, C. R. Conductive-Polymer Bronzes. Intercalated Polyaniline in Vanadium Oxide Xerogels. *J. Am. Chem. Soc.* **1989,** *111*, 4139.

9. Kanatzidis, M. G.; Tonge, L. M.; Marks, T. J.; Marcy, H. O.; Kannewurf, C. R. In situ intercalative polymerization of pyrrole in FeOCl: a new class of layered, conducting polymer-inorganic hybrid materials. *J. Am. Chem. Soc.* **1987,** *109*, 3797.

10. Zou, S.; Burke, M. S.; Kast, M. G.; Fan, J.; Danilovic, N.; Boettcher, S. W. Fe(Oxy)hydroxide Oxygen Evolution Reaction Electrocatalysis: Intrinsic Activity and the Roles of Electrical Conductivity, Substrate, and Dissolution. *Chem. Mater.* **2015,** *27*, 8011.

11. Wurster, B.; Grumelli, D.; Hötger, D.; Gutzler, R.; Kern, K. Driving the Oxygen Evolution Reaction by Nonlinear Cooperativity in Bimetallic Coordination Catalysts. *J. Am. Chem. Soc.* **2016,** *138*, 3623.

12. Lyons, M. E. G.; Doyle, R. L.; Brandon, M. P. Redox switching and oxygen evolution at oxidized metal and metal oxide electrodes: iron in base. *Phys. Chem. Chem. Phys.* **2011,** *13*, 21530.

13. Burke, M. S.; Zou, S.; Enman, L. J.; Kellon, J. E.; Gabor, C. A.; Pledger, E.; Boettcher, S. W. Revised Oxygen Evolution Reaction Activity Trends for First-Row Transition-Metal (Oxy)hydroxides in Alkaline Media. *J. Phys. Chem. Lett.*, **2015,** *6*, 3737.

14. Friebel, D.; Louie, M. W.; Bajdich, M.; Sanwald, K. E.; Cai, Y.; Wise, A. M.; Cheng, M.-J.; Sokaras, D.; Weng, T.-C.; Alonso-Mori, R.; Davis, R. C.; Bargar, J. R.; Nørskov, J. K.;

Nilsson, A.; Bell, A. T. Identification of Highly Active Fe Sites in (Ni,Fe)OOH for Electrocatalytic Water Splitting. *J. Am. Chem. Soc.* **2015,** *137*, 1305.